Typy pulsacji gwiazd

Wzbudzanie pulsacji
w klasycznym pasie niestabilności
i na Ciągu Głównym:
mechanizm „kappa”
i Z-maksimum

Typy pulsacji gwiazd

Według geometrii pulsacji:

Radialne - drgania z zachowaniem symetrii sferycznej, węzły dla obertonów - tylko wzdłuż promienia, jako koncentryczne sfery.
Nieradialne – na sferze mamy obszary, które drgają w przeciwfazie.

Według fizycznej natury:

Akustyczne (ciśnieniowe) [np. fale dźwiękowe] , dla których siłą zwracającą jest gradient ciśnienia. Radialne pulsacje należą do akustycznych.
Grawitacyjne [np. fale na wodzie], dla których siłą zwracającą jest grawitacja. Tylko nieradialne pulsacje.

1D oscillations

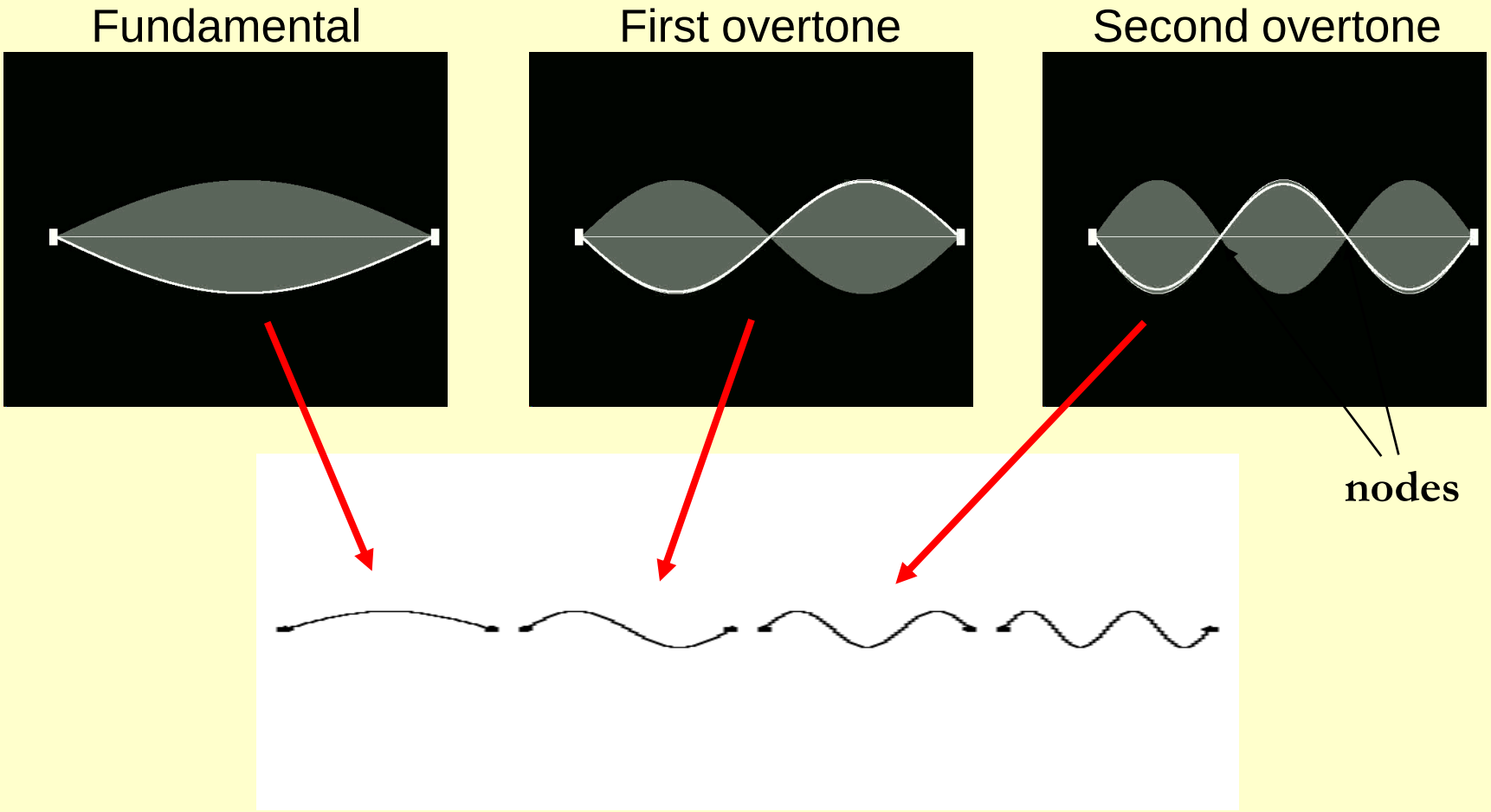

From a course of asteroseismology

Trzy najniższe mody drgań struny i trzy najniższe mody pulsacji radialnych gwiazdy

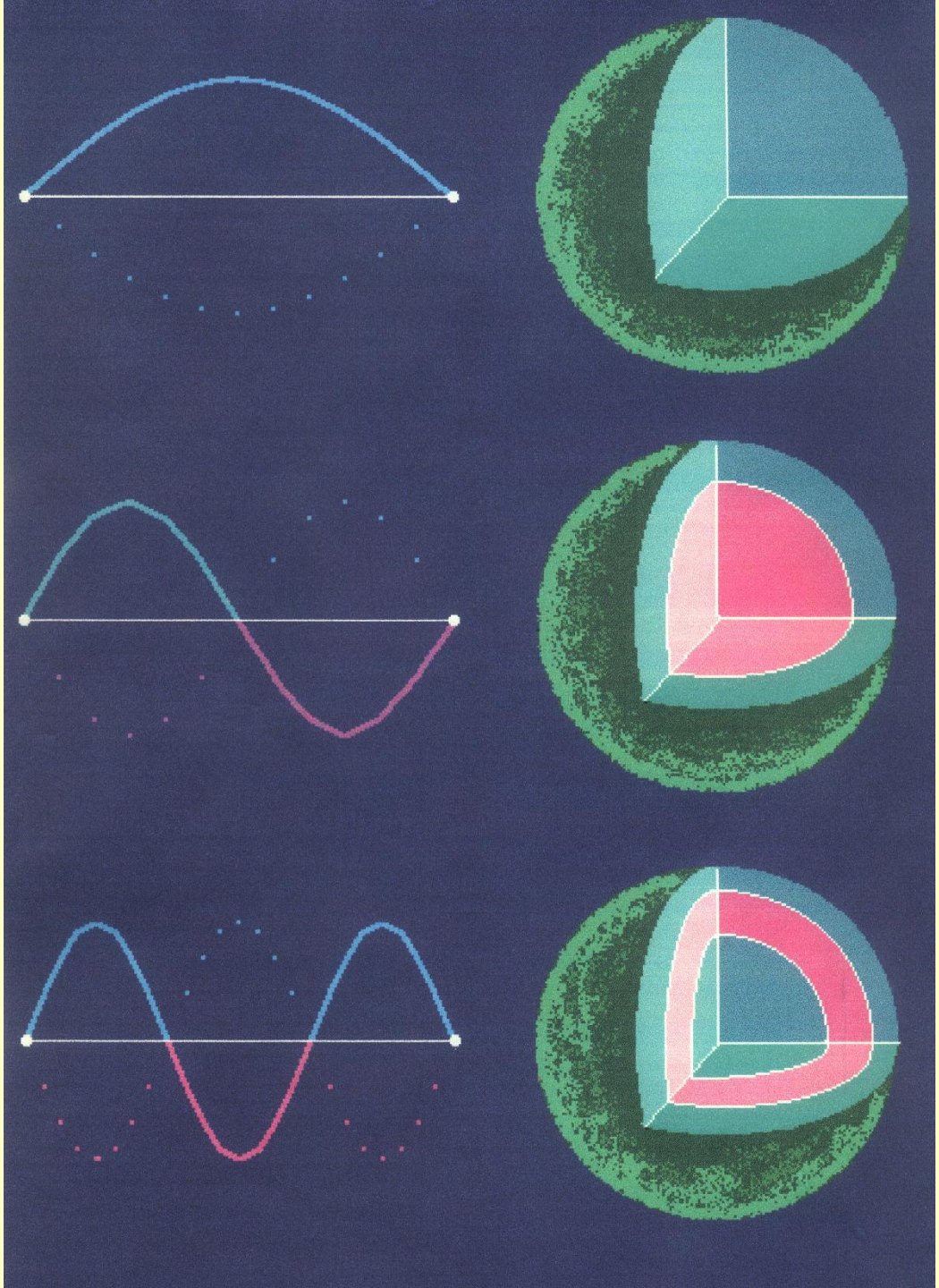

Radialne pulsacje

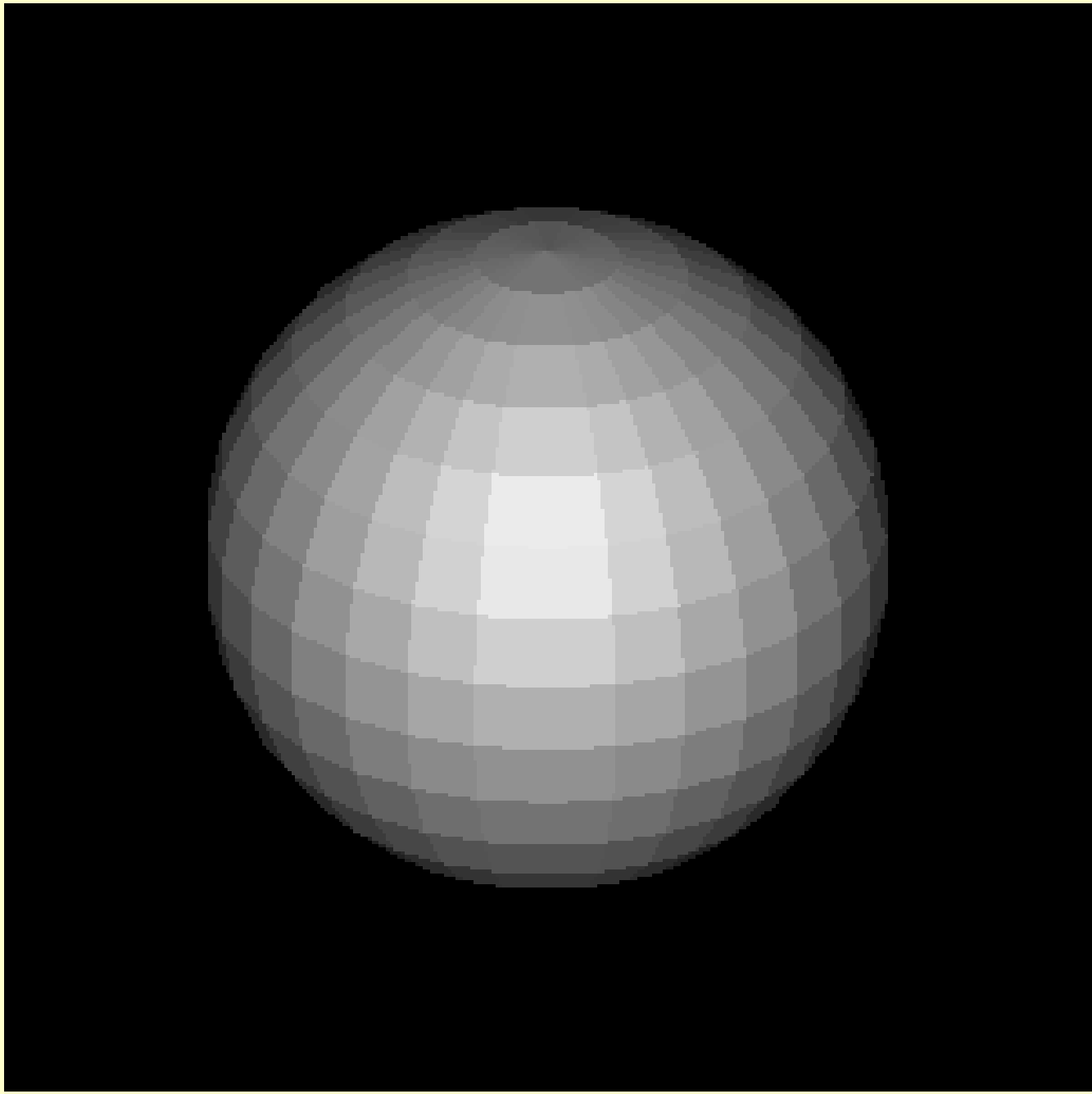

MODY

$$\frac{\delta T}{T} = y_{T,n}(r) Y_\ell^m(\theta,\phi) \exp(-\mathrm{i}\omega_{n\ell m} t)$$

$y_{T,n}(r)$ radialna funkcja własna

n radialny rząd modu

$n < 0$ mody **g** $(\ell > 0)$

$n = 0$ mody **f** $(\ell > 1)$

$n > 0$ mody **p**

$Y_\ell^m(\theta,\phi)$ sferyczna harmonika

$\nabla_H^2 Y = -\ell(\ell+1)Y$

ℓ stopień modu

$m = -\ell, ...0, ...\ell$ rząd azymutalny

W. A. Dziembowski

MODY

$$\frac{\delta T}{T} = y_{T,n}(r) Y_\ell^m(\theta,\phi)\exp(-\mathrm{i}\omega_{n\ell m}t)$$

$y_{T,n}(r)$ radialna funkcja własna

$Y_\ell^m(\theta,\phi)$ sferyczna harmonika

n radialny rząd modu

$\nabla_H^2 Y = -\ell(\ell+1)Y$

$n<0$ mody **g** $(\ell>0)$

ℓ stopień modu

$n=0$ mody **f** $(\ell>1)$

$m=-\ell,\ldots 0,\ldots \ell$ rząd azymutalny

$n>0$ mody **p**

$$Y_\ell^m(\theta,\phi) = (-1)^m \mathcal{N}_\ell^{|m|} P_\ell^{|m|}(\mu)\exp(\mathrm{i}m\phi)$$

$$\mathcal{N}_\ell^{|m|} = \sqrt{\frac{(2\ell+1)(\ell-|m|)!}{4\pi(\ell+|m|)!}}$$

$\mu = \cos\theta$

$$P_\ell^{|m|}(\mu) = (1-\mu^2)^{\frac{|m|}{2}} \frac{d^{|m|}P_\ell}{d\mu^{|m|}}$$

- stowarzyszone funkcje Legendra

P_ℓ - wielomiany Legendra

W. A. Dziembowski

Harmoniki sferyczne Y_l^m

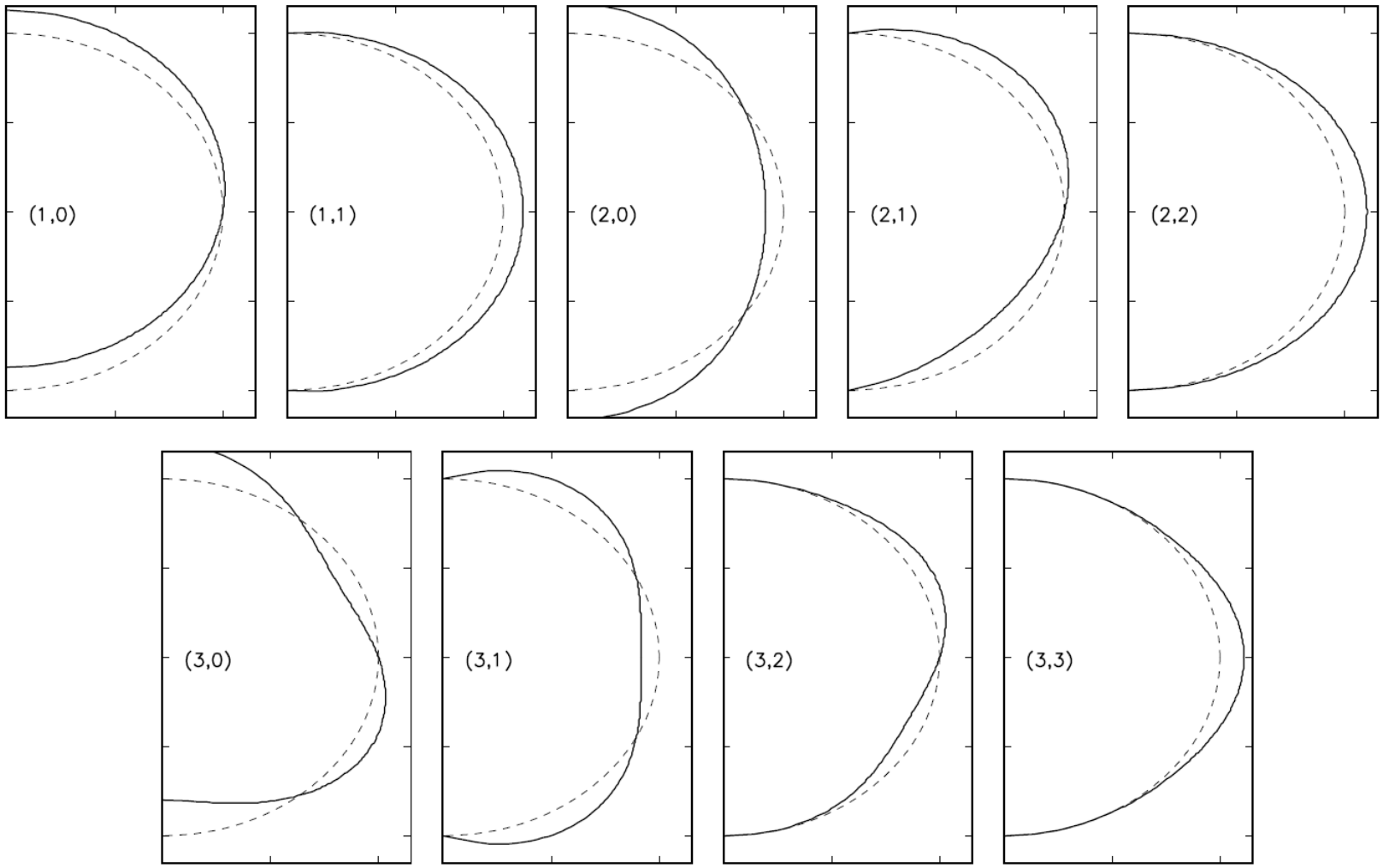

Rysunek 1: Sferyczne harmoniki stopni $\ell = 1, 2$ i 3 na półpłaszczyźnie $\phi = 0$.

W. A. Dziembowski

MODY

$$\frac{\delta T}{T} = y_{T,n}(r) Y_\ell^m(\theta,\phi) \exp(-\mathrm{i}\omega_{n\ell m} t)$$

$y_{T,n}(r)$ radialna funkcja własna

$Y_\ell^m(\theta,\phi)$ sferyczna harmonika

n radialny rząd modu

$\nabla_H^2 Y = -\ell(\ell+1)Y$

ℓ stopień modu

$n < 0$ mody **g** $(\ell > 0)$

$n = 0$ mody **f** $(\ell > 1)$

$n > 0$ mody **p**

$m = -\ell, \ldots 0, \ldots \ell$ rząd azymutalny

częstotliwość kołowa $\omega_{n,\ell,m} = 2\pi\nu_{n,\ell,m}$

najniższy mod radialny $\omega_{1,0,0} = \sigma_{1,0,0}\sqrt{4\pi G\bar{\rho}}$ $\sigma_{1,0,0} \in (1.4, 2)$

mody wyższe (owertony) $\omega_{n+1,0,0} > \omega_{n,0,0}$

W. A. Dziembowski

MODY

$$\frac{\delta T}{T} = y_{T,n}(r) Y_\ell^m(\theta,\phi) \exp(-\mathrm{i}\omega_{n\ell m} t)$$

$y_{T,n}(r)$ radialna funkcja własna

$Y_\ell^m(\theta,\phi)$ sferyczna harmonika

n radialny rząd modu

$\nabla_H^2 Y = -\ell(\ell+1)Y$

$n<0$ mody **g** $(\ell > 0)$

ℓ stopień modu

$n=0$ mody **f** $(\ell > 1)$

$m = -\ell, \ldots 0, \ldots \ell$ rząd azymutalny

$n>0$ mody **p**

częstotliwość kołowa $\omega_{n,\ell,m} = 2\pi\nu_{n,\ell,m}$

najniższy mod radialny $\omega_{1,0,0} = \sigma_{1,0,0}\sqrt{4\pi G\bar{\rho}}$ $\sigma_{1,0,0} \in (1.4, 2)$

mody wyższe (owertony) $\omega_{n+1,0,0} > \omega_{n,0,0}$

mody nieradialne $\omega_{n+1,\ell,m} > \omega_{n\ell,m}$

gwiazdy sferyczne $\omega_{n,\ell,m} = \omega_{n,\ell,0}$

W. A. Dziembowski

MODY

$$\frac{\delta T}{T} = y_{T,n}(r) Y_\ell^m(\theta,\phi) \exp(-\mathrm{i}\omega_{n\ell m} t)$$

$y_{T,n}(r)$ radialna funkcja własna

$Y_\ell^m(\theta,\phi)$ sferyczna harmonika

n radialny rząd modu

$\nabla_H^2 Y = -\ell(\ell+1)Y$

ℓ stopień modu

$n < 0$ mody **g** $(\ell > 0)$

$n = 0$ mody **f** $(\ell > 1)$

$n > 0$ mody **p**

$m = -\ell, \ldots 0, \ldots \ell$ rząd azymutalny

częstotliwość kołowa $\omega_{n,\ell,m} = 2\pi\nu_{n,\ell,m}$

najniższy mod radialny $\omega_{1,0,0} = \sigma_{1,0,0}\sqrt{4\pi G\bar{\rho}}$ $\sigma_{1,0,0} \in (1.4, 2)$

mody wyższe (owertony) $\omega_{n+1,0,0} > \omega_{n,0,0}$

mody nieradialne $\omega_{n+1,\ell,m} > \omega_{n\ell,m}$

gwiazdy sferyczne $\omega_{n,\ell,m} = \omega_{n,\ell,0}$

gwiazdy wolno rotujące $\omega_{n,\ell,m} = \omega_{n,\ell,0} - m\Omega C_{n,\ell}$

W. A. Dziembowski

Pulsacje z ℓ=3

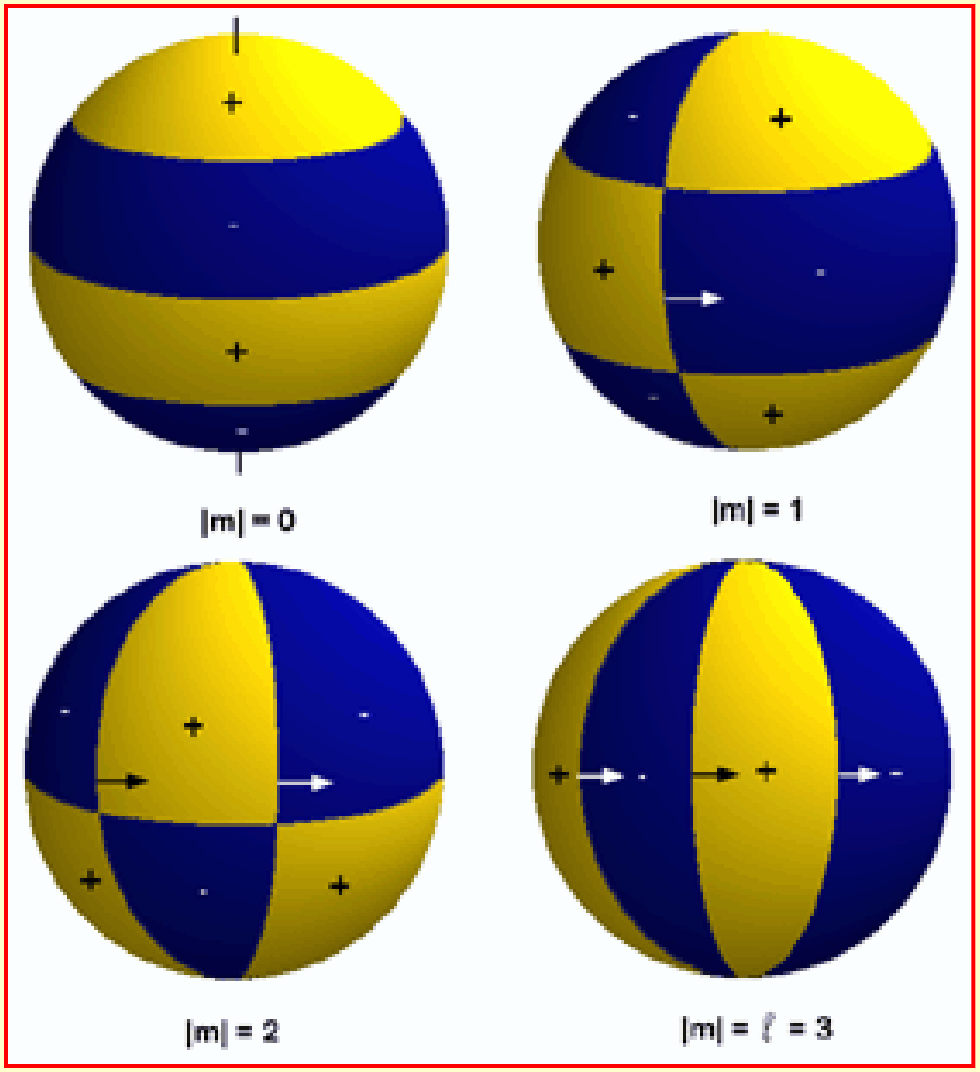

Z wykładu J. Daszyńskiej-Daszkiewicz

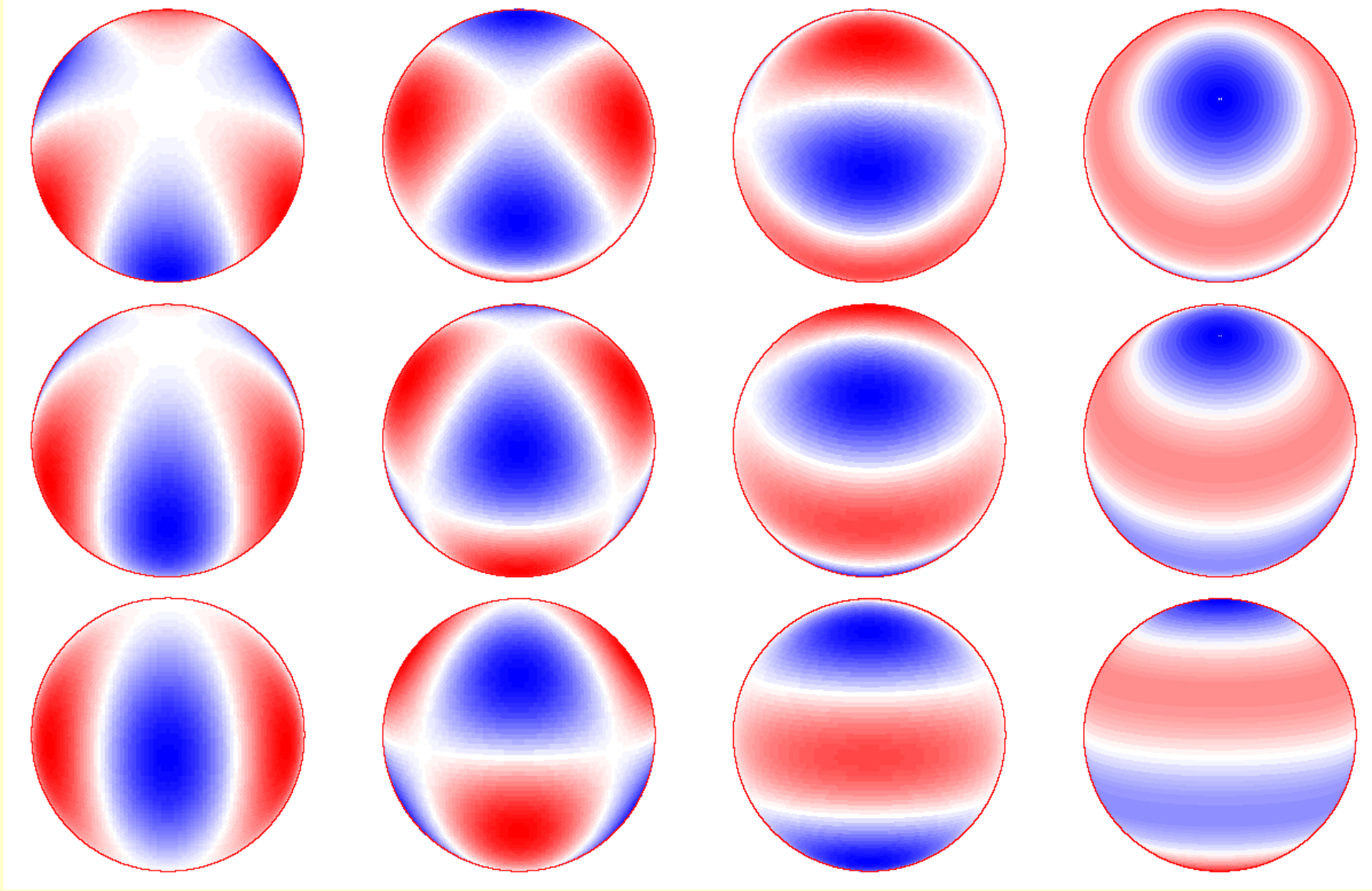

C. Aerts

Przykłady geometrii oscylacji nieradialnych:

a) l=1, m=0
b) l=1, m=1

c) l=2, m=0
d) l=2, m=1
e) l=2, m=2

f) l=3, m=0
g) l=3, m=1
h) l=3, m=2
i) l=3, m=3

j) l=5, m=5
k) l=10, m=5
l) l=10, m=10

J. Christensen-Dalsgaard

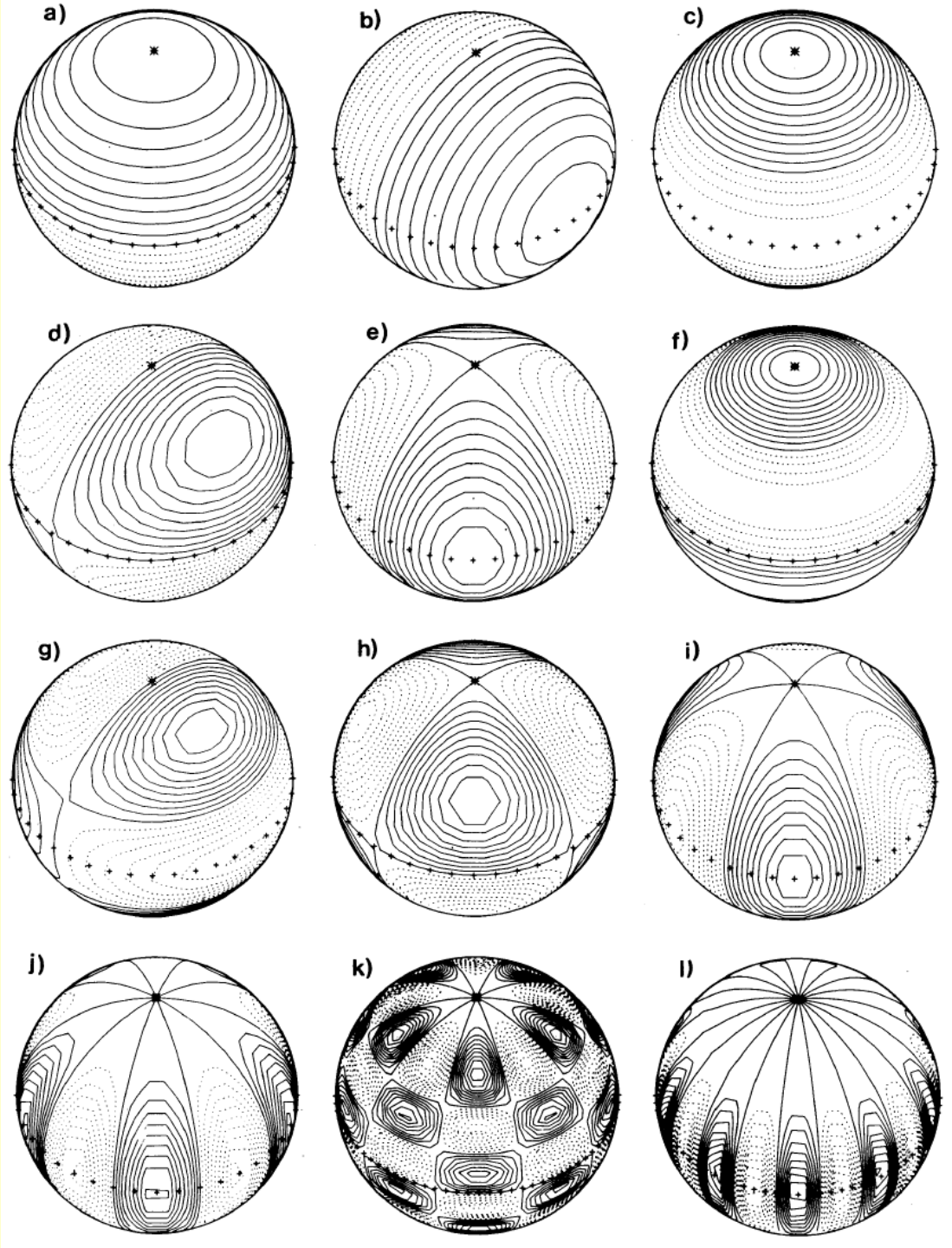

Oscylacje nieradialne dipolowe, *l*=1:

m=0

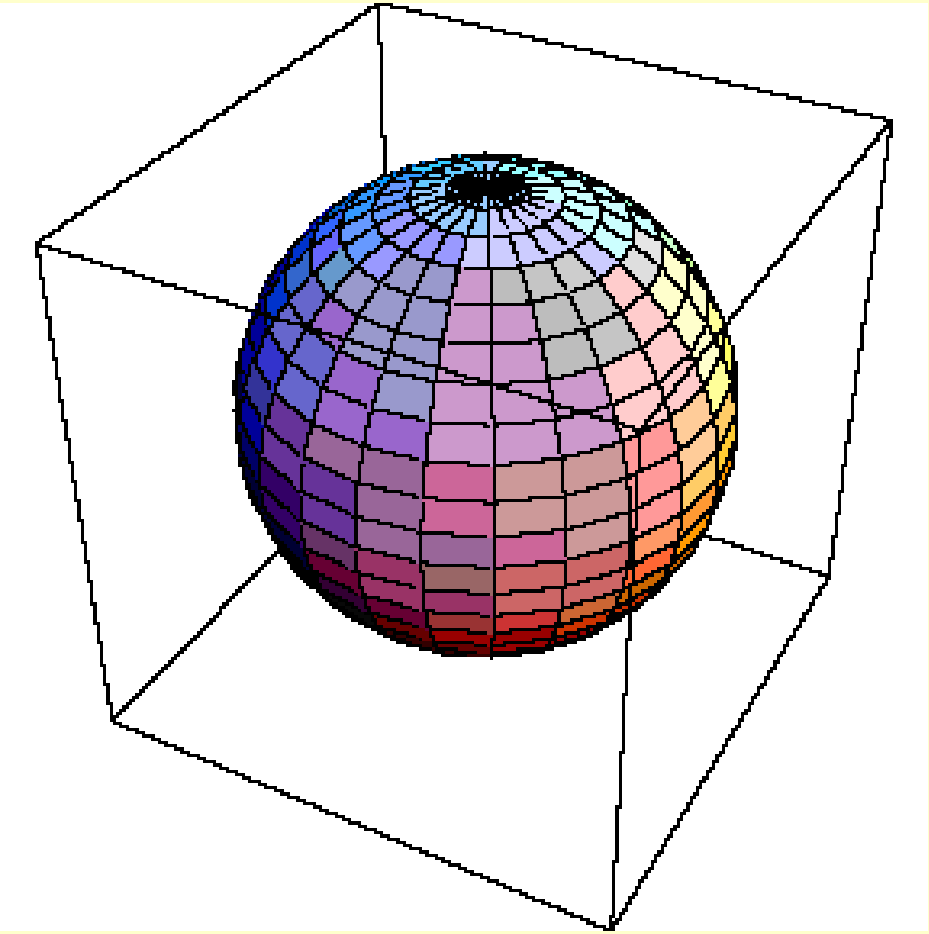

m=1

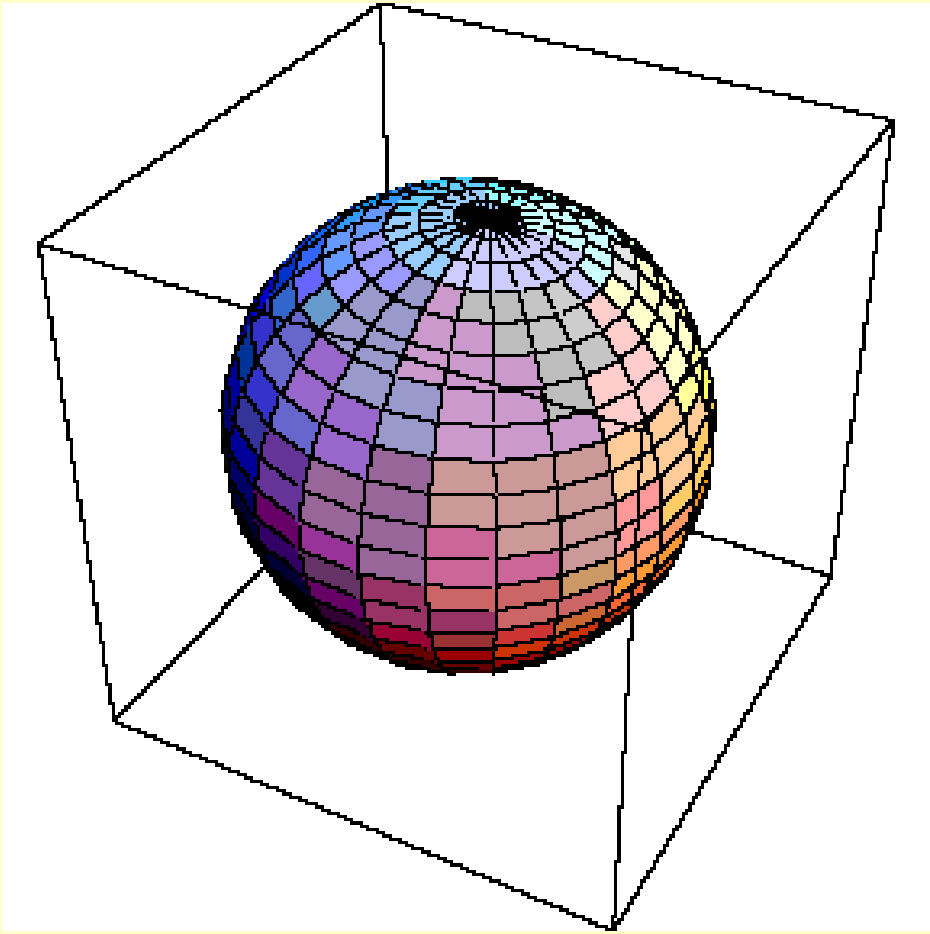

Tim Bedding

Oscylacje nieradialne oktupolowe, *l*=3:

m=0

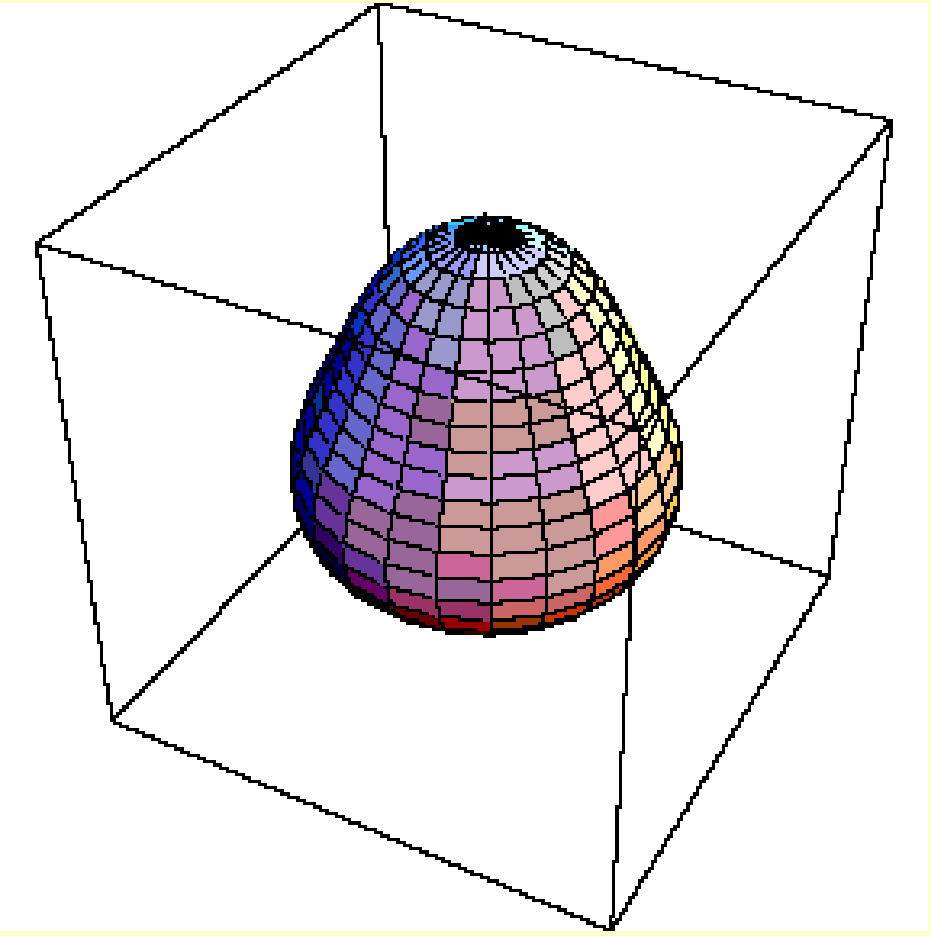

m=3

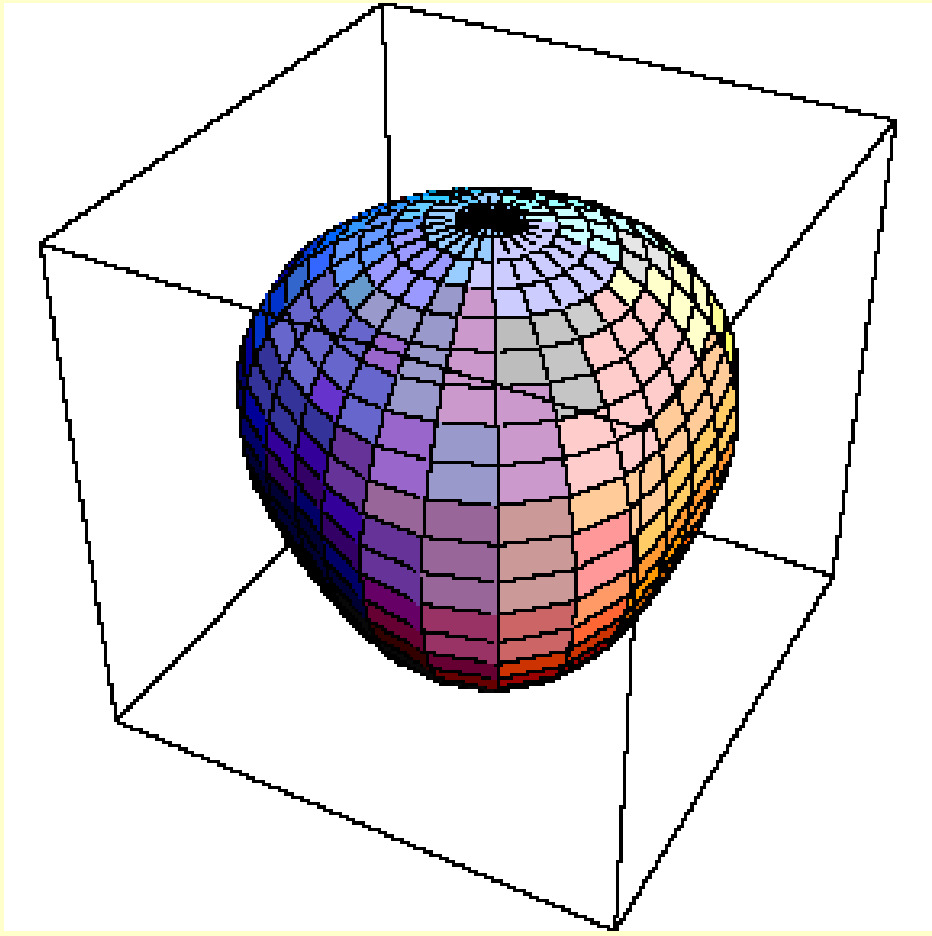

Tim Bedding

Oscylacje nieradialne, *l*=8, m=3:

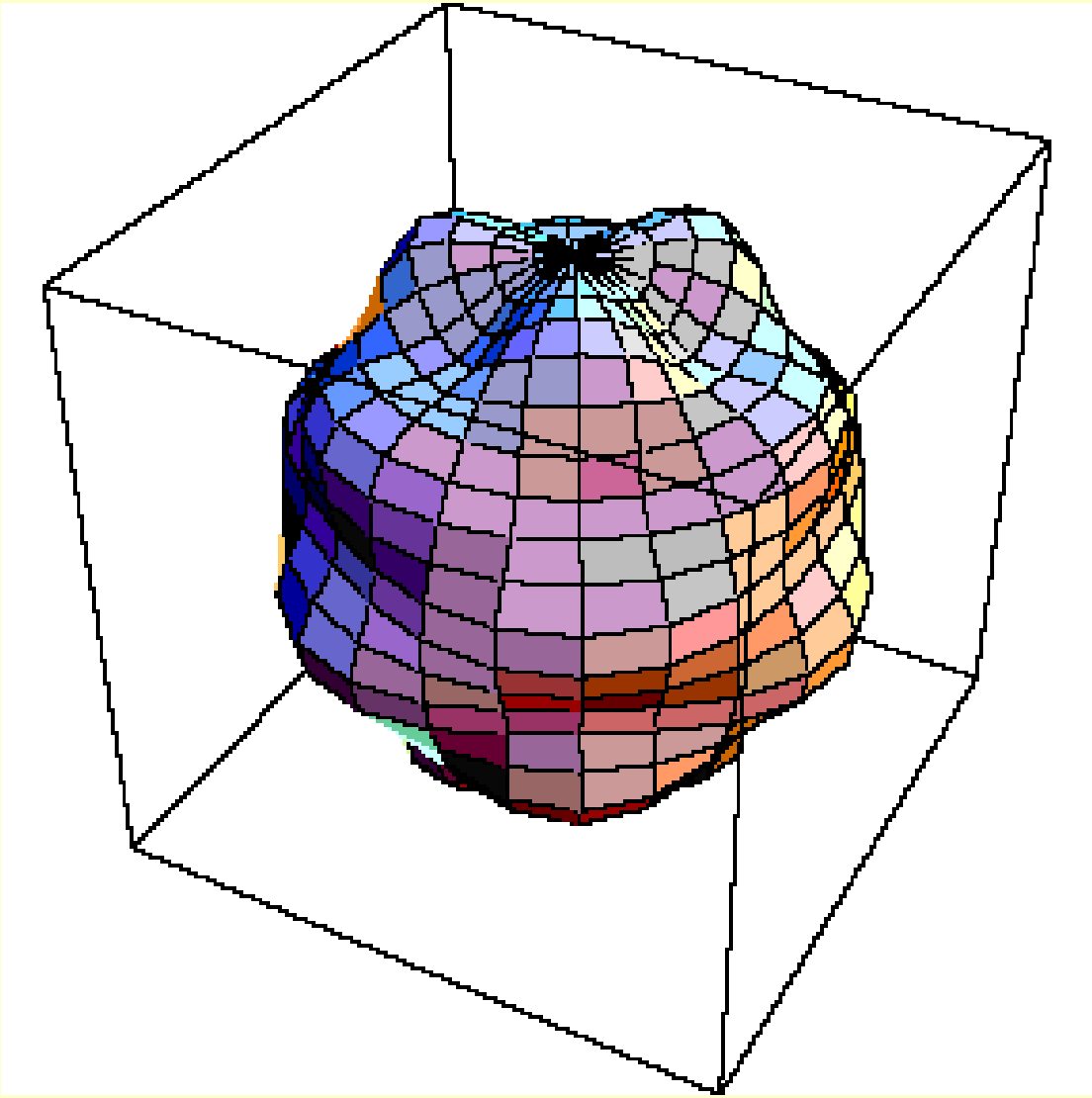

Tim Bedding

Pole prędkości i zmiany profilu linii widmowej wskutek efektu Doplera.

Radialne pulsacje (*l*=0)

Efekt Doplera – zmiana obserwowanej długości fali w stosunku do długości fali wysłanej, spowodowana względnym ruchem źródła i obserwatora.

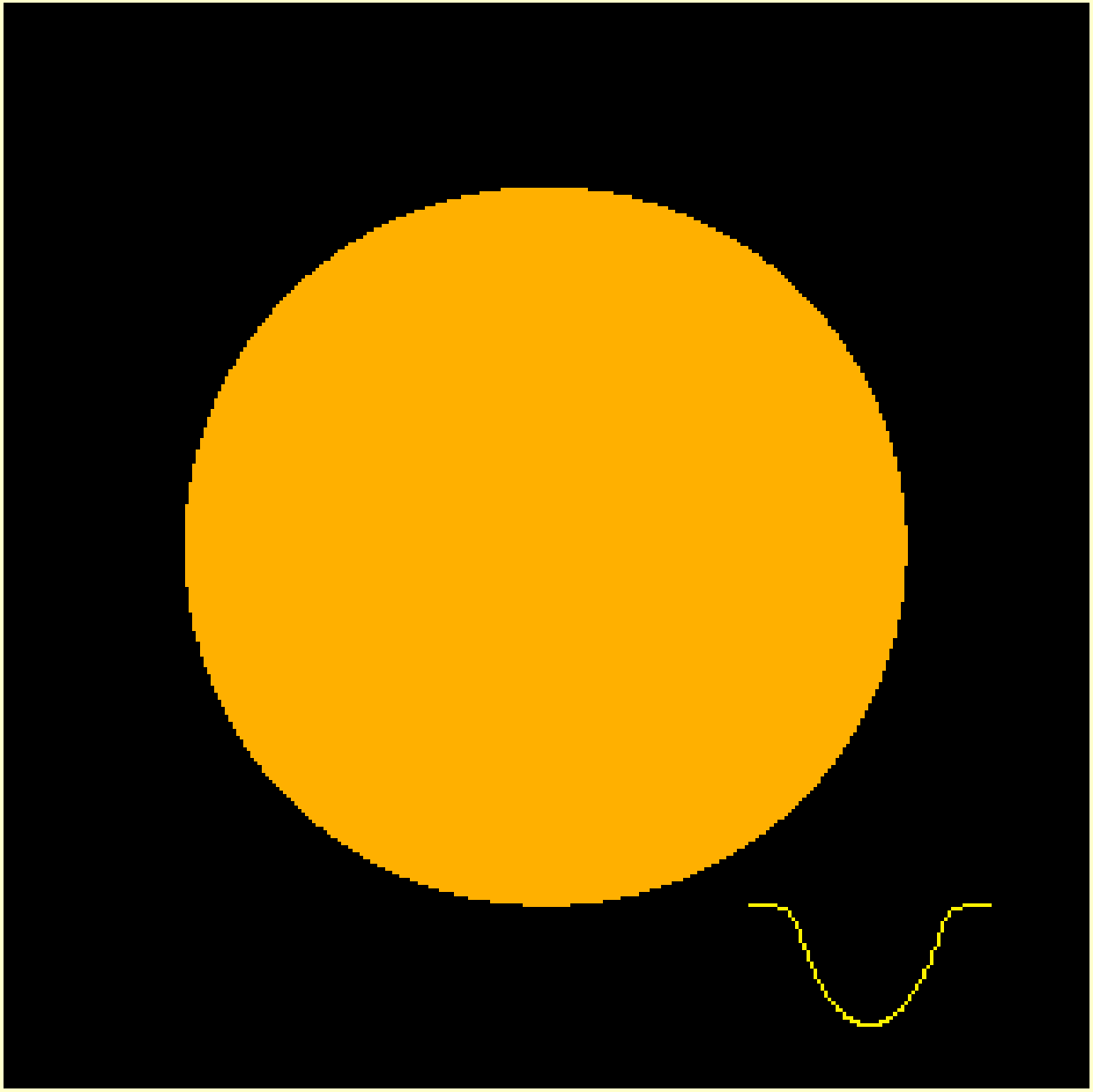

Pole prędkości i zmiany profilu linii widmowej wskutek efektu Doplera.

Radialne pulsacje (*l*=0)

Efekt Doplera – zmiana obserwowanej długości fali w stosunku do długości fali wysłanej, spowodowana względnym ruchem źródła i obserwatora.

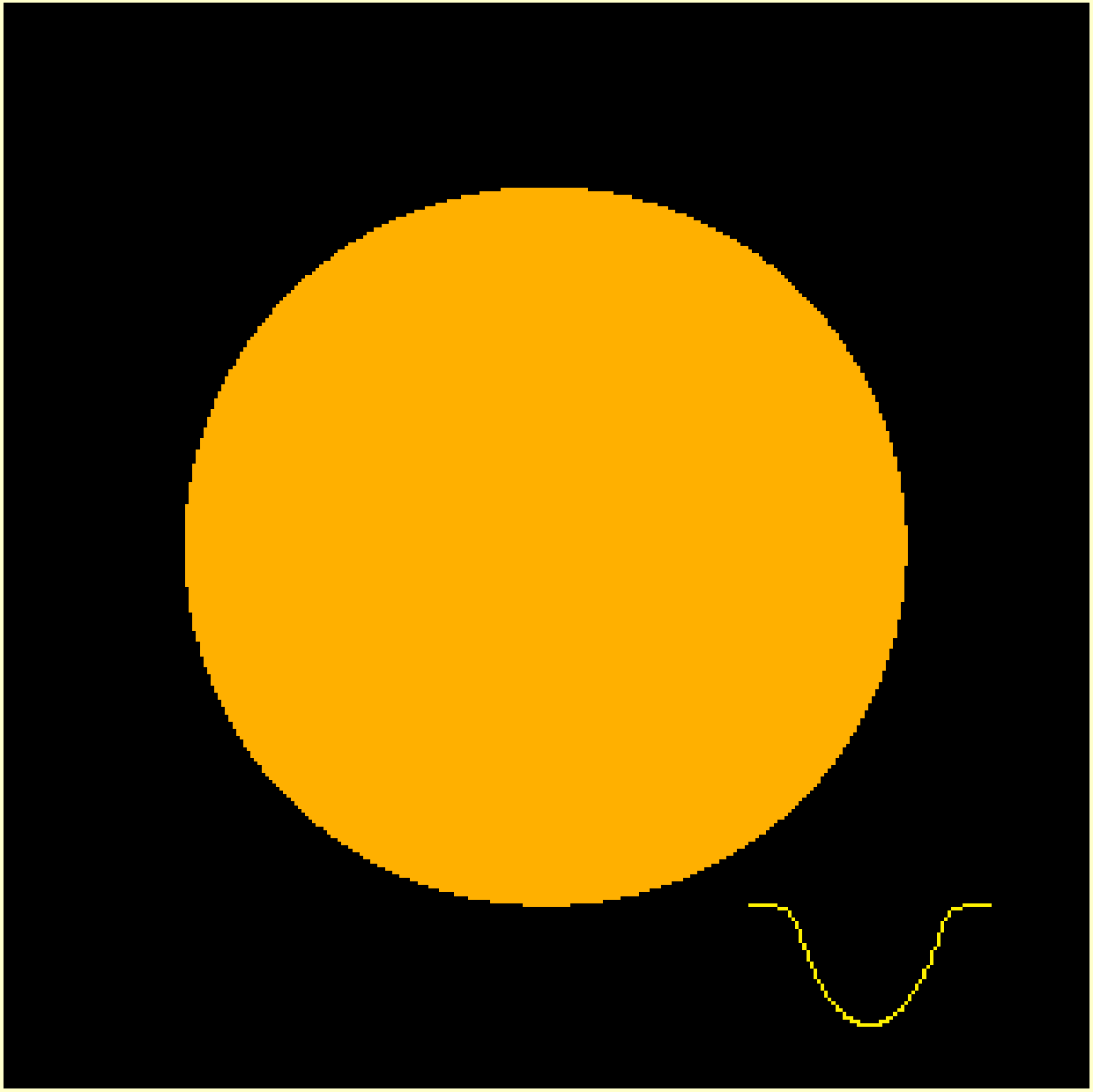

Pole prędkości i zmiany profilu linii widmowej

Dipolowe pulsacje
***l*=1, m=0**

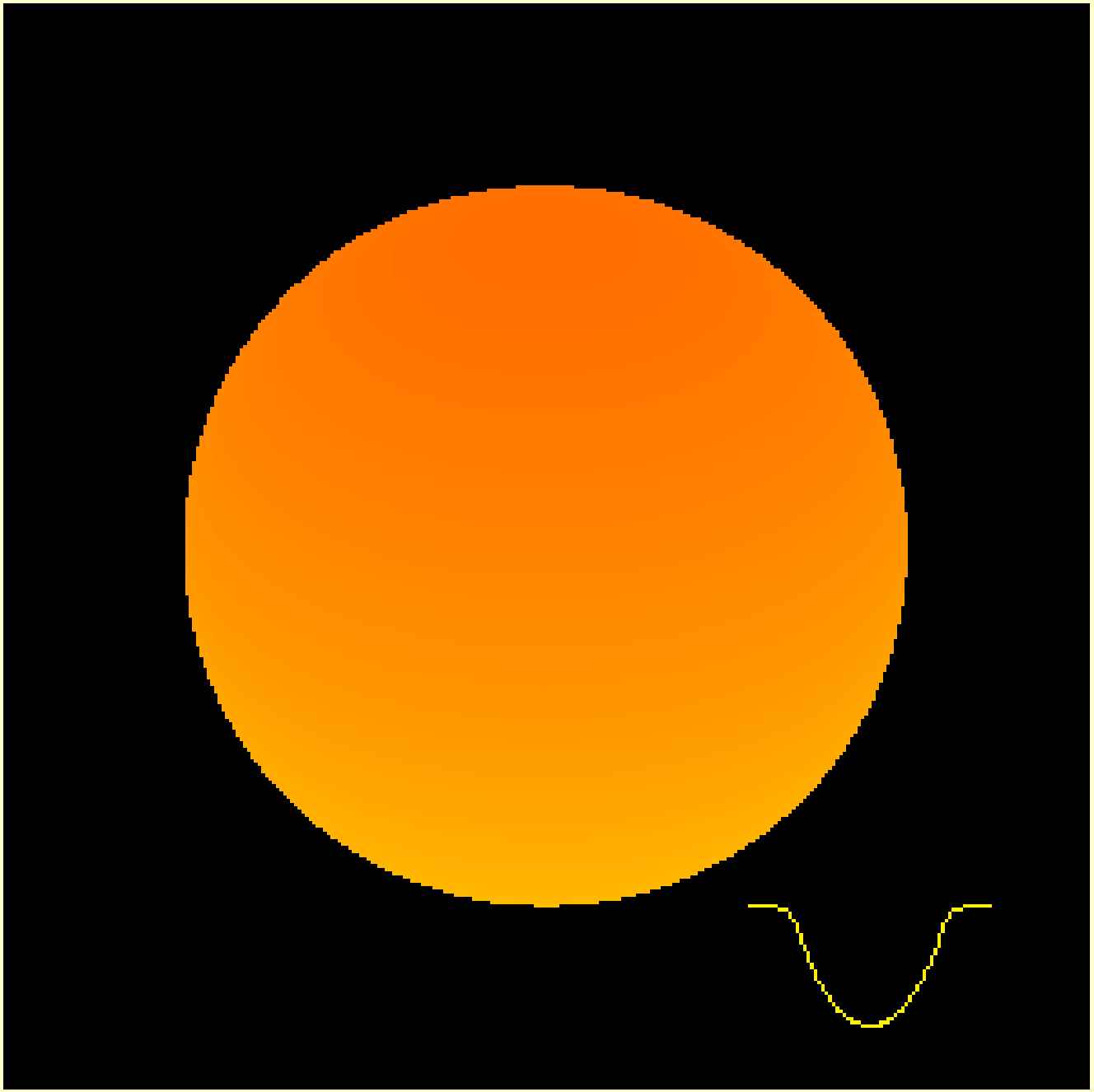

Pole prędkości i zmiany profilu linii widmowej

Oktupolowe pulsacje
***l*=3, m=0**

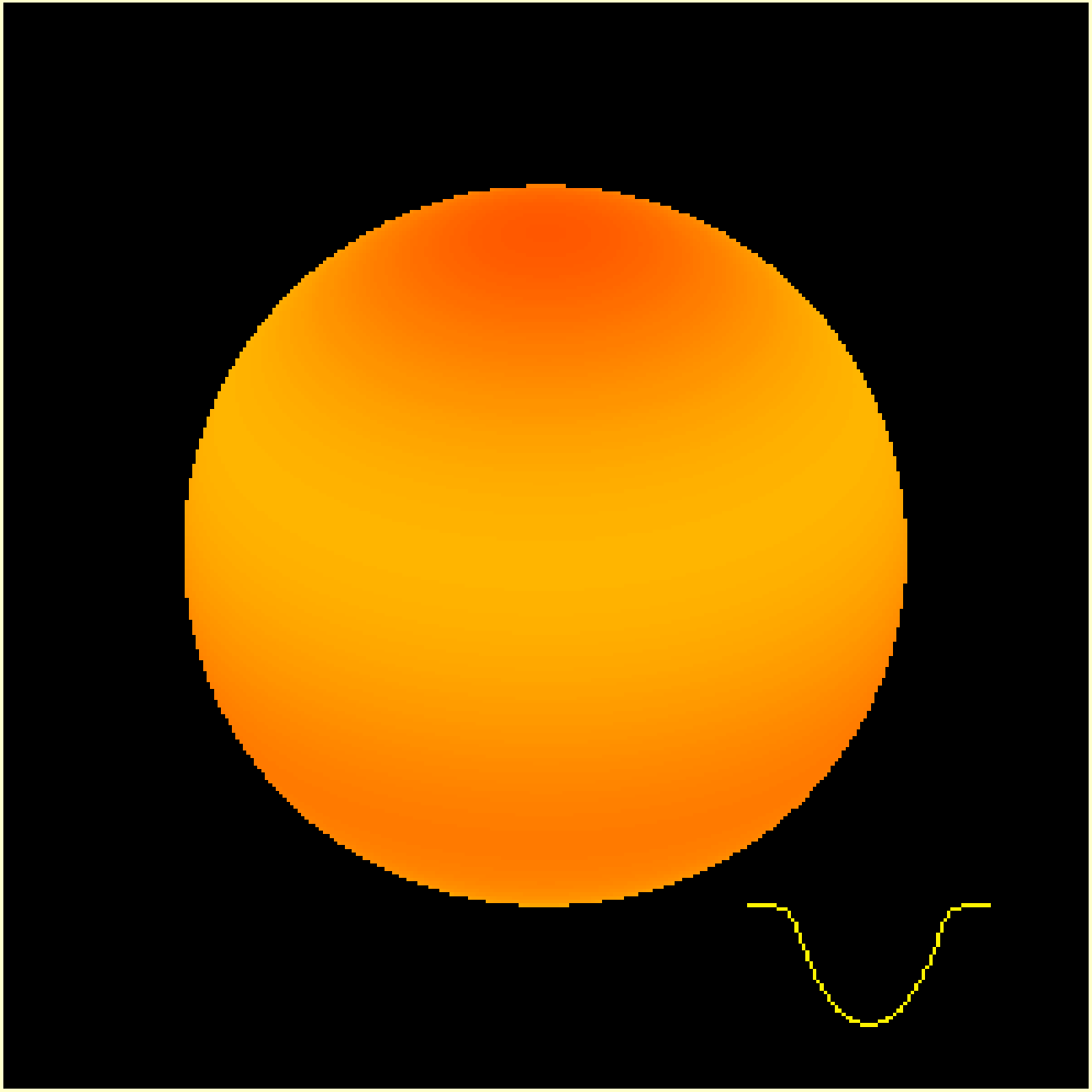

Pole prędkości i zmiany profilu linii widmowej

Oktupolowe pulsacje
***l*=3, m=3**

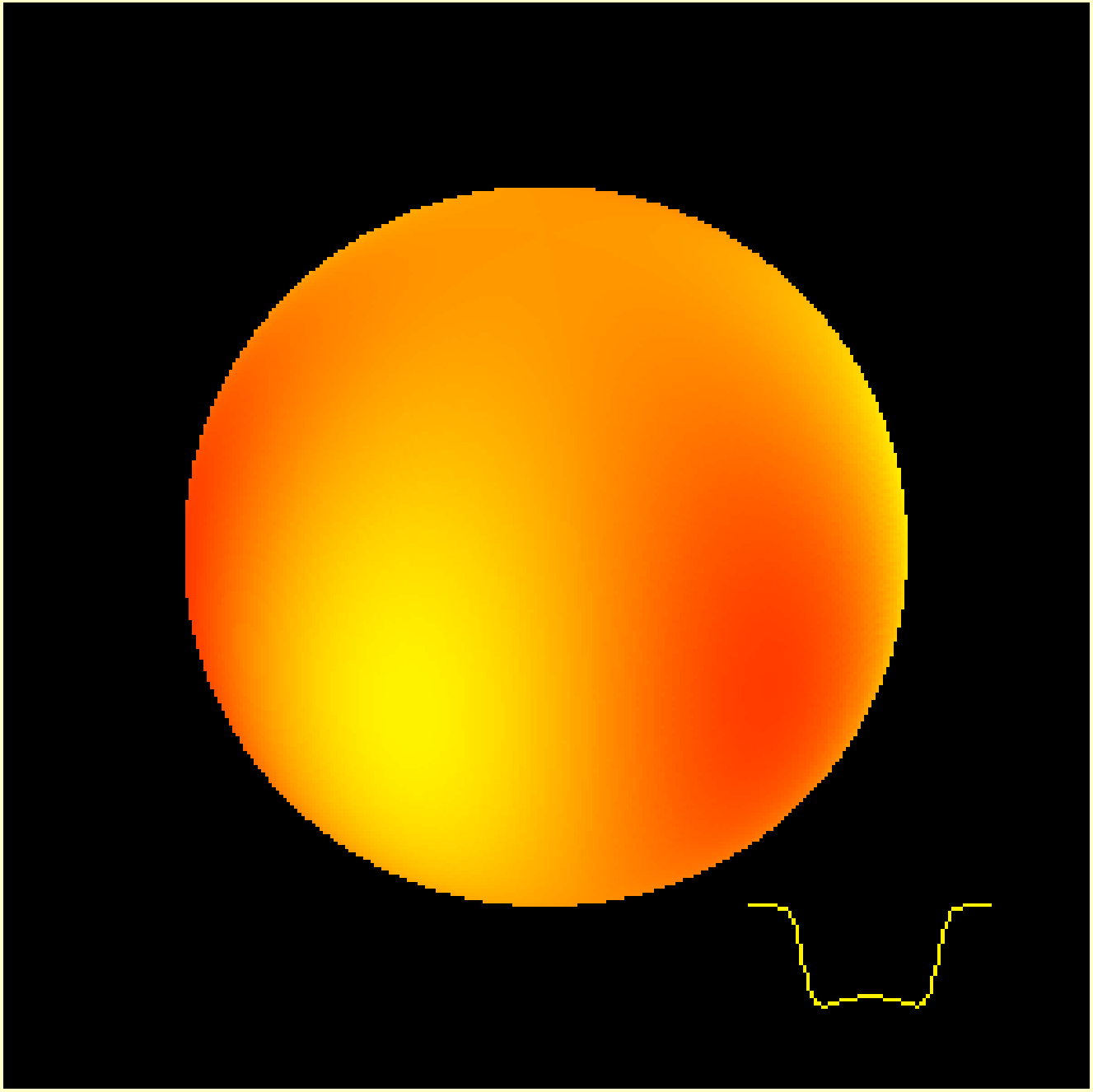

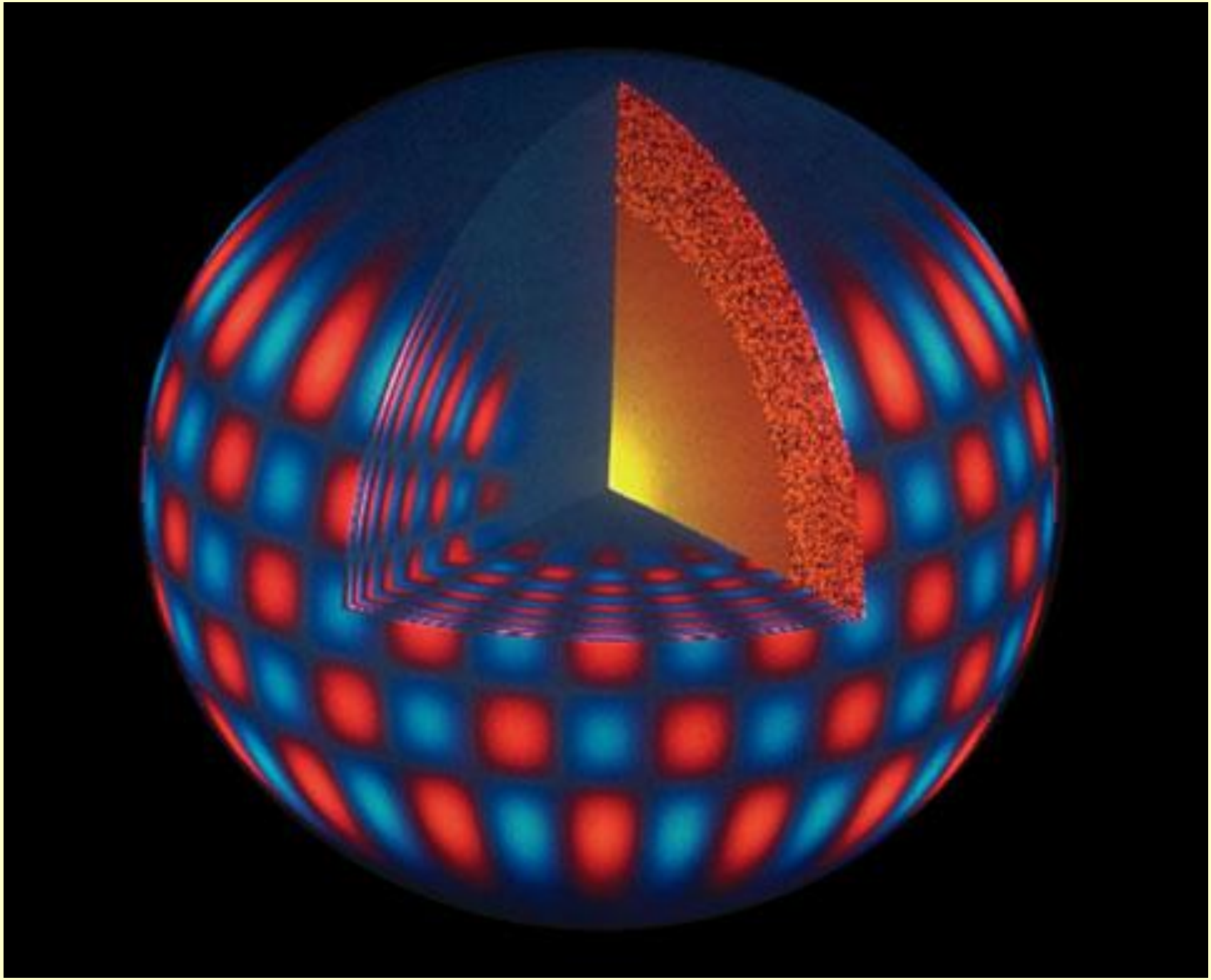

Pole prędkości radialnych na powierzchni Słońca

(łącznie z rotacja Słońca)

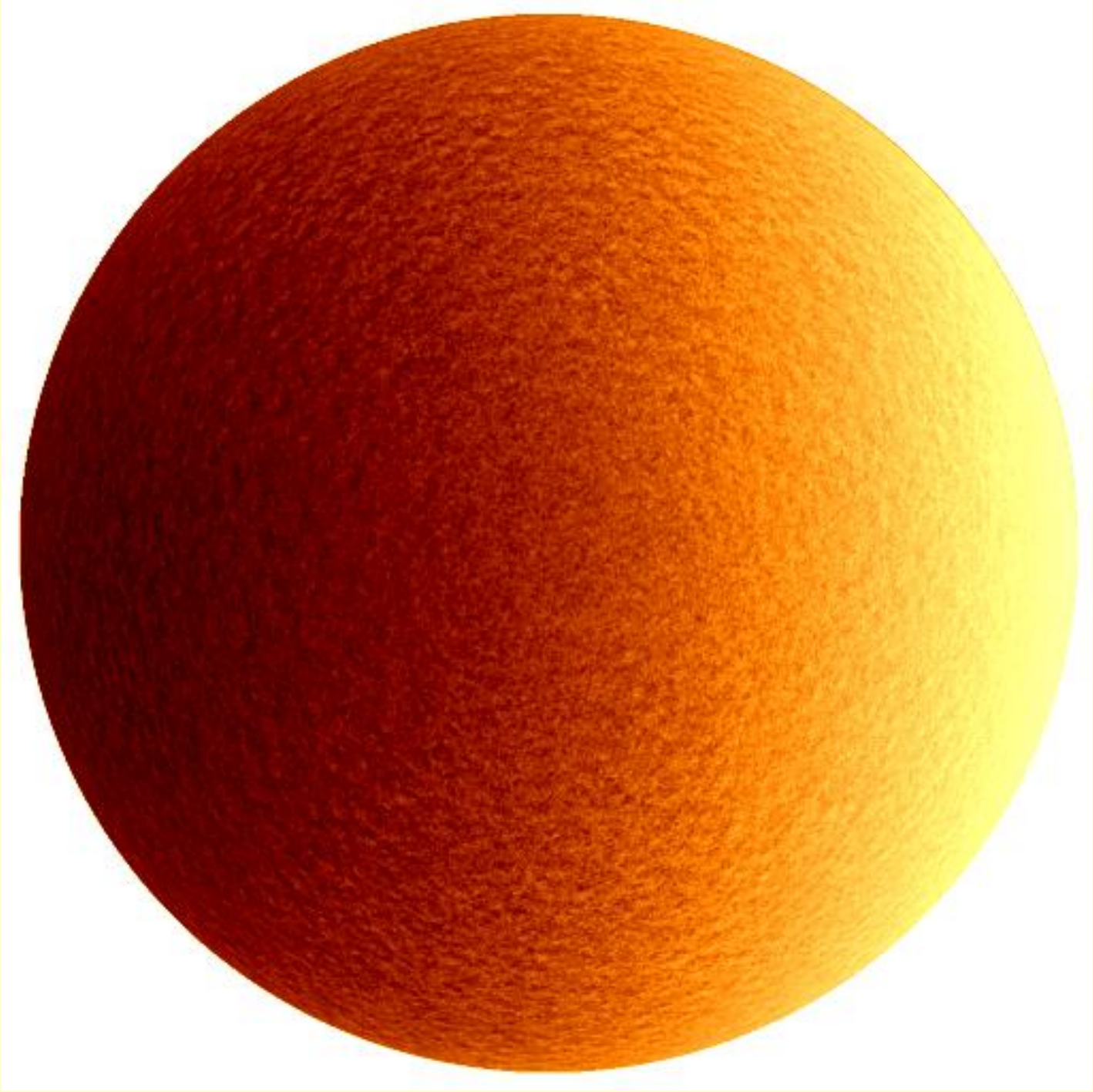

Pole prędkości radialnych na powierzchni Słońca po usunięciu efektu rotacji

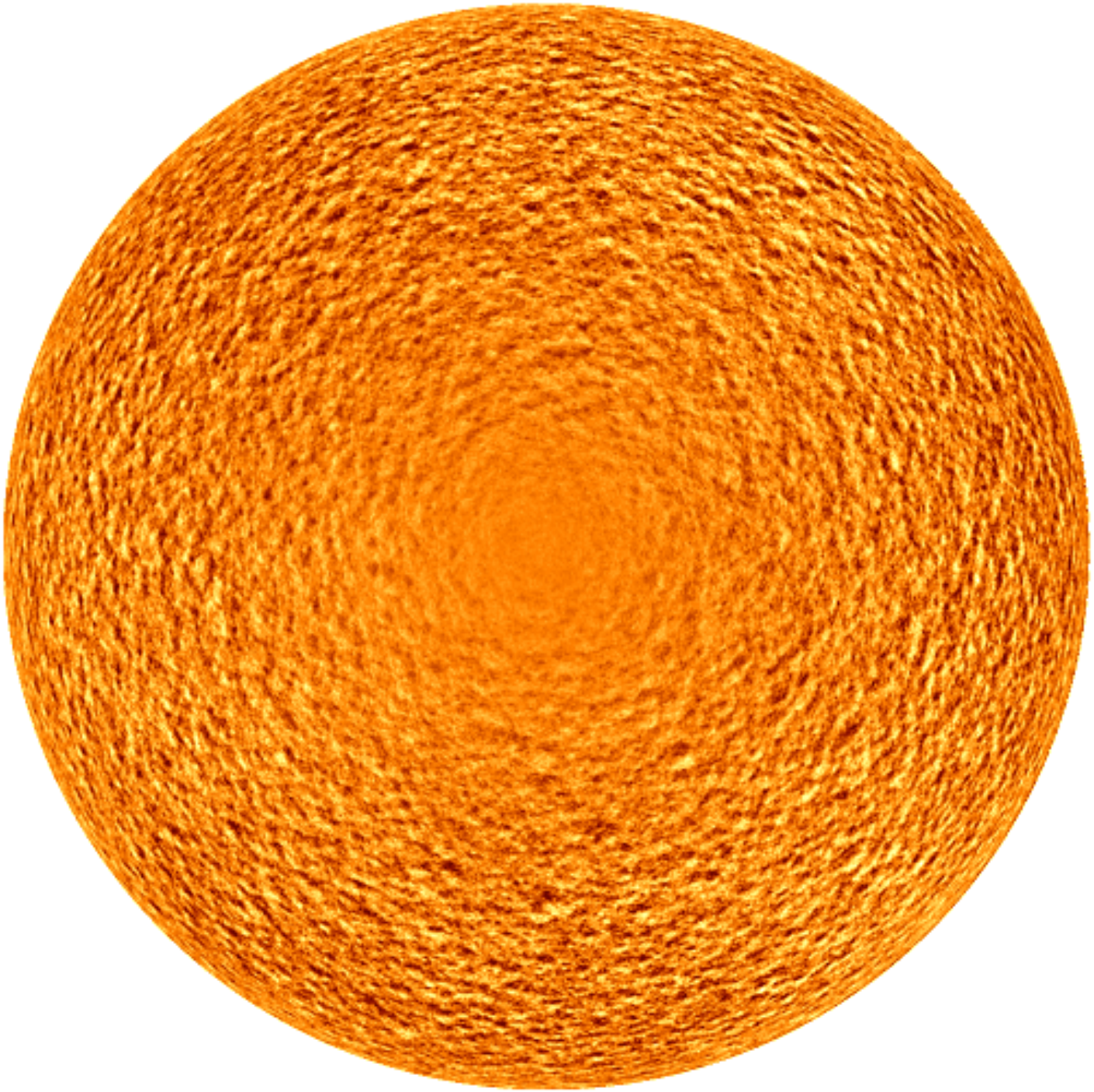

Widmo 5-minutowych oscylacji Słońca

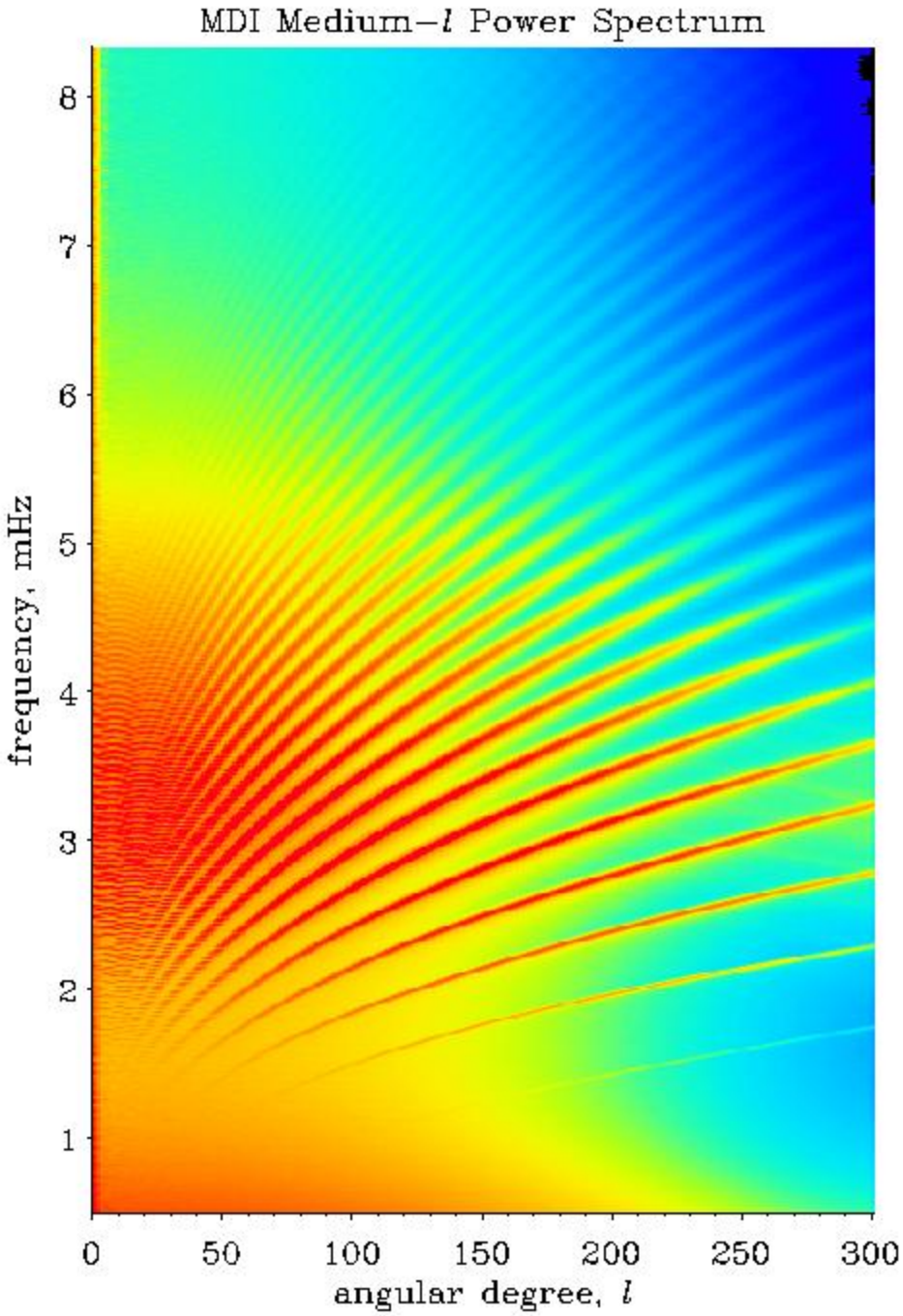

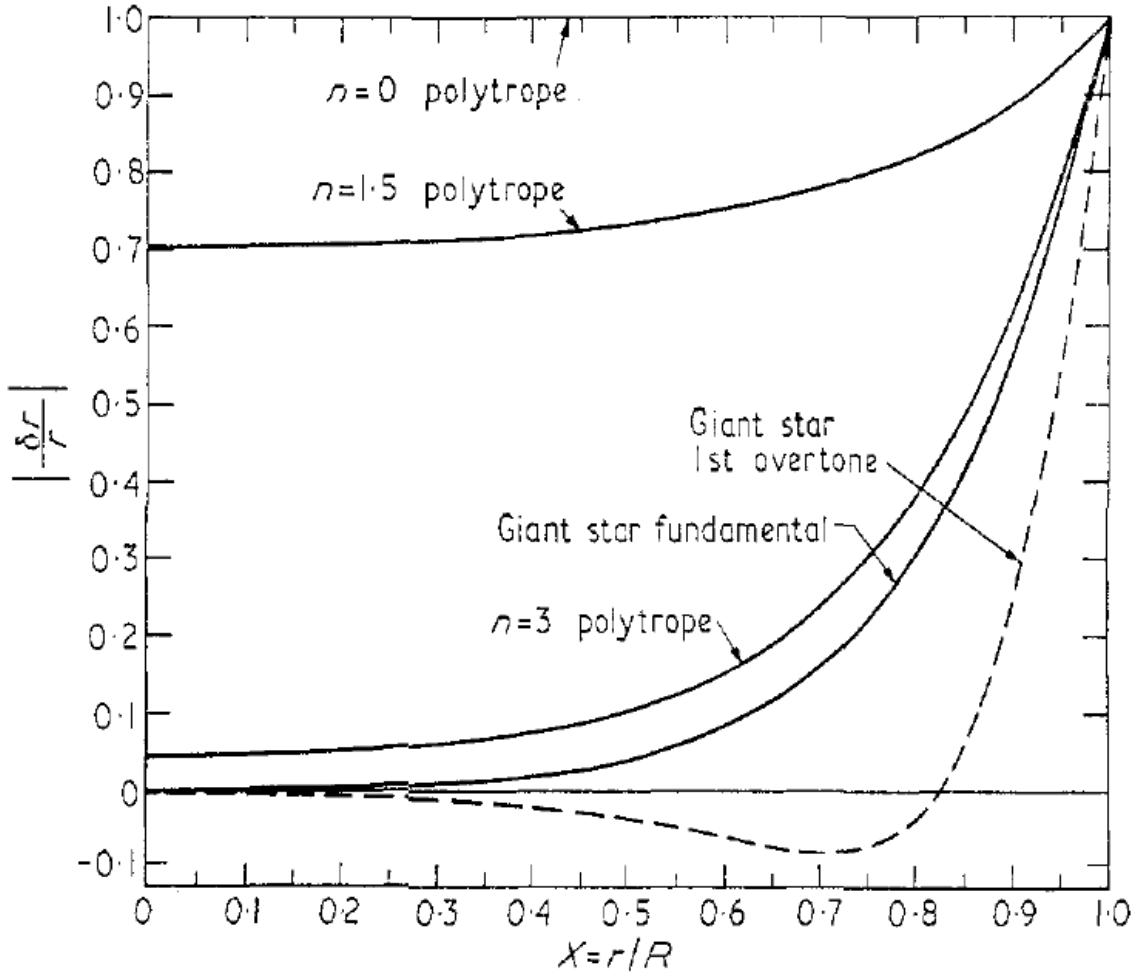

Figure 14. Eigenfunctions for the fundamental (solid lines) and first harmonic (broken line) modes for selected stellar models. Abscissa is fractional distance from the stellar centre; ordinate is relative radius semi-amplitude.

Cox 1974

Frequencies of non radial modes of the homogeneous model

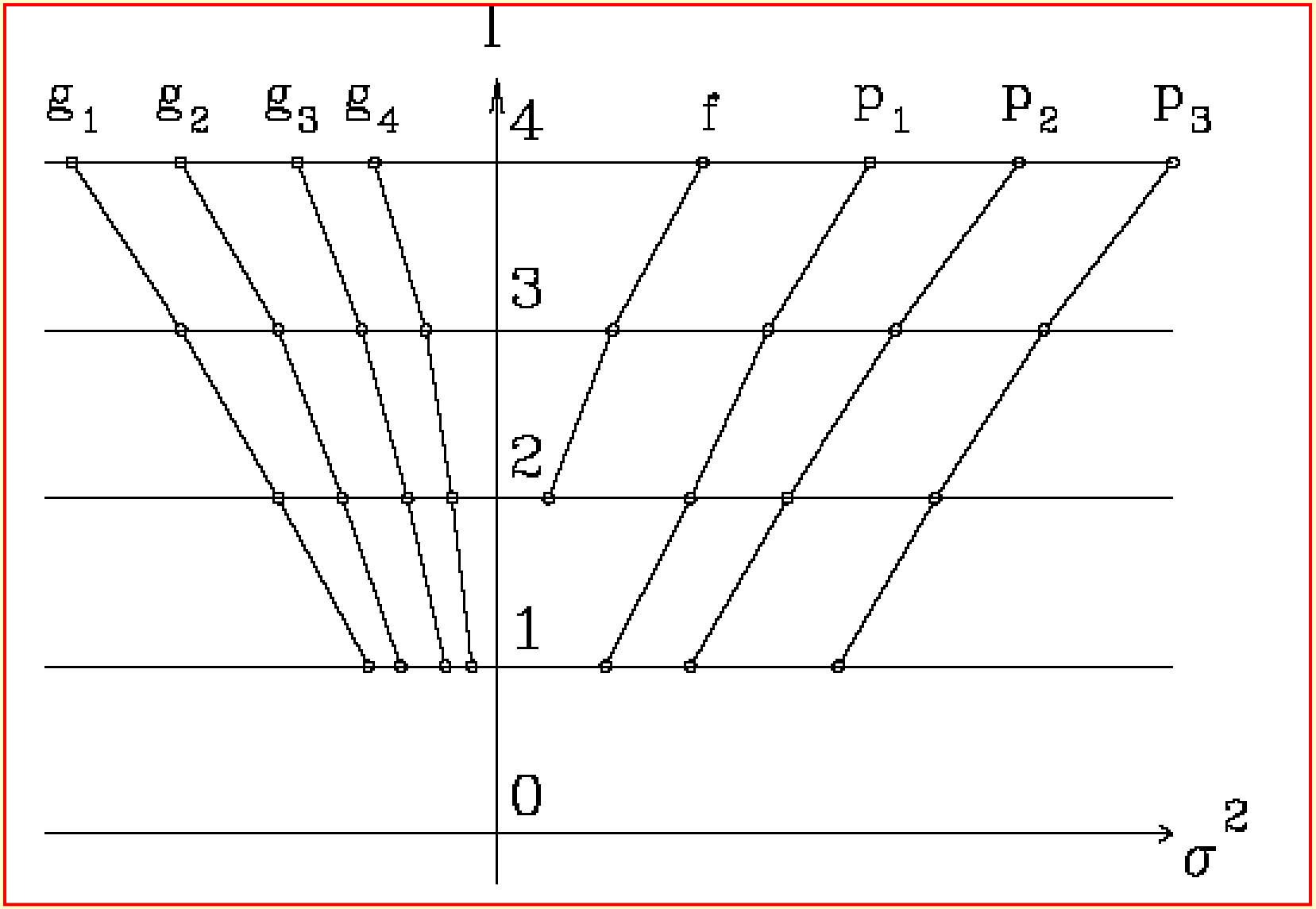

R. Scuflaire

Characteristic frequencies

Acoustic frequency

$$S_l^2 = \frac{l(l+1)c^2}{r^2}$$

Buoyancy frequency:

$$N^2 = g\left(\frac{1}{\Gamma_1}\frac{\mathrm{d}\ln p}{\mathrm{d}r} - \frac{\mathrm{d}\ln\rho}{\mathrm{d}r}\right) \simeq \frac{g^2\rho}{p}(\nabla_{\mathrm{ad}} - \nabla + \nabla_\mu)$$

$$\nabla = \frac{\mathrm{d}\ln T}{\mathrm{d}\ln p}, \qquad \nabla_{\mathrm{ad}} = \left(\frac{\partial \ln T}{\partial \ln p}\right)_{\mathrm{ad}}, \qquad \nabla_\mu = \frac{\mathrm{d}\ln\mu}{\mathrm{d}\ln p}.$$

Lokalne własności oscylacji są opisane przez dwie charakterystyczne częstotliwości:

1. ***częstotliwość Lamba, L_ℓ^2***
2. ***częstotliwość Brunta-Väisälä, N^2***

$$L_\ell^2=(k_h c)^2= \ell(\ell+1)\, c^2/r^2$$

$$k_h = 2\pi/\lambda_h\,, \quad c^2=\Gamma_1 p/\rho\,, \quad \Gamma_1=(d\ln p/d\ln\rho)_{ad}$$

k_h - falowa liczba horyzontalna, Γ_1 - wykładnik adiabaty
λ_h – horyzontalna długość fali

$$k_h= [\ell(\ell+1)]^{1/2}/r \approx \ell/r$$

Fala akustyczna pokonuje drogę $\lambda_h = 2\pi r/\ell$ ruchem horyzontalnym z okresem $2\pi/L$, gdzie $L= [\ell(\ell+1)]^{1/2}$.

Z wykładu J. Daszyńskiej-Daszkiewicz

Częstotliwość Brunta-Väisälä, N^2

$$N^2 = g\left(\frac{1}{\Gamma_1}\frac{d\ln p}{dr} - \frac{d\ln \rho}{dr}\right)$$

N^2 – częstotliwość z jaką element gazu może oscylować wokół położenia równowagi po wpływem siły grawitacji

Z wykładu J. Daszyńskiej-Daszkiewicz

$\omega^2 > L_\ell^2, N^2$

mody o wysokich częstotliwościach (ciśnieniowe)

$\omega^2 < L_\ell^2, N^2$

mody o niskich częstotliwościach (grawitacyjne)

$L_\ell^2 > \omega^2 > N^2$ ***lub*** $L_\ell^2 < \omega^2 < N^2$

obszary znoszenia oscylacji

Z wykładu J. Daszyńskiej-Daszkiewicz

Diagram propagacji dla politropy N=3

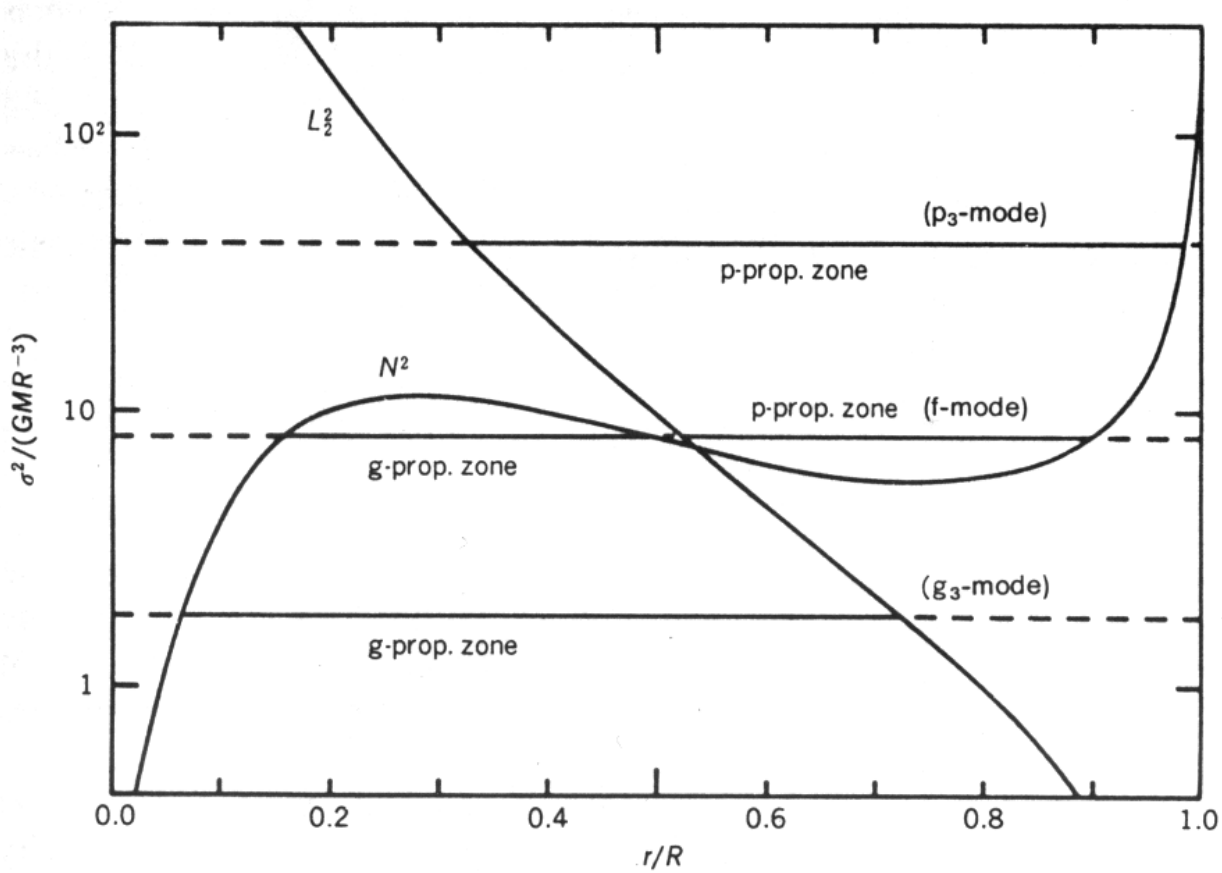

Fig. 4.2 Variations of N^2 and L_2^2 (normalized by GM/R^3) with respect to r/R for a polytrope (with the polytropic index 3) model. Three horizontal lines show the wave propagation zones (thin full lines) for the p_3-mode, the f-mode, and g_3-mode of spherical harmonic degree $l = 2$.

Unno at al.

Diagramy propagacji akustycznych i grawitacyjnysh oscylacji

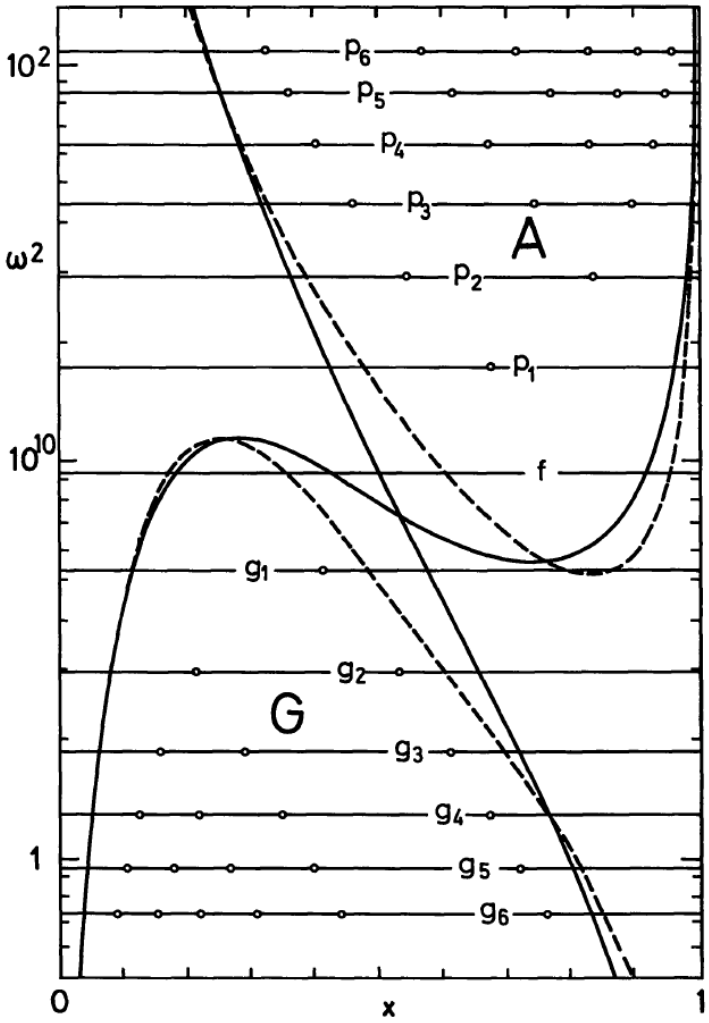

Fig. 4. Polytrope of index 3. The solid lines delimit A and G regions. The horizontal lines give the frequencies of a few modes ($l=2$) and the circles represent the positions of their nodes. The dashed lines represent the cut-off frequencies for plane waves

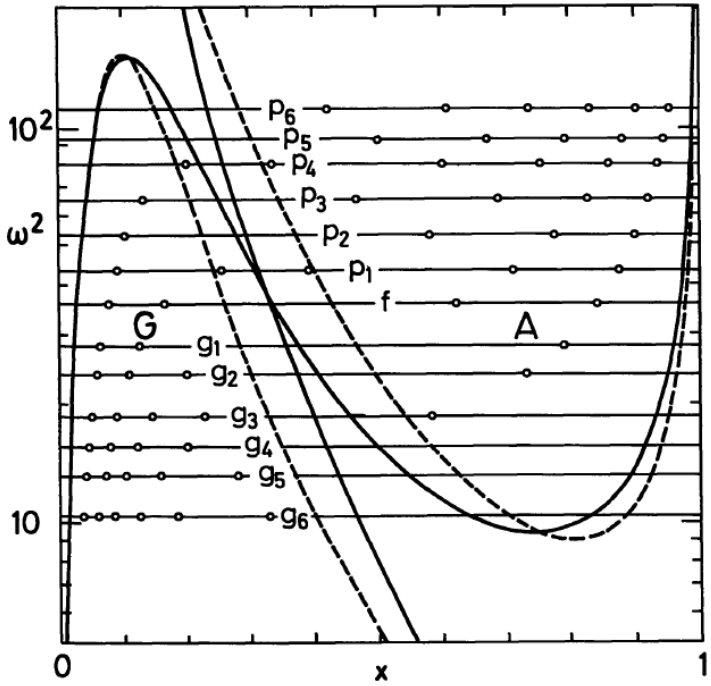

Fig. 5. Same as Fig. 4 but for the polytrope of index 4

the A region and all the nodes of the g modes lie in the G region as it is expected. But for the more condensed polytrope $n=4$ ($\varrho_c/\overline{\varrho}=622.4$, Fig. 5) the f mode and the first p and g modes have nodes in both regions. We can no longer say that these p modes are purely acoustic modes. They have rather a mixed character: gravity waves in the internal regions and acoustic waves in the external layers. The same is true for the first g modes. This transition from a gravity wave to

Scuflaire 1974

Mody grawitacyjne

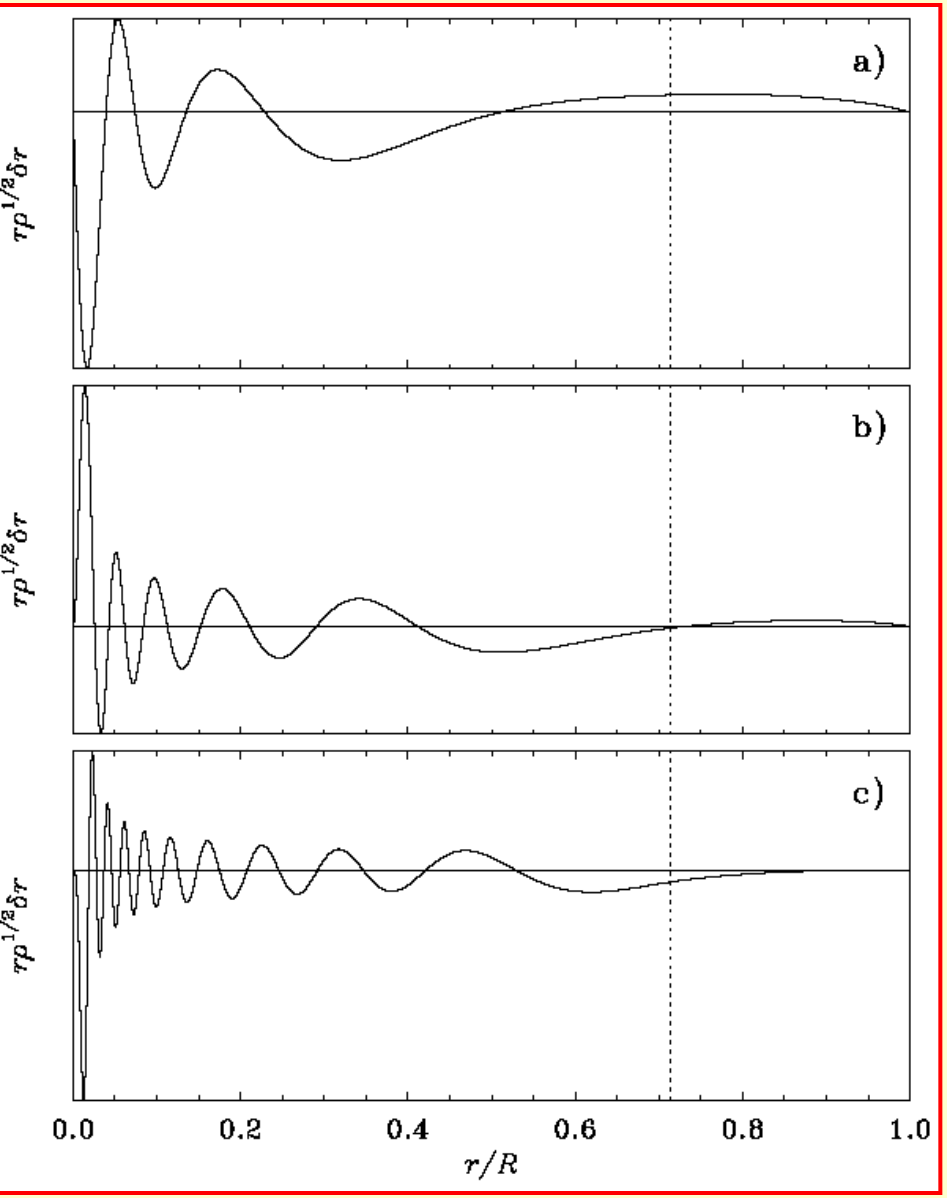

(l,n)=(1,5), (2,10), (4,19), ν=100μHz

Mody akustyczne (ciśnieniowe)

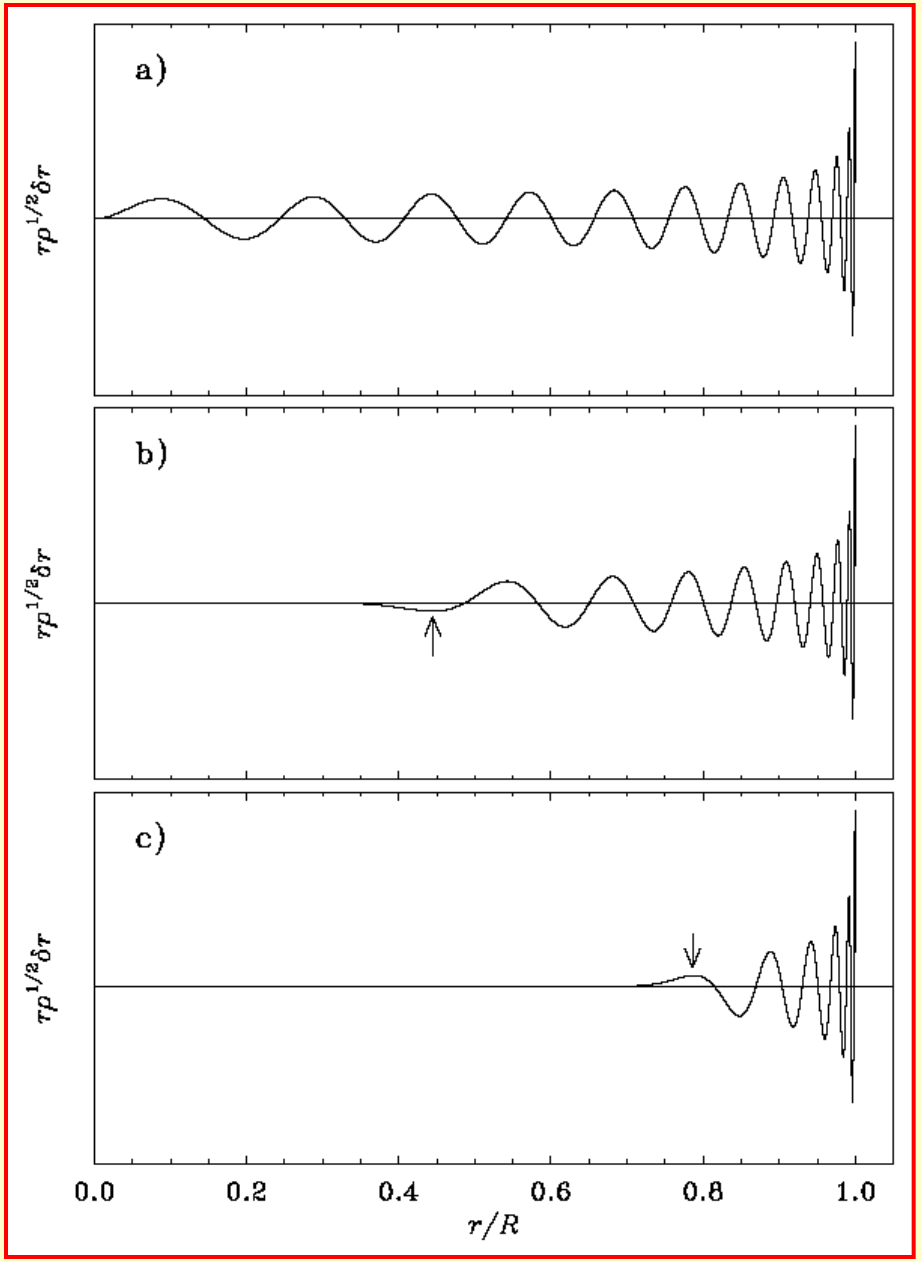

(l,n)=(0,23), (20,17), (60,10), ν=3300μHz

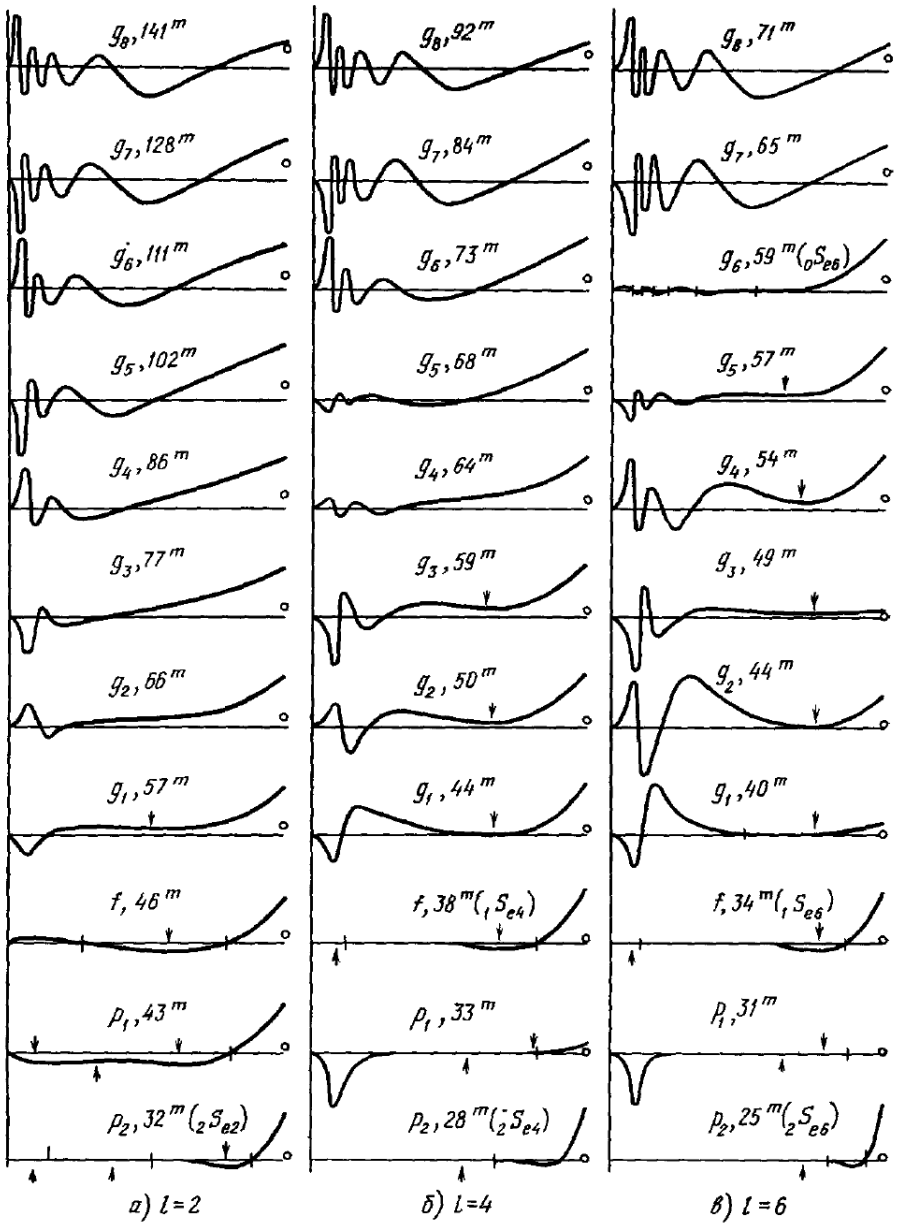

Рис. 5. Собственные функции различных нерадиальных ($l = 2, 4, 6$) колебаний стандартной модели Солнца [32].

Обозначения те же, что на рис. 3. Для некоторых мод в скобках приведена их классификация по дополнительной схеме. *а*) $l = 2$, *б*) $l = 4$; *в*) $l = 6$.

Vorontsov & Zharkov 1981

Oscillation frequencies of typical Beta Cephei and Delta Scuti models on the main sequence

(from the ZAMS to the TAMS)

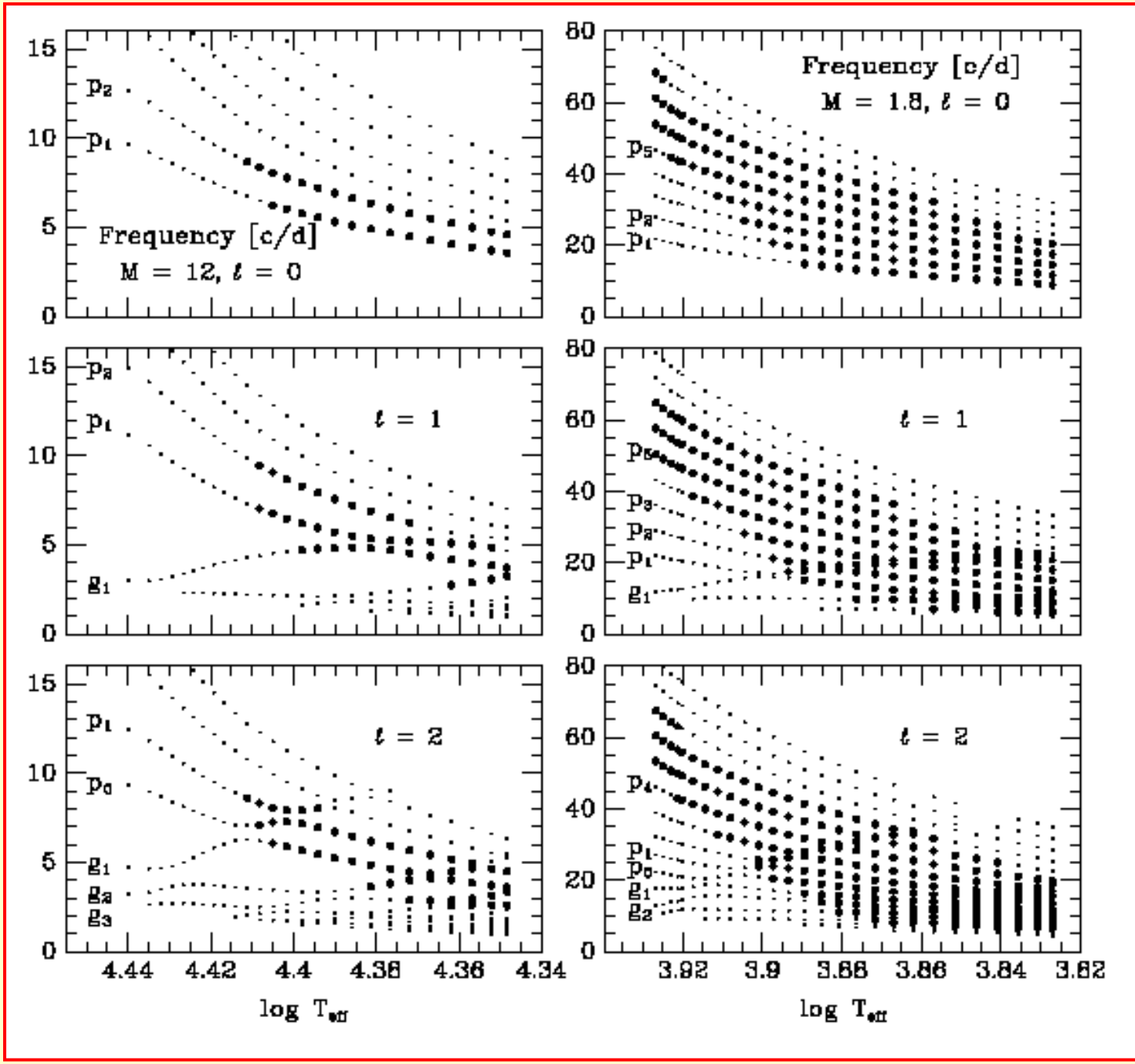

Lines of constant period in the HRD

Rough estimate of the position of the constant period lines in HR diagram:

$\Pi\sqrt{\rho} \sim const \Rightarrow \Pi \sim M^{-1/2} R^{3/2}$

$\Rightarrow M \sim R^3$ for const Π

$M \sim L^{1/3}$ (mass-luminosity relation for ~MS stars)

$\Rightarrow L \sim R^9$ for const Π

$L \sim R^2 T_e^4 \Rightarrow R \sim L^{1/2} T_e^{-2}$

$\Rightarrow L \sim L^{9/2} T_e^{-18}$ for const Π

$\Rightarrow L \sim T_e^5$

$\lg L \sim 5 \cdot \lg T_e$

Main sequence: $\frac{\Delta \lg L}{\Delta \lg T_e} \sim \frac{6.5}{0.9} \sim 7$

or $\lg L \sim 7 \cdot \lg T_e$

$\Rightarrow$ The constant period lines are, roughly, parallel to the main sequence. (they have slightly lower slope)

Regularities in theoretical frequency spectra:

- high-order p-modes:

$$\nu_{nl} \approx \Delta\nu \cdot \left(n + \frac{l}{2} + \alpha\right) - \frac{l(l+1)}{4\pi^2 n} \cdot f_c$$

$$\Delta\nu = \left(2\int \frac{dr}{c}\right)^{-1}, \quad f_c = \int \frac{dc}{dr} \cdot \frac{dr}{r}$$

large separation:

$$\nu_{nl} - \nu_{n-1,l} \approx \Delta\nu$$

small separation:

$$\nu_{nl} - \nu_{n-1,l+2} = \delta\nu_{nl} \approx -\frac{4l+6}{4\pi^2 n} \cdot f_c$$

- high-order g-modes:

$$\Pi_{nl} \approx \frac{n}{\sqrt{l(l+1)}} \cdot \Delta\Pi, \quad \Delta\Pi = 2\pi^2 \left(\int \frac{N}{r}\, dr\right)^{-1}$$

$$N = g\left(\frac{1}{\Gamma_1}\frac{d\ln P}{dr} - \frac{d\ln \rho}{dr}\right)$$

- Rotational splitting: (~ Goupil et al. 2000)

$$\nu_m = \nu_0 + m\left(1 - C_{nl}\right)\frac{\Omega}{2\pi} + \frac{\Omega^2}{2\pi\nu_0}\left(D_0 + m^2 D_1\right) + m\frac{\Omega^3}{\nu_0^2}T$$

$$\Rightarrow \frac{\nu_m - \nu_{m=0}}{m} = \frac{\Omega}{2\pi}\left(1 - C_{nl} + m\mu D_1 + \mu^2 T\right)$$

$$\mu = \frac{\Omega}{\nu_0}$$

- rotation rate:

$$\frac{\nu_m - \nu_{-m}}{2m} = \Omega\left(1 - C_{nl} + \mu^2 T\right)$$

- Effective gravity:

$$g_{eff} = g - \frac{2}{3}\Omega^2 r$$

- Ledoux constant:

$$C_{nl} = \frac{\int (2yz + z^2)\rho r^4 dr}{\int (y^2 + \Lambda z^2)\rho r^4 dr} \qquad \Lambda = l(l+1)$$

y, z – radial and horizontal components of displacement

$C_{nl} \ll 1$ for high-order p-modes $(y \gg z)$

$C_{nl} \simeq \frac{1}{l(l+1)}$ for g-modes $(z \gg y)$

$C \sim \frac{1}{2}$ for gravity modes of $l = 1$

Wzbudzanie pulsacji w klasycznym pasie niestabilności i na Ciągu Głównym: mechanizm „kappa” i Z-maksimum

Kilka referencji:

- **Cox J. P.,**
  „The linear theory: initiation of pulsational instability in stars”,
  1967, Proc. IAU Symp. 28, p. 3

- **Gautschy A., Saio H.,**
  „Stellar pulsations across the HR diagram”,
  Part1: 1995, Ann. Rev. Astron. Astrophys., vol. 33, p. 75.
  Part2: 1996, Ann. Rev. Astron. Astrophys., vol. 34, p. 551.

- **Pamyatnykh A. A.,**
  „Pulsational instability domains in the upper main sequence”,
  1999, Acta Astronomica, 49, 119.

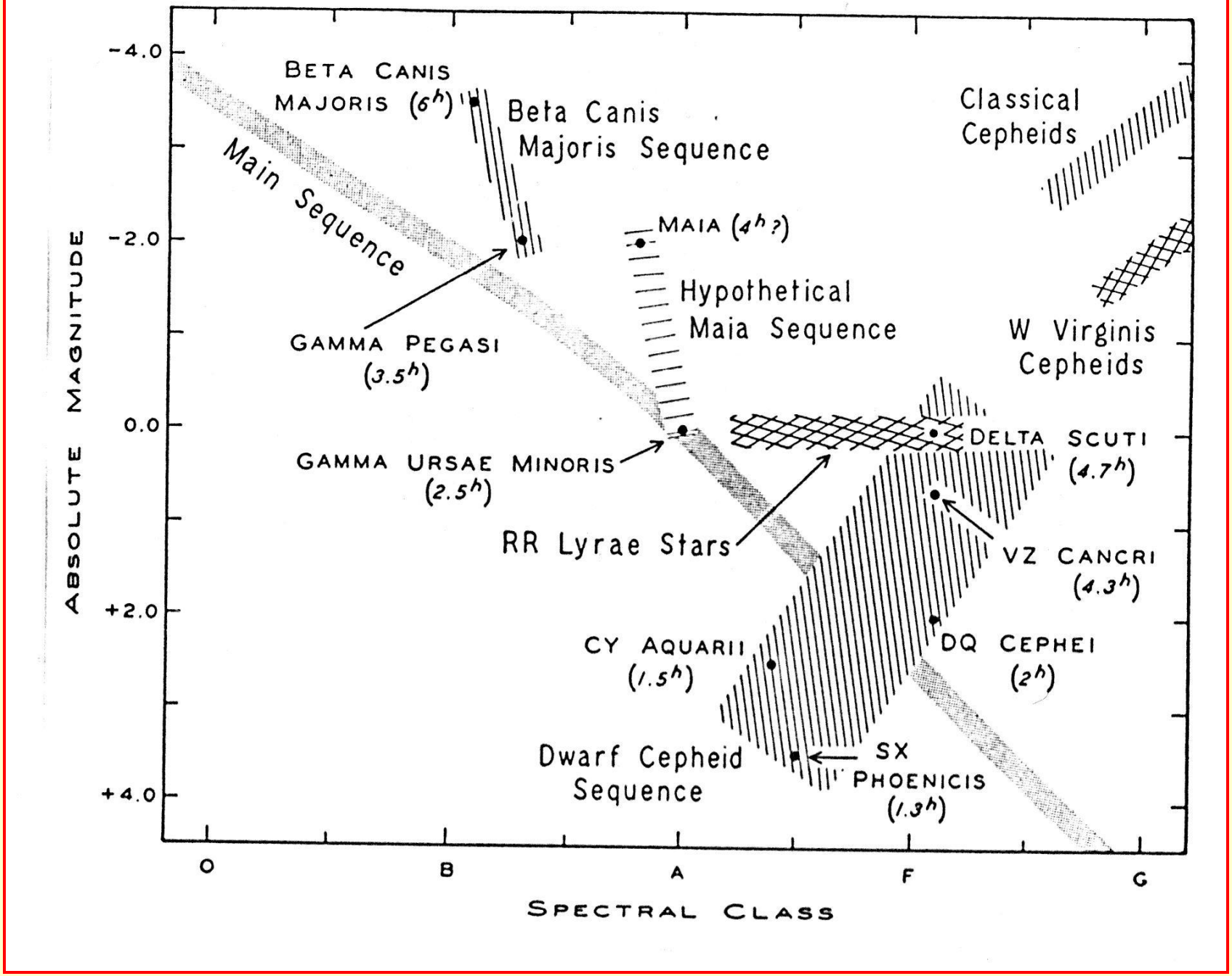

O. Struve, *Some unusual short-period variables.* Sky and Telescope, 1955, 14, 461.

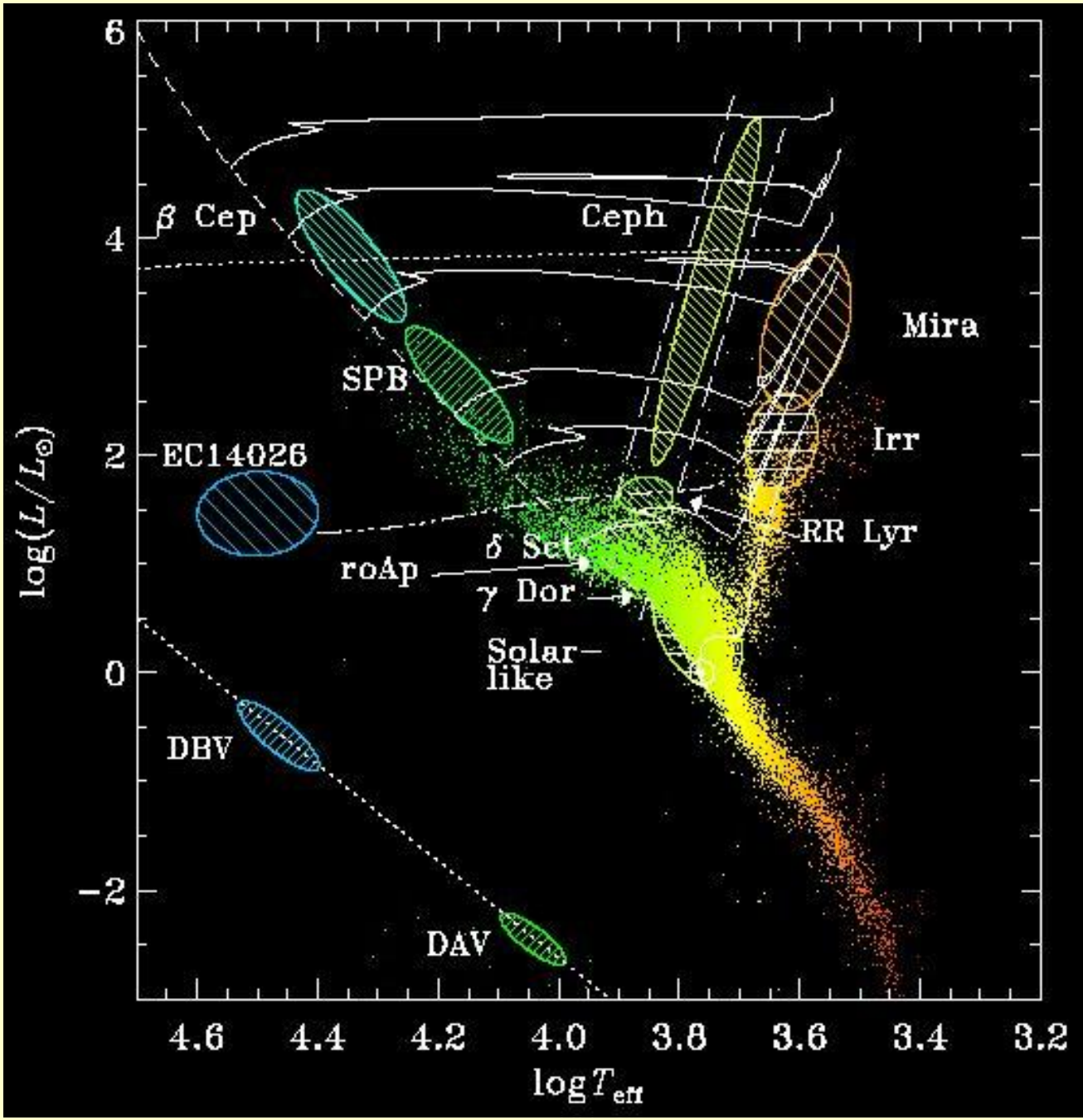

J. Christensen-Dalsgaard

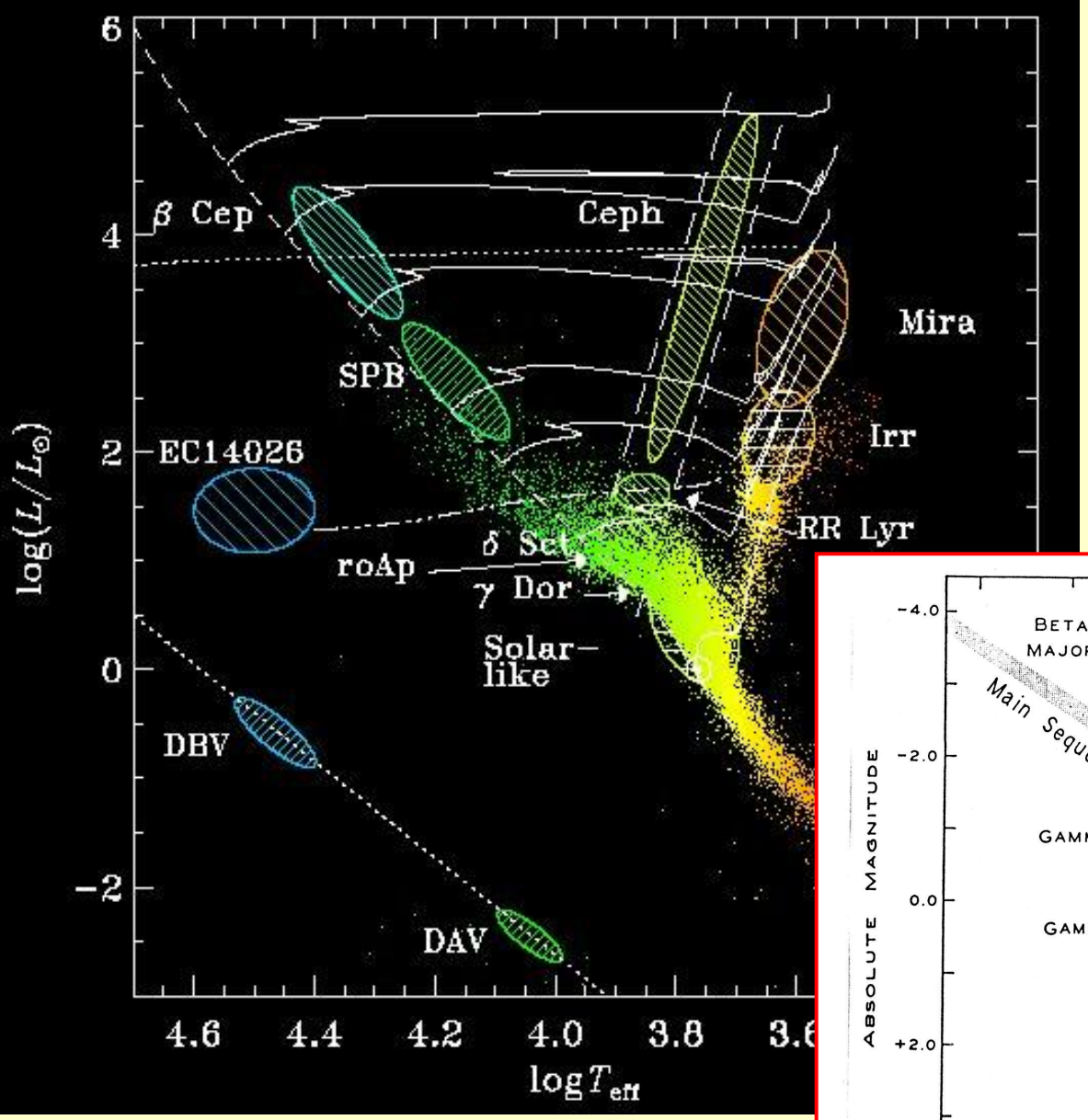

J. Christensen-Dalsgaard

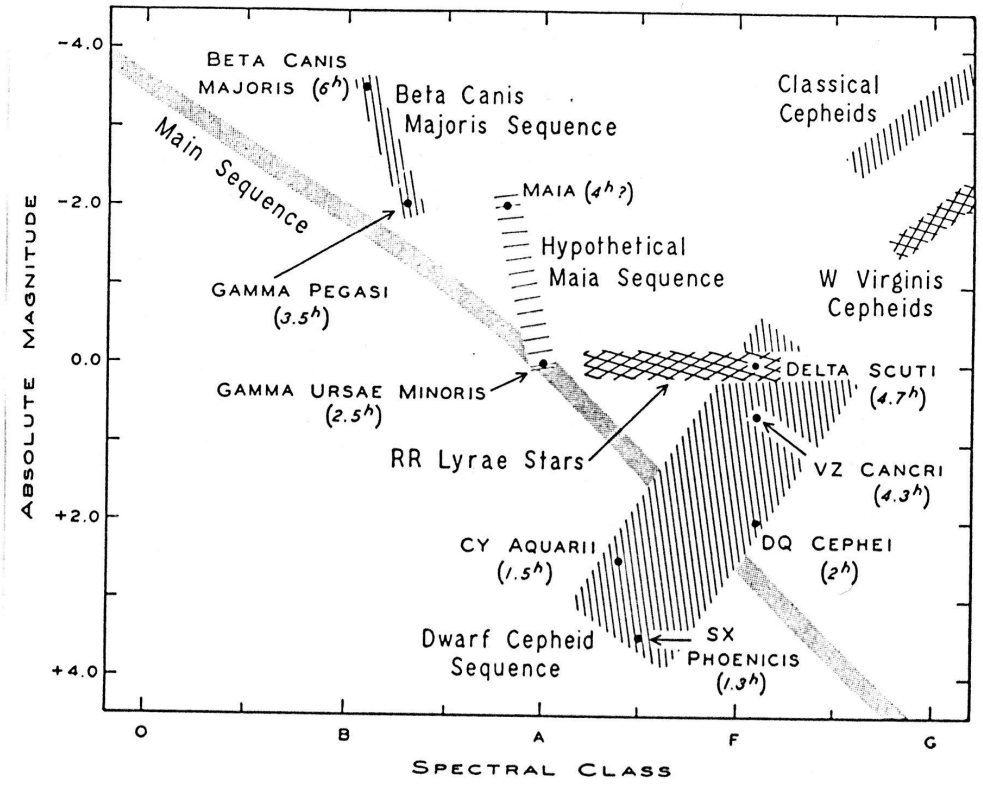

O. Struve

Całka pracy (Work integral)

Explicitly, we have

$$W = \int_M \mathrm{d}m \oint P\,\mathrm{d}V = \int_M \mathrm{d}m \int_0^{\Pi} P \frac{\partial}{\partial t}\left(\frac{1}{\rho}\right) \mathrm{d}\cancel{m}\,\mathrm{dt} \qquad (5.63)$$

and growth or decay correspond, respectively, to $W > 0$ or $W < 0$.

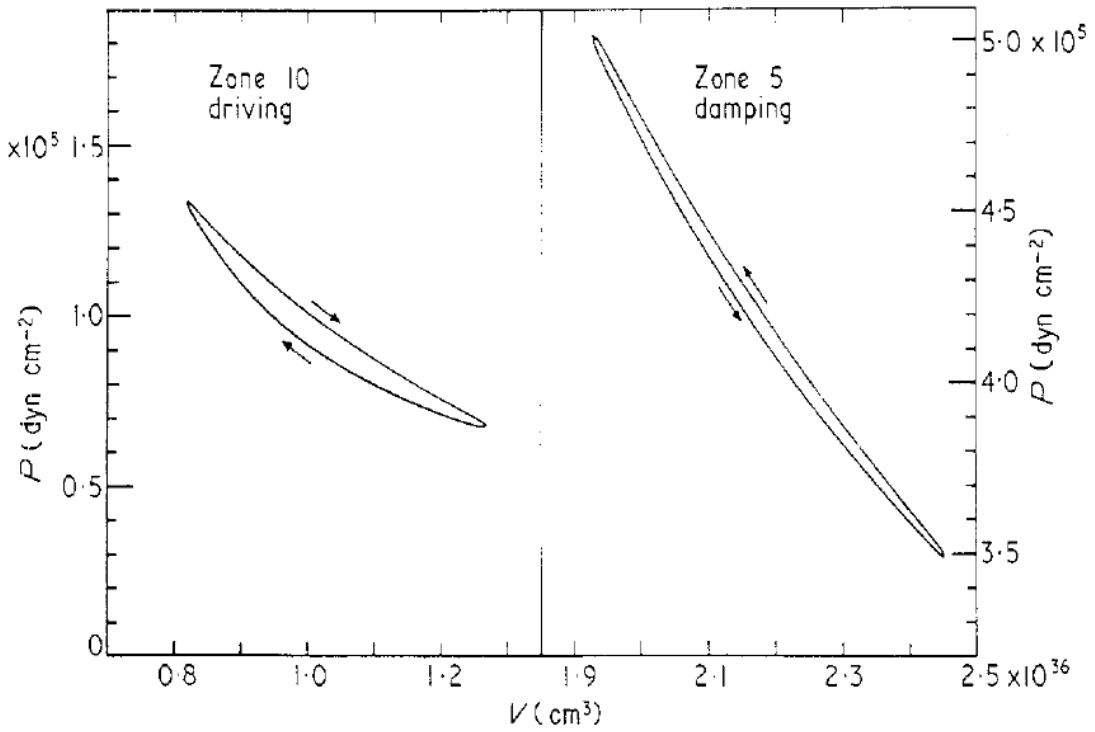

Figure 15. P–V plots for zones 10 and 5 for one of the classical cepheid envelope models investigated by Cox *et al* (1966) at limiting amplitude. The directions of the arrows show that driving is present in zone 10 (coinciding approximately with the region of 50% He^+ ionization, see text), while damping is present in zone 5 (below the He^+ ionization region). In the figure V denotes the total volume of the zone (from King and Cox 1968).

Cox 1974

$$W = -\int \mathrm{d}^3x\, \nabla_{\mathrm{ad}} \oint \mathrm{d}t\, \mathrm{Re}\left[\left(\frac{\delta P}{P}\right)^* \delta\, \mathrm{div}\, \mathbf{F}_{\mathrm{R}}\right]$$

$$\nabla_{\mathrm{ad}} = (\mathrm{d}\ln T/\mathrm{d}\ln P)_{\mathrm{ad}}$$

$$\delta\, \mathrm{div}\, \mathbf{F}_{\mathrm{R}} = \frac{1}{4\pi r^2}\frac{d\,\delta L_r}{dr}$$

$$\frac{\delta L_r}{L_r} = \frac{\mathrm{d}r}{\mathrm{d}\ln T}\frac{\mathrm{d}}{\mathrm{d}r}\left(\frac{\delta T}{T}\right) - \frac{\delta\kappa}{\kappa} + 4\left(\frac{\delta T}{T} + \frac{\delta r}{r}\right)$$

$$\frac{1}{\kappa}\cdot\int \frac{dB_\nu}{dT}d\nu = \int \frac{1}{\kappa_\nu}\frac{dB_\nu}{dT}d\nu$$

$$\kappa_T + \kappa_\rho/(\Gamma_3 - 1)$$

$$\Gamma_3 - 1 = (\mathrm{d}\ln T/\mathrm{d}\ln\rho)_{\mathrm{ad}}$$

$$\kappa_T = (\partial\ln\kappa/\partial\ln T)_\rho$$

$$\kappa_\rho = (\partial\ln\kappa/\partial\ln\rho)_T$$

$$\tau_{\mathrm{th}}(r) = \int_r^R Tc_P\,\mathrm{d}M/L$$

Pamyatnykh 1999 (due Dziembowski 1994)

$$W = -\int \mathrm{d}^3x\, \nabla_{\mathrm{ad}} \oint \mathrm{d}t\, \mathrm{Re}\left[\left(\frac{\delta P}{P}\right)^* \delta\, \mathrm{div}\, \mathbf{F}_{\mathrm{R}}\right]$$

$$\nabla_{\mathrm{ad}} = (\mathrm{d}\ln T/\mathrm{d}\ln P)_{\mathrm{ad}}$$

$$\delta\, \mathrm{div}\, \mathbf{F}_{\mathrm{R}} = \frac{1}{4\pi r^2}\frac{d\,\delta L_r}{dr}$$

$$\frac{\delta L_r}{L_r} = \frac{\mathrm{d}r}{\mathrm{d}\ln T}\frac{\mathrm{d}}{\mathrm{d}r}\left(\frac{\delta T}{T}\right) - \frac{\delta\kappa}{\kappa} + 4\left(\frac{\delta T}{T} + \frac{\delta r}{r}\right)$$

$$\frac{1}{\kappa}\cdot\int \frac{dB_\nu}{dT}d\nu = \int \frac{1}{\kappa_\nu}\frac{dB_\nu}{dT}d\nu$$

$$\kappa_T + \kappa_\rho/(\Gamma_3 - 1)$$

$$\Gamma_3 - 1 = (\mathrm{d}\ln T/\mathrm{d}\ln\rho)_{\mathrm{ad}}$$

$$\kappa_T = (\partial\ln\kappa/\partial\ln T)_\rho$$

$$\kappa_\rho = (\partial\ln\kappa/\partial\ln\rho)_T$$

$$\tau_{\mathrm{th}}(r) = \int_r^R Tc_P\,\mathrm{d}M/L$$

Pamyatnykh 1999 (due Dziembowski 1994)

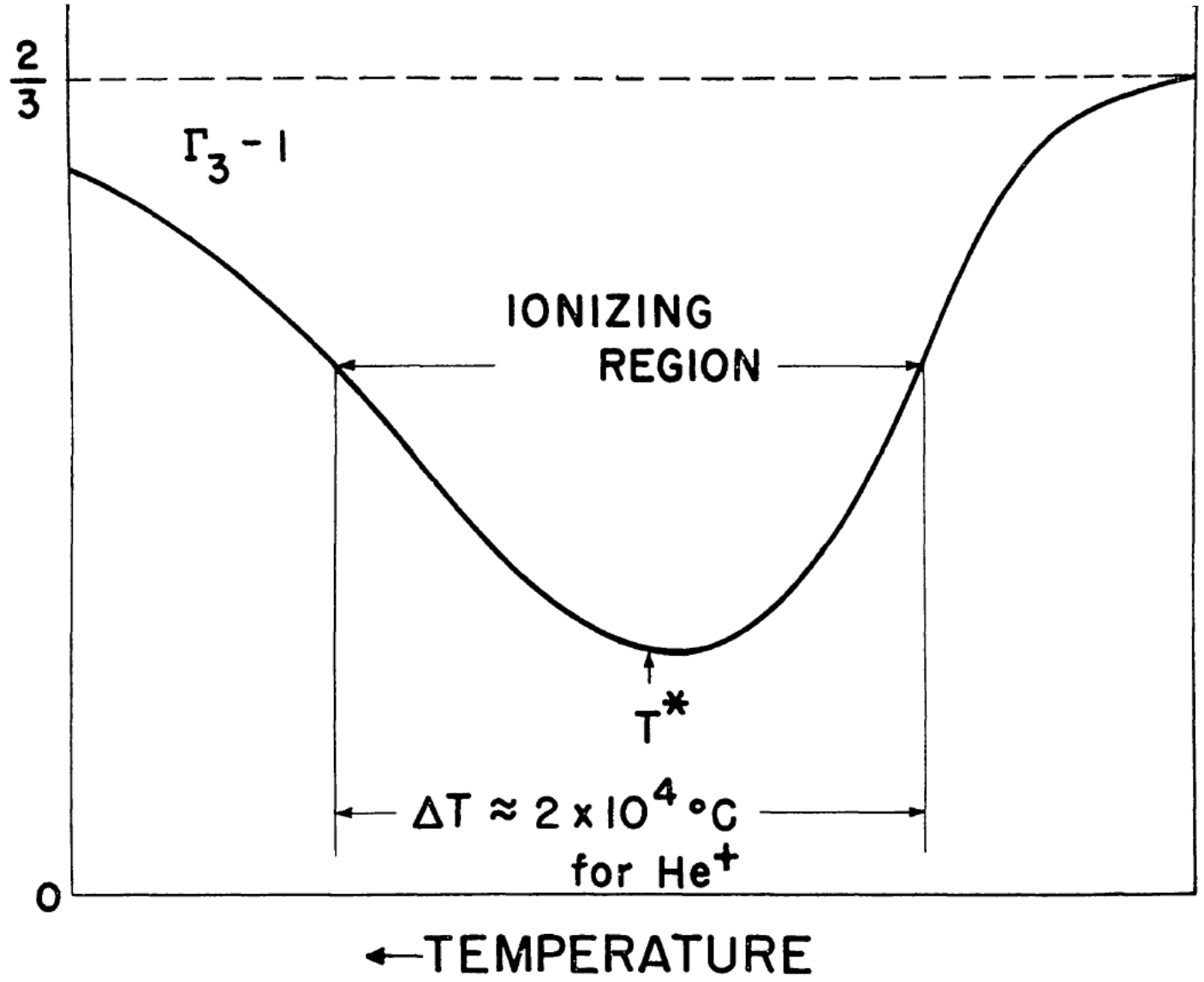

FIG. 4. $\Gamma_3 - 1$ vs. temperature (schematic) in the region of He^+ ionization in the equilibrium model of a stellar envelope.

Cox 1967

Kappa-mechanism

On excitation of pulsations

$\varkappa$ - mechanism :

$$\varkappa \sim \varkappa_0 \rho^n T^{-s}, \quad \begin{matrix} n \sim 1 \\ s \sim 3.5 \end{matrix}$$

($\varkappa$ - opacity coefficient)

(1) $$\frac{\delta T}{T} \sim (\gamma - 1) \frac{\delta \rho}{\rho}$$

In H- and He-ionization zones $\gamma \downarrow$ from $\sim 5/3$ to $\sim 1.1 - 1.2$

$\Rightarrow$ increasing effect of density variations on opacity variations during pulsations

$\Rightarrow \varkappa \uparrow$ at compression $\Rightarrow$ energy flux is blocked $\Rightarrow$ driving

Moreover, $n, s \neq$ const, their behaviour may also be in favour of driving ($s < 0$ in H-ioniz. zone)

(2) $$\text{Flux} \sim \frac{T^4}{\varkappa}$$

(due to ionization)

Direct influence of decreased temperature variations - **γ - mechanism.** (see (1) and (2)).

Usually: „$\varkappa$-mechanism" = ($\varkappa$-mechanism) + (γ-mechanism).

Opacity mechanism

Work integral – net energy gained by an oscillation mode during one cycle:

$$W = -\int d^3x \cdot \nabla_{ad} \oint dt \, \frac{\delta P}{P} \, \delta \mathrm{div}\, \vec{F}$$

$$\delta \mathrm{div}\, \vec{F} = \frac{1}{4\pi r^2} \frac{d\, \delta L_r}{dr}$$

$$\frac{\delta L_r}{L} = \frac{dr}{d\ln T} \frac{d}{dr} \frac{\delta T}{T} - \frac{\delta \varkappa}{\varkappa} + 4\left(\frac{\delta T}{T} + \frac{\delta r}{r}\right)$$

- $\frac{d}{dr}\left(\varkappa_T + \frac{\varkappa_\rho}{\Gamma_3 - 1}\right) > 0$ for driving effect

Two additional conditions to excite an oscillation:

- In the driving zone, eigenfunction $\delta P/P$ must be large and must vary only slowly with r.
- In the driving zone, the thermal timescale

$$\tau_{th}(T) = \frac{1}{L} \int_{\text{surface}}^{M(T)} T c_p \, dM$$

must be $\gtrsim$ oscillation period.
Otherwise, the potentially driving region remains in thermal equilibrium during pulsation.

$$\tau_{\mathrm{th}}(r) = \int_{r}^{R} T c_P \, \mathrm{d}M / L$$

Scala cieplna w obszarze wzbudzania
danego modu powinna być porównywalna z okresem oscylacji

$T_{eff} > T_{eff,\ crit}$

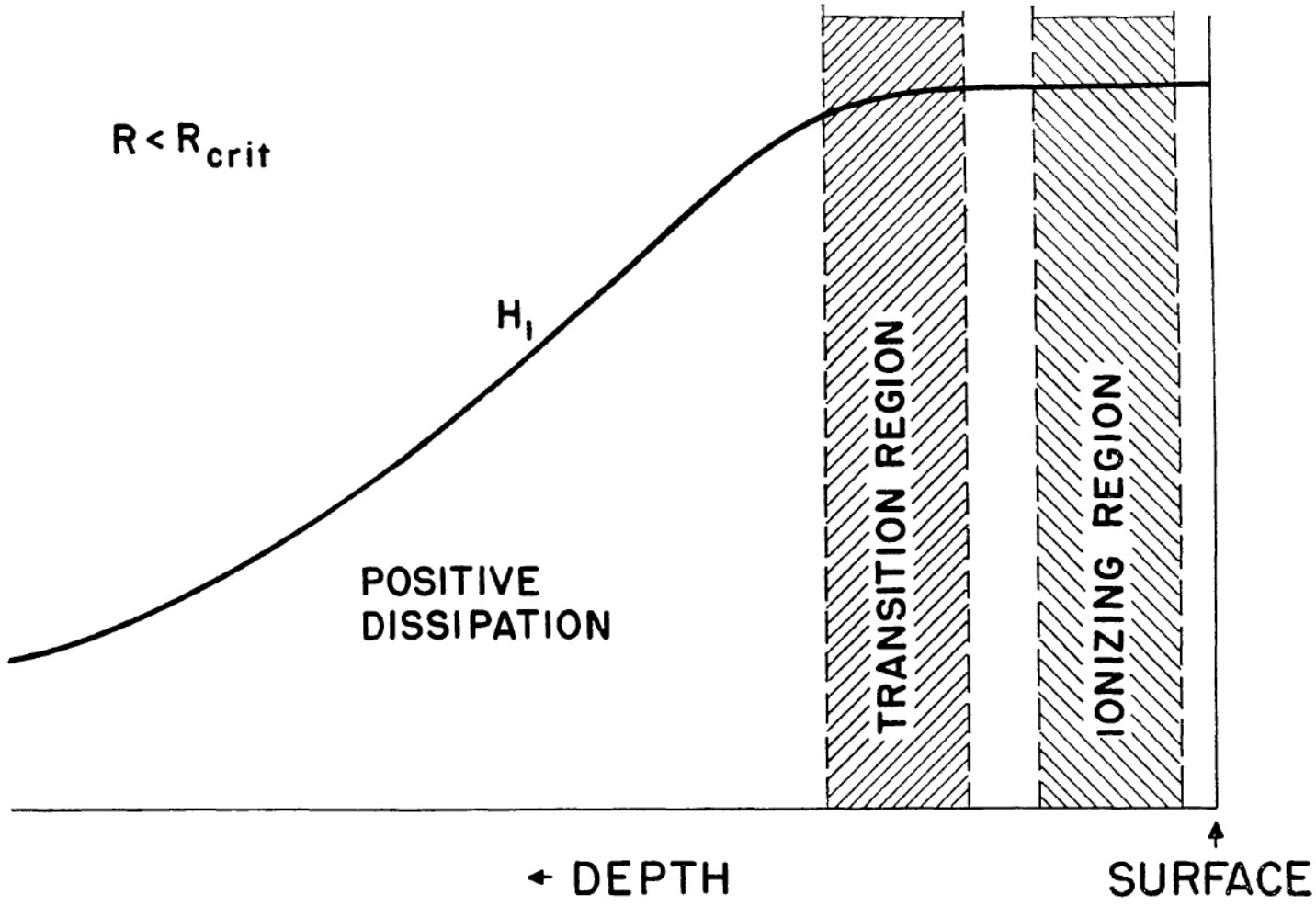

FIG. 5. H_1 vs. depth below the stellar surface (schematic) for $R < R_{crit}$ (see text for explanation of symbols).

$H_1 = Re(\delta L/L)$

Cox 1967

$T_{eff} < T_{eff,\,crit}$

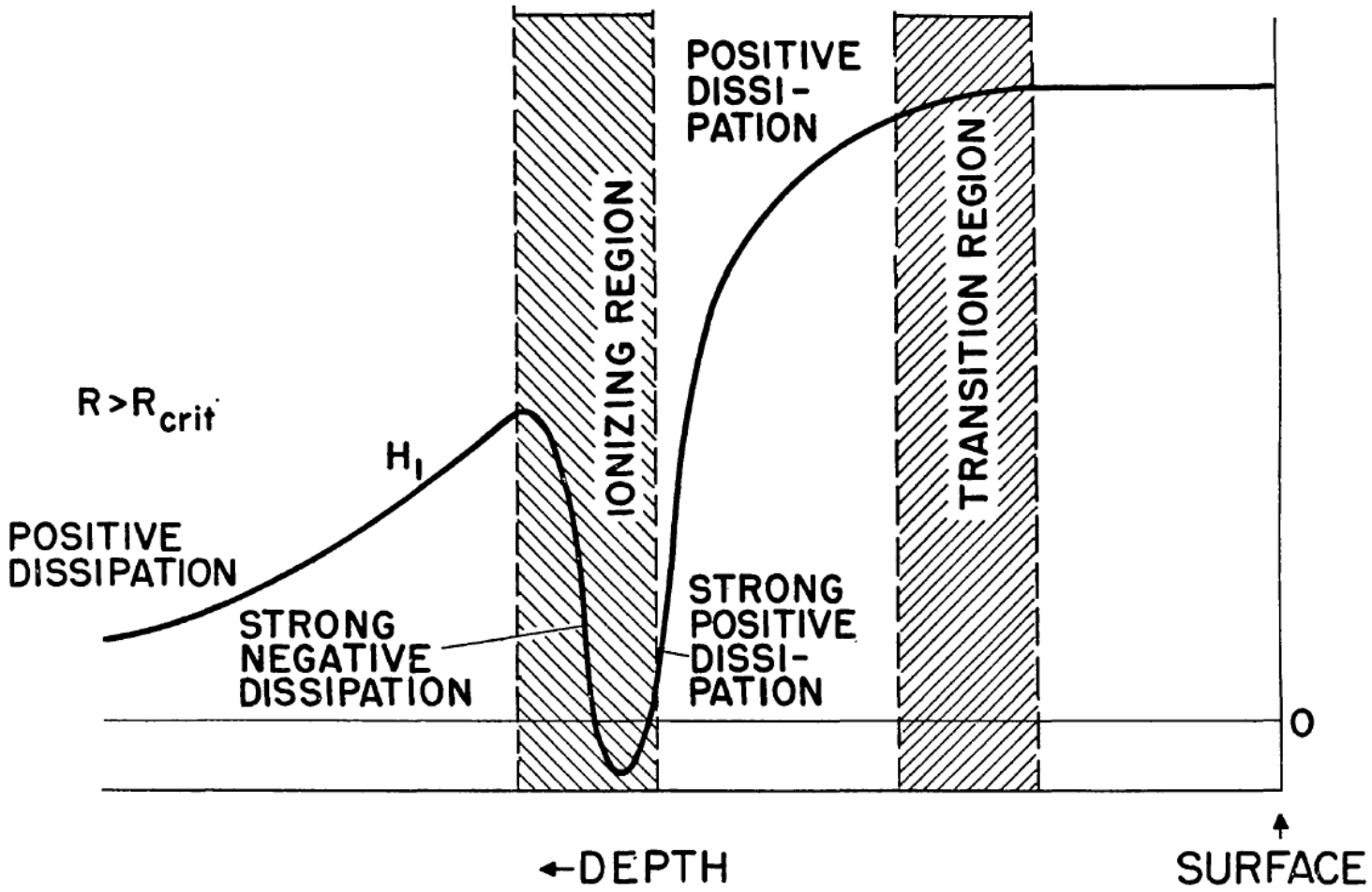

FIG. 6. H_1 vs. depth below the stellar surface (schematic) for $R > R_{crit}$ (see text for explanation of symbols).

Cox 1967

$T_{eff} = T_{eff,\,crit}$

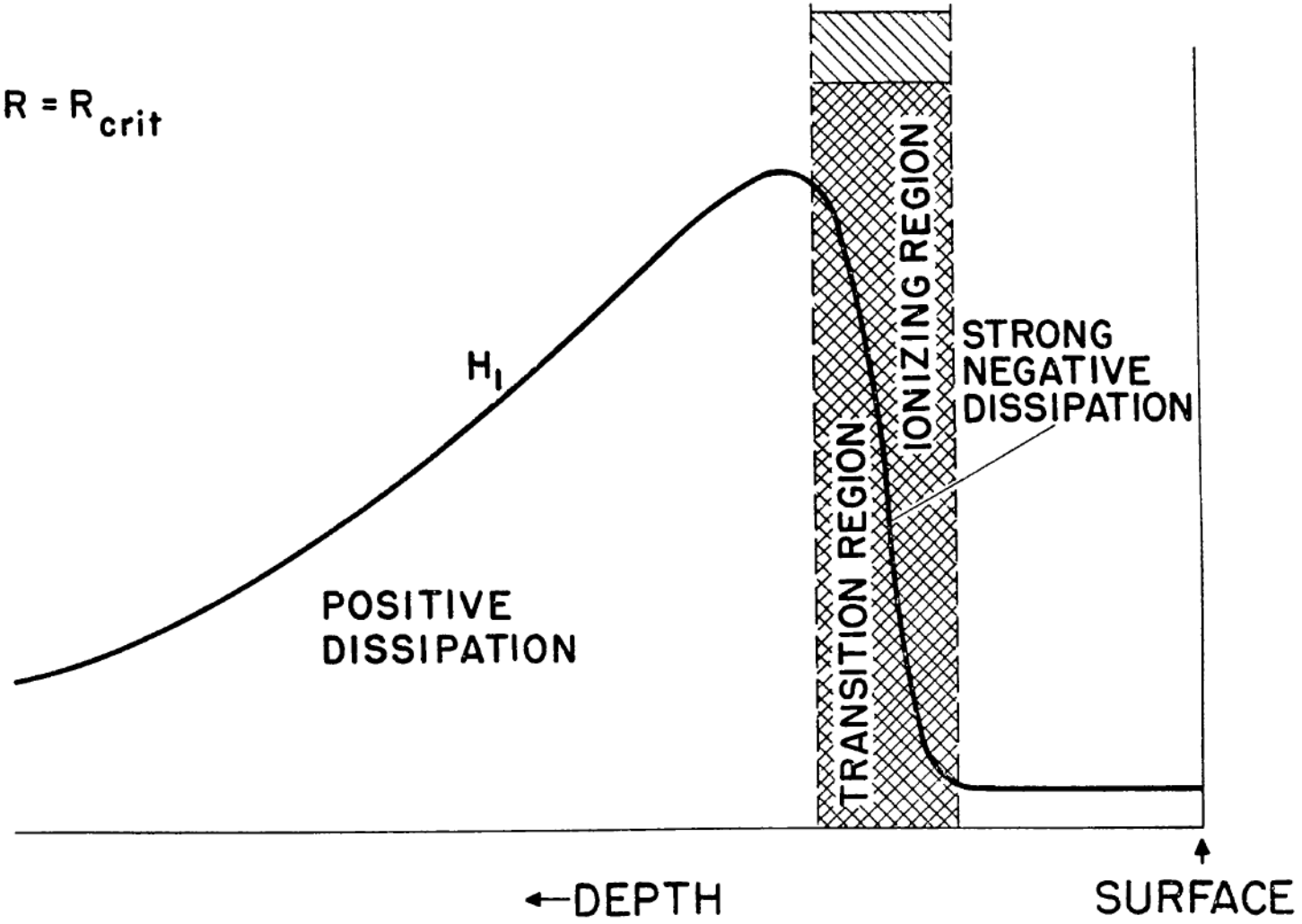

FIG. 7. H_1 vs. depth below the stellar surface (schematic) for $R = R_{crit}$ (see text for explanation of symbols).

Cox 1967

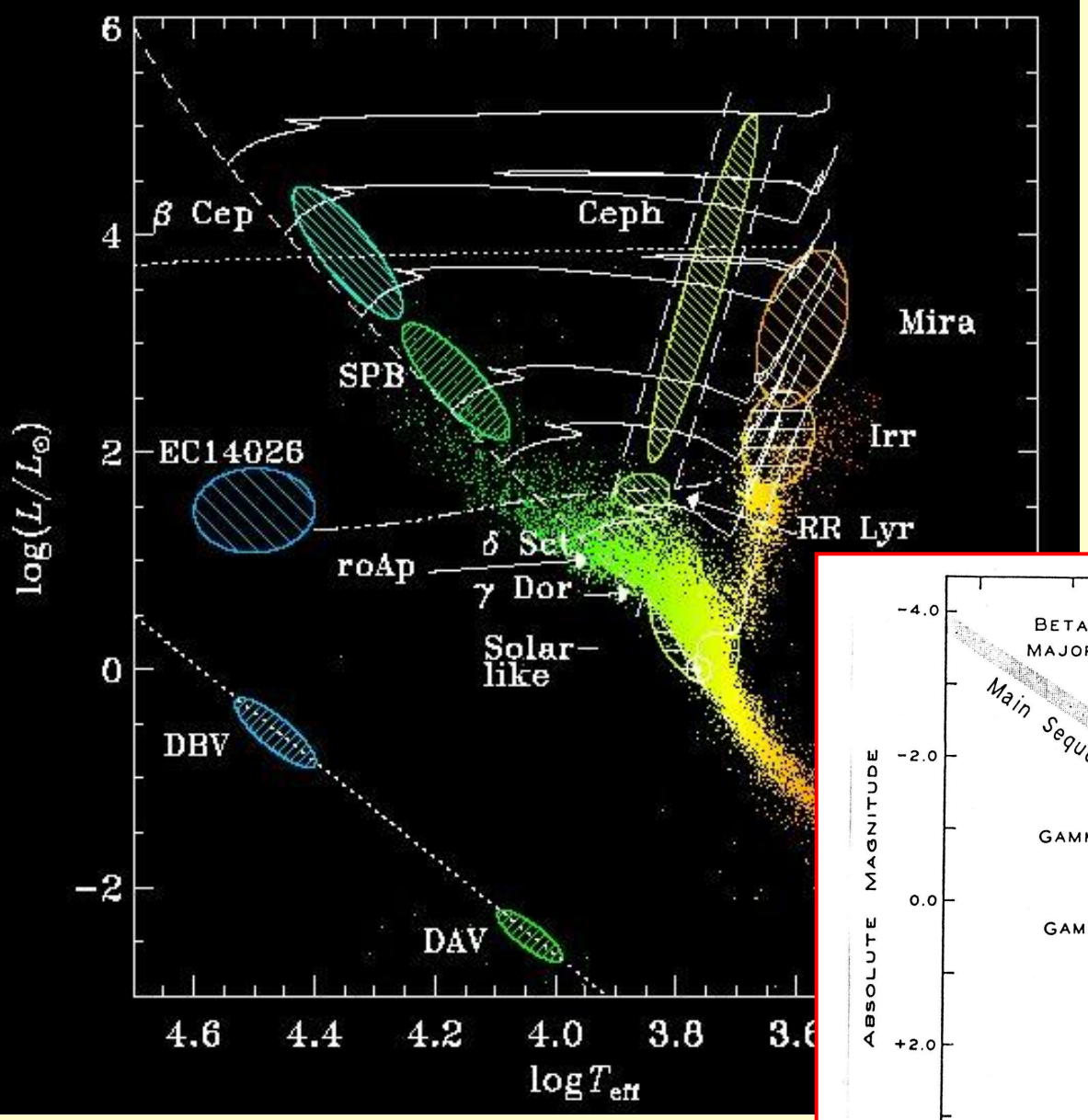

J. Christensen-Dalsgaard

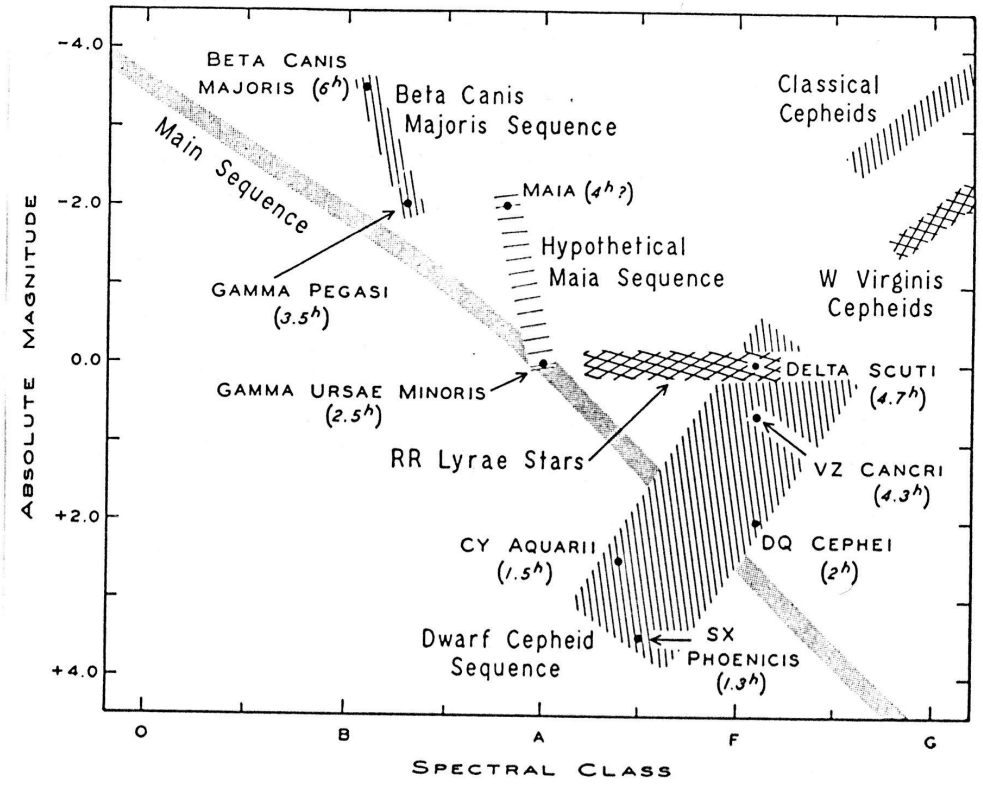

O. Struve

Sergey A. Zhevakin (11.04.1916 – 21.02.2001)

Zhevakin S. A.,
Physical basis of the pulsation theory of variable stars.
Ann.Rev.Astron.Astrophys., 1963, Vol. 1, 367-400.

http://vivovoco.rsl.ru/VV/JOURNAL/NATURE/08_06/STARS.HTM
http://sundry.wmsite.ru/moja-genealogija/kulikov/sergej-aleksandrovich-zhevakin/

Norman Baker (23.10.1931 – 11.10.2005)

N. Baker, R. Kippenhahn,
The pulsations of models of
Delta Cephei stars.
1962, Z.f.Ap., 54, 114-151

N. Baker, R. Kippenhahn,
The pulsations of models of
Delta Cephei stars. II.
1965, Ap. J., 142, 868-889

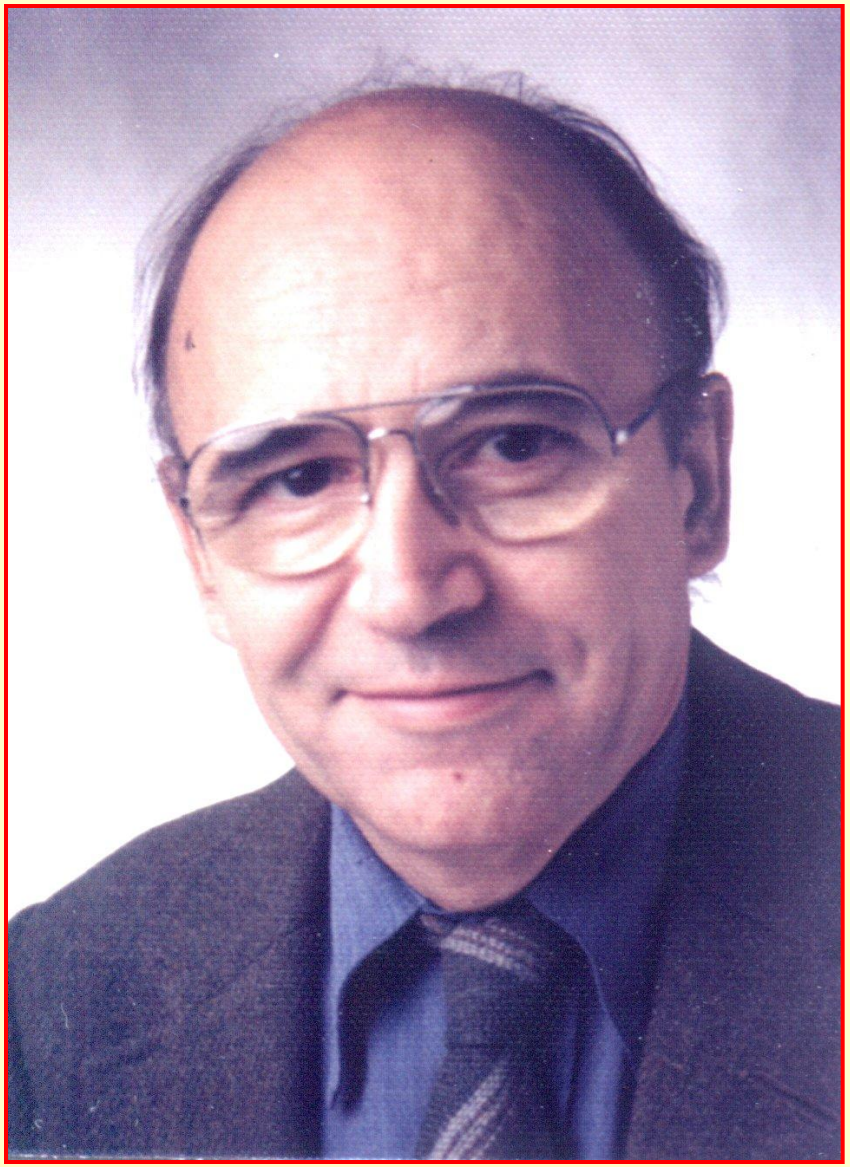

http://iau-c35.stsci.edu/News/nhbobit.pdf

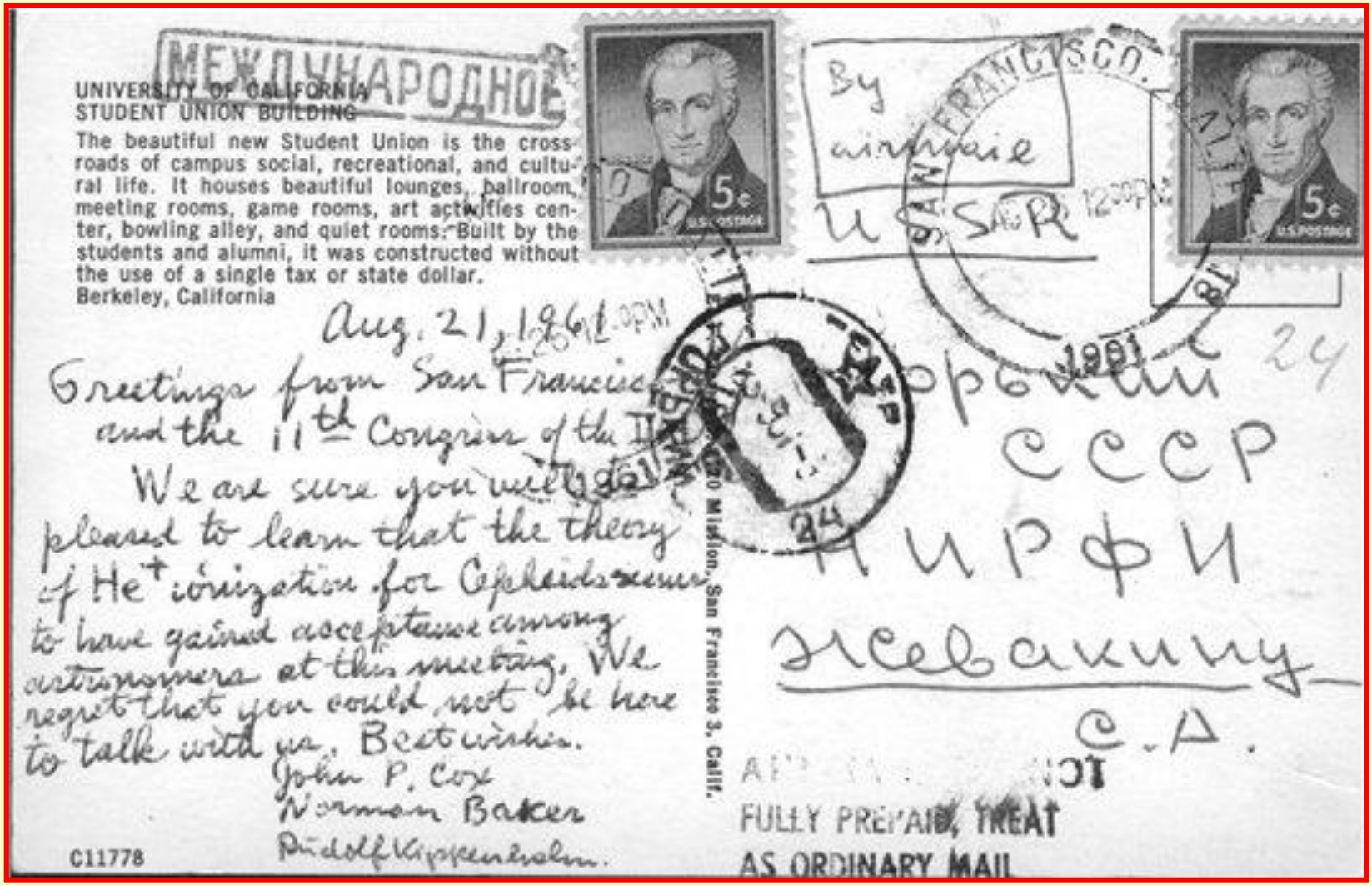

http://sundry.wmsite.ru/moja-genealogija/kulikov/sergej-aleksandrovich-zhevakin/

Wzbudzanie pulsacji na Ciągu Głównym: Z-maksimum

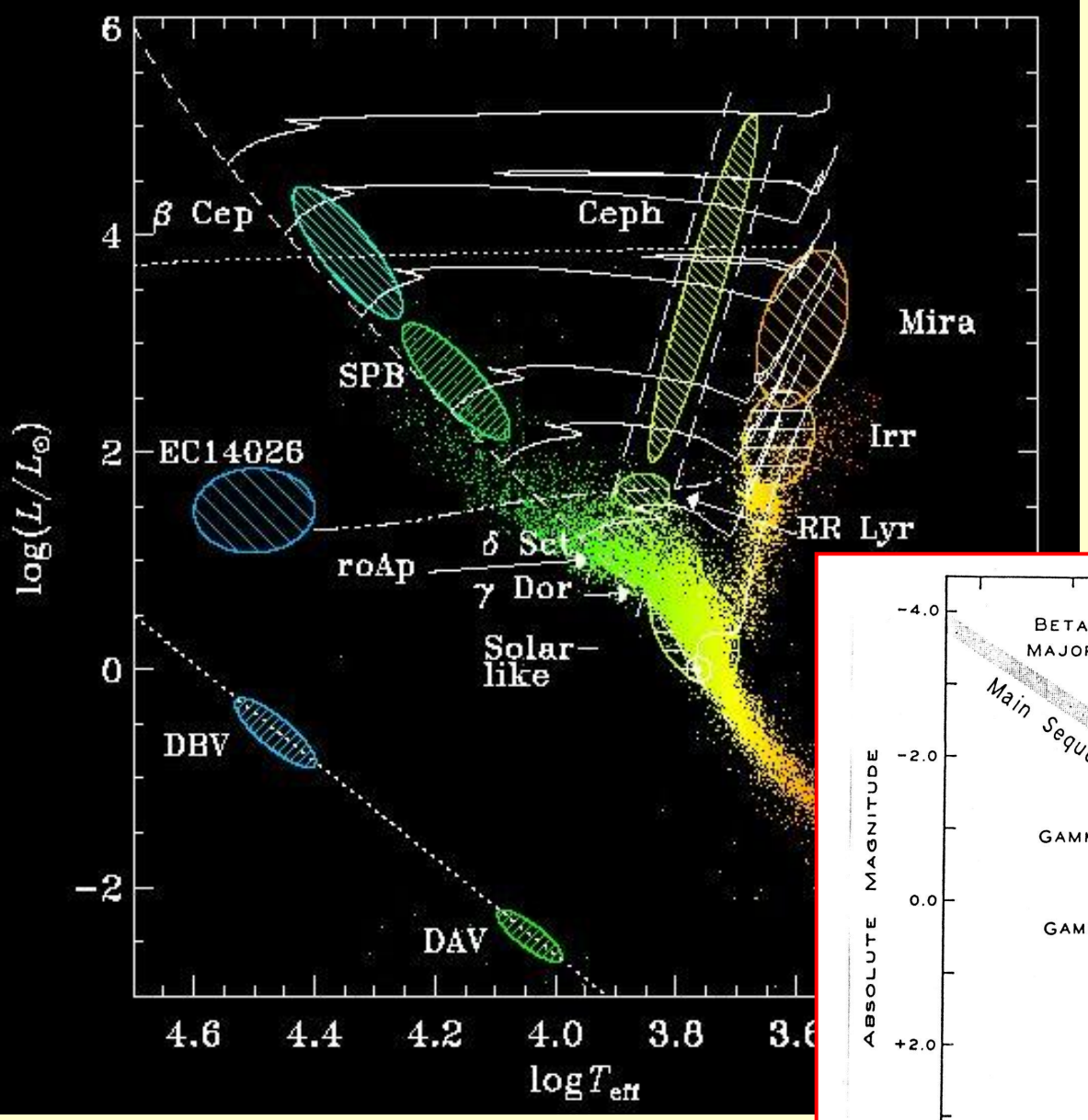

J. Christensen-Dalsgaard

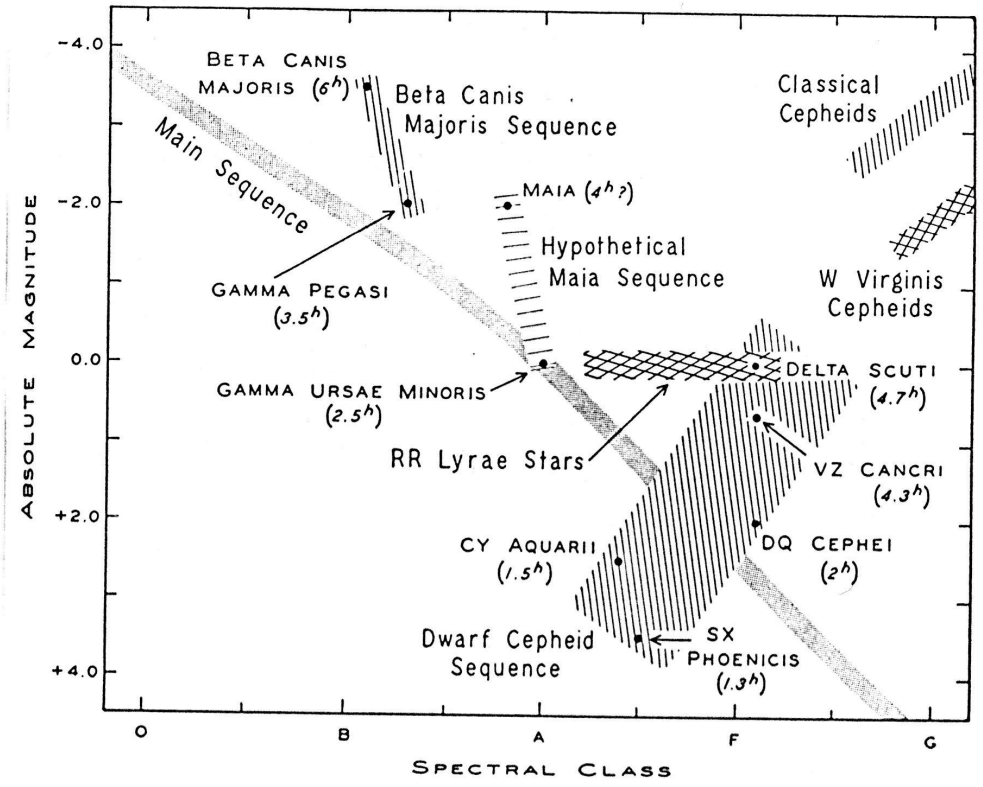

O. Struve

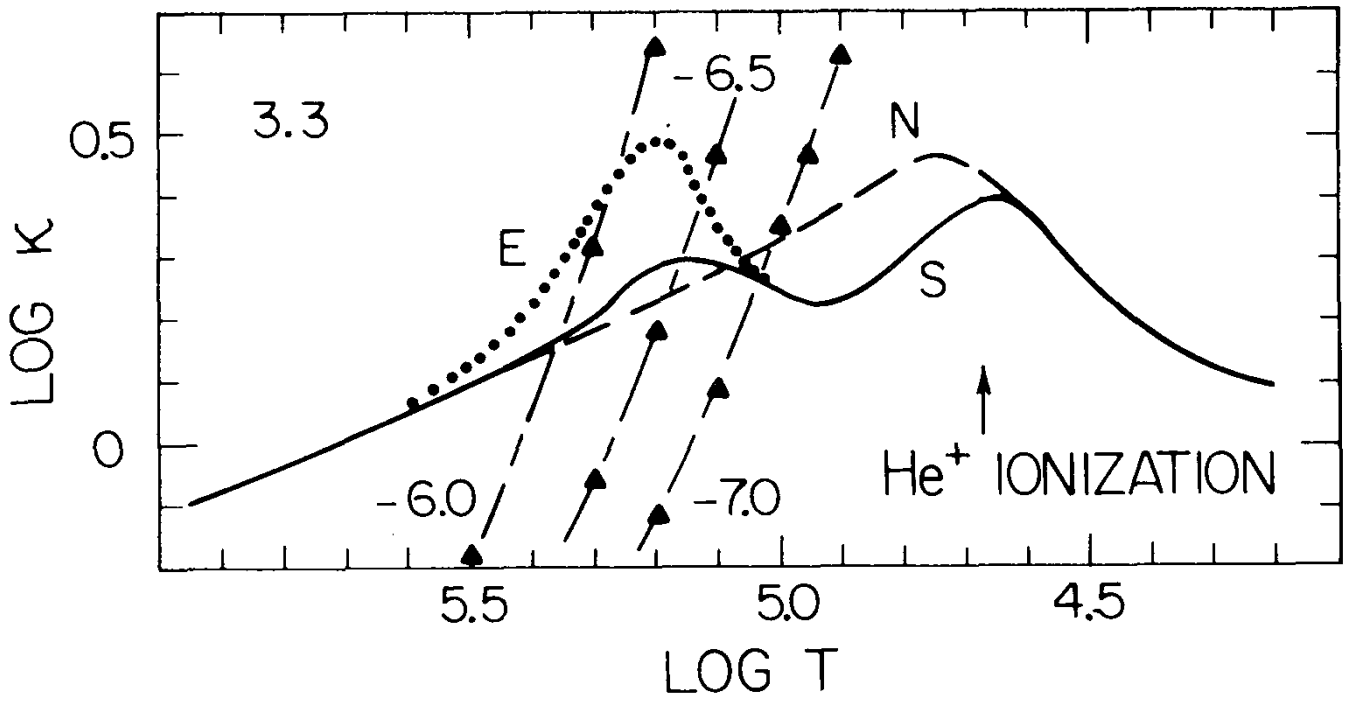

FIG. 5. Run of opacity versus temperature for models 3.3S, N, and E, as labeled. Triangles are opacity points taken directly from the King IVA table at densities of $\log\rho = -6.0, -6.5$, and -7.0, as indicated.

Stellingwerf 1978

Opacity inside a Beta Cephei star model (M=12 Msun, X=0.70, Z=0.02): OP (Seaton et al.) *versus* OPAL (Livermore) *versus* LAOL (Los Alamos)

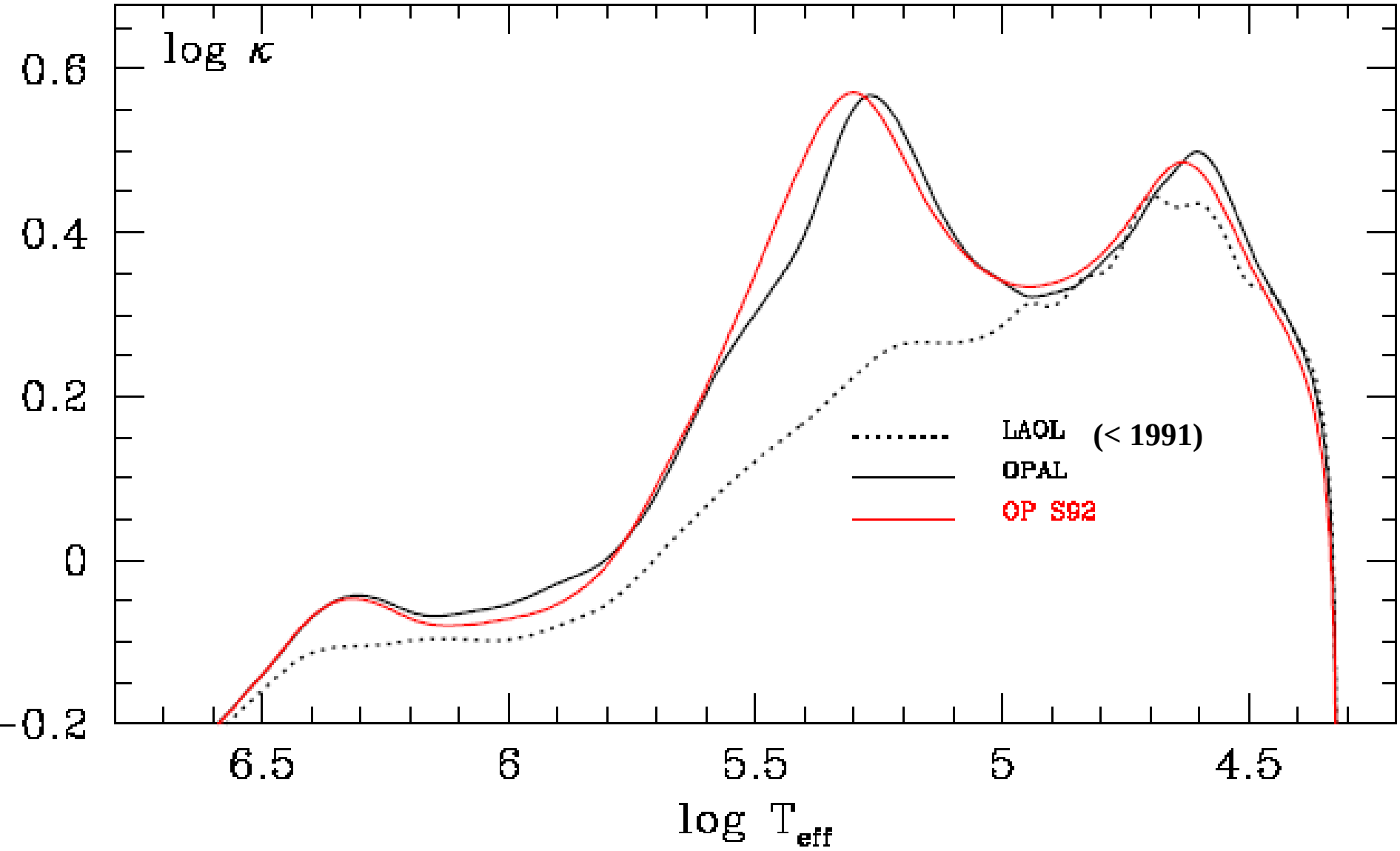

κ OPAL (1992) vs
κ OPAL (1991)

Metal opacity bump is considerably increased and so is the driving effect

Work integral
(>0 for instability)

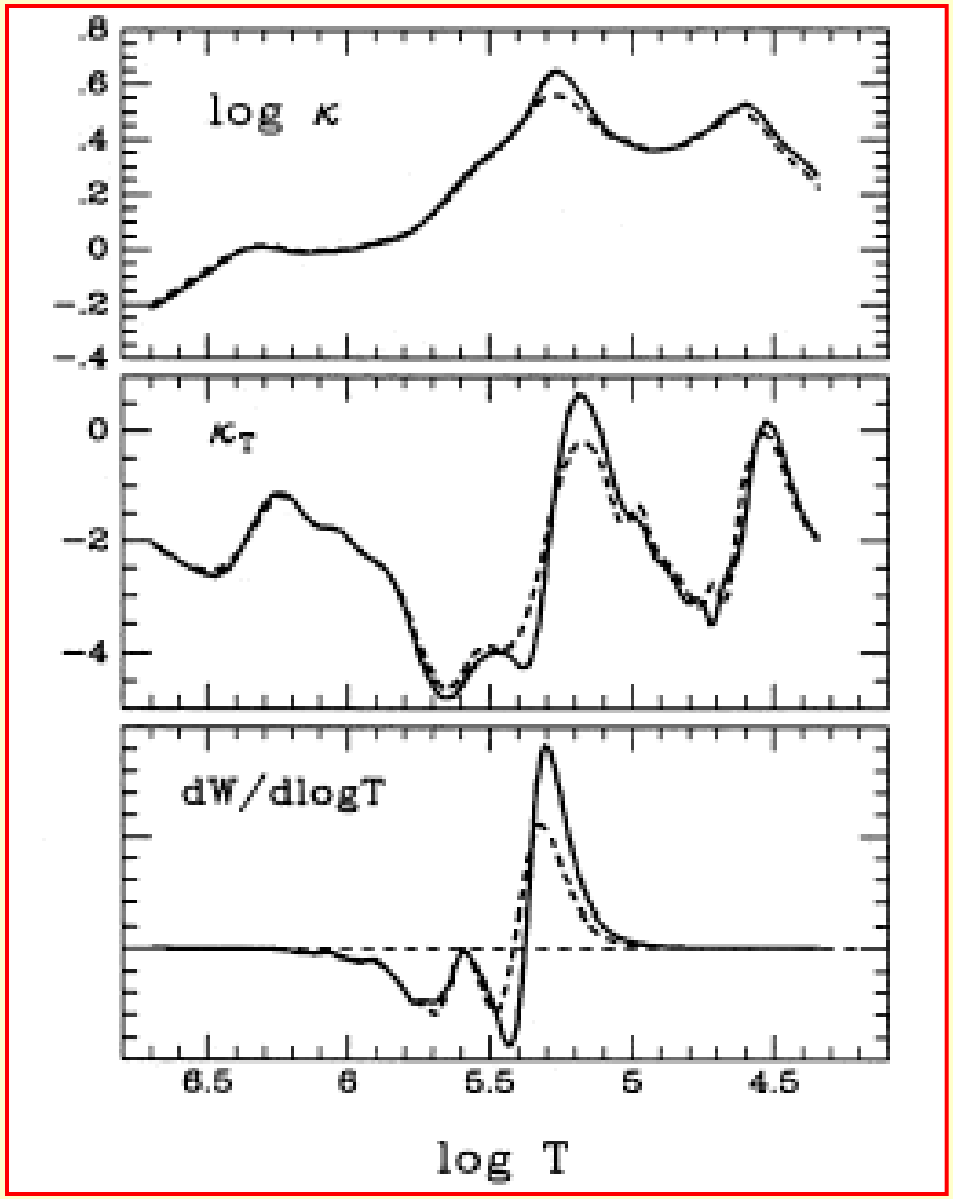

Dziembowski & Pamyatnykh, 1993, A&A, 262, 204

Beta Cephei instability domain. Opacities from OPAL 1991

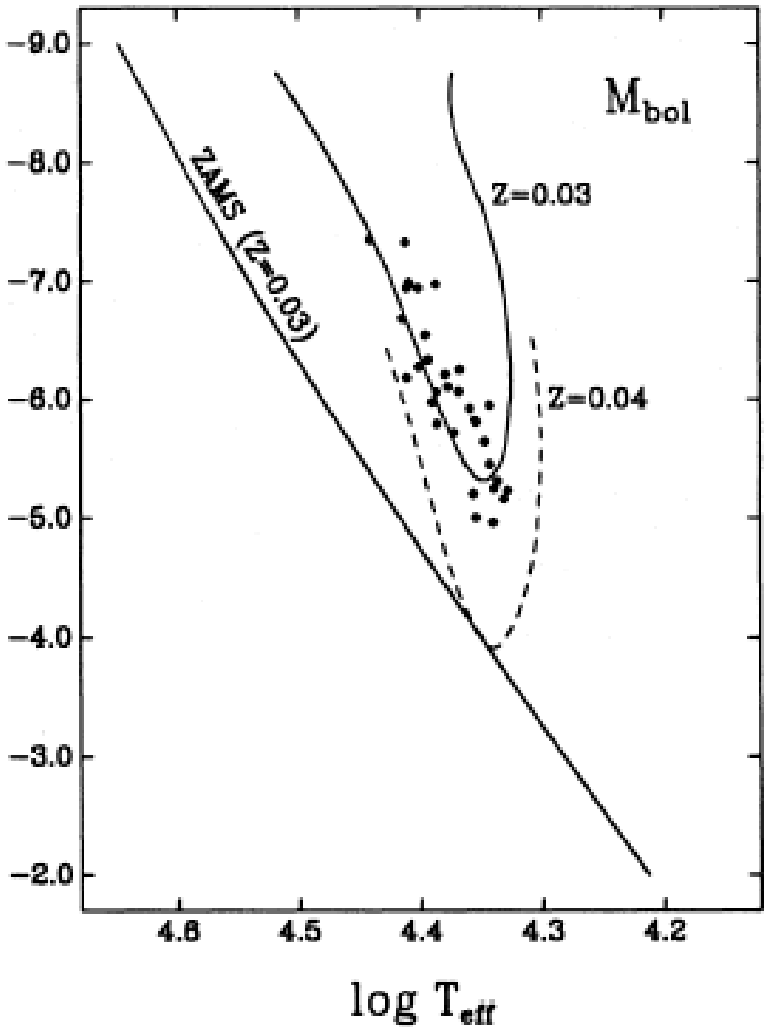

Fig. 4 The H-R diagram showing positions of β Cep stars (dots) and the domain of the radial fundamental mode instability, calculated for two values of the heavy element content.

Moskalik & Dziembowski, 1992, A&A 256, L5

For many years, explaining the cause of Beta Cephei variability has been a major challenge to stellar pulsation theory.
The problem is now solved, but we owe the solution to progress in opacity calculation and not to new astrophysical ideas.
In fact, if the OPAL opacities were available the problem would have been solved many years ago (Baker & Dziembowski 1969, unpublished).

W. Dziembowski,
IAU Symp. 162, France, 1993.

Opacity behaviour at astrophysical conditions [κ OPAL 1996]

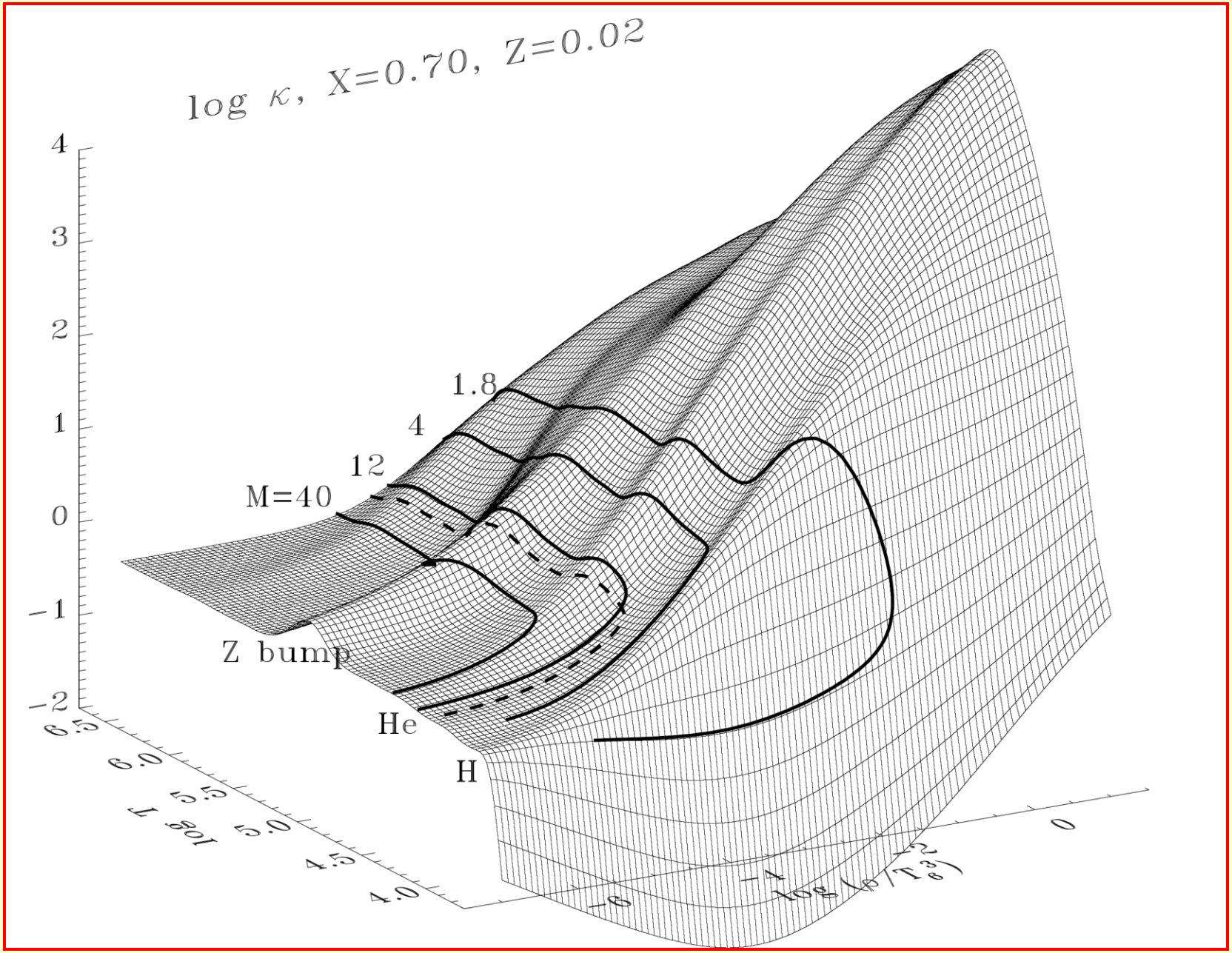

Pamyatnykh, 1999, Acta Astronomica, 49, 119

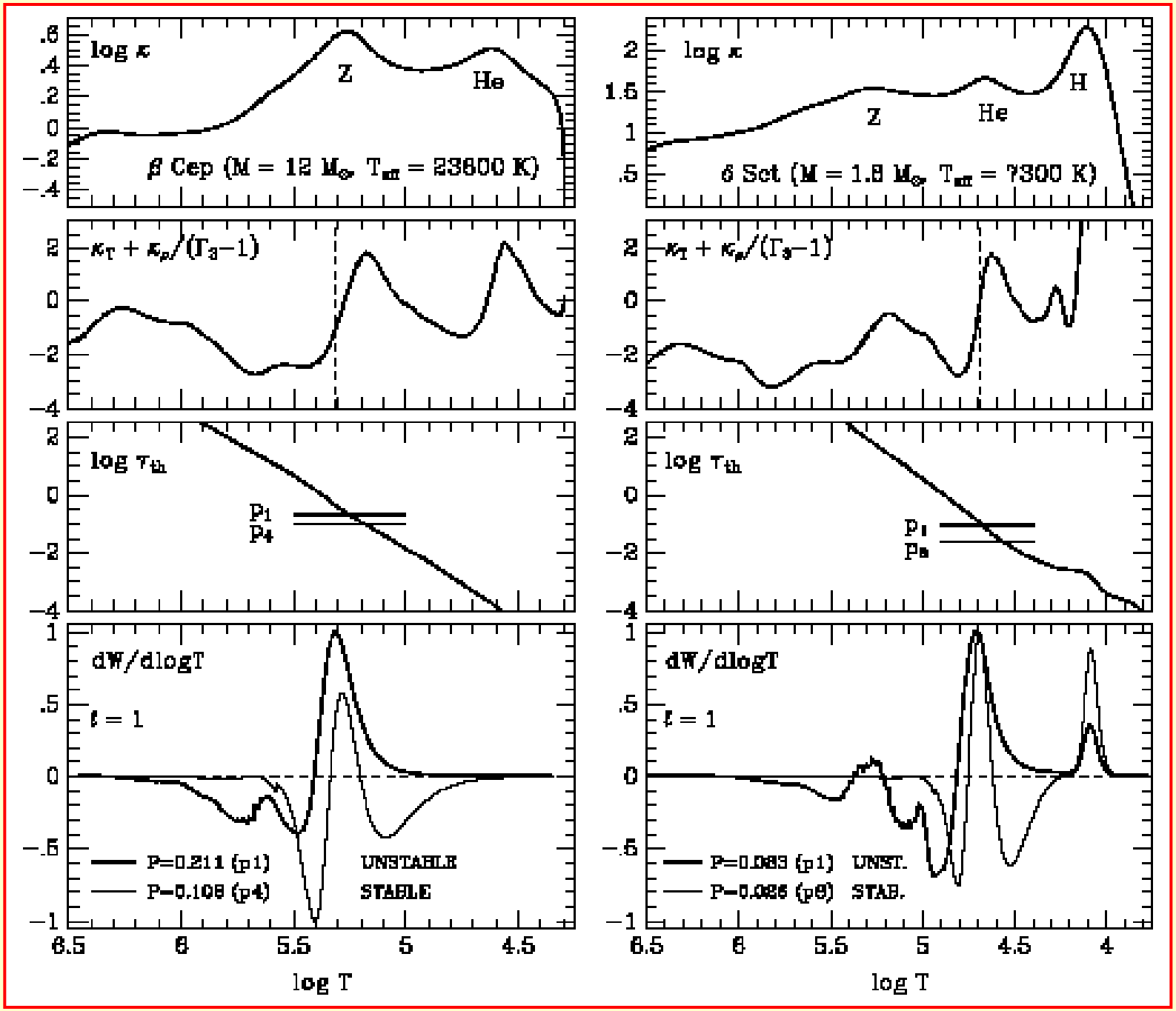

Pamyatnykh, 2000

Opacity, thermal timescale and work integral for selested pulasation modes for three representative models of β Cephei, SPB and δ Scuti variables

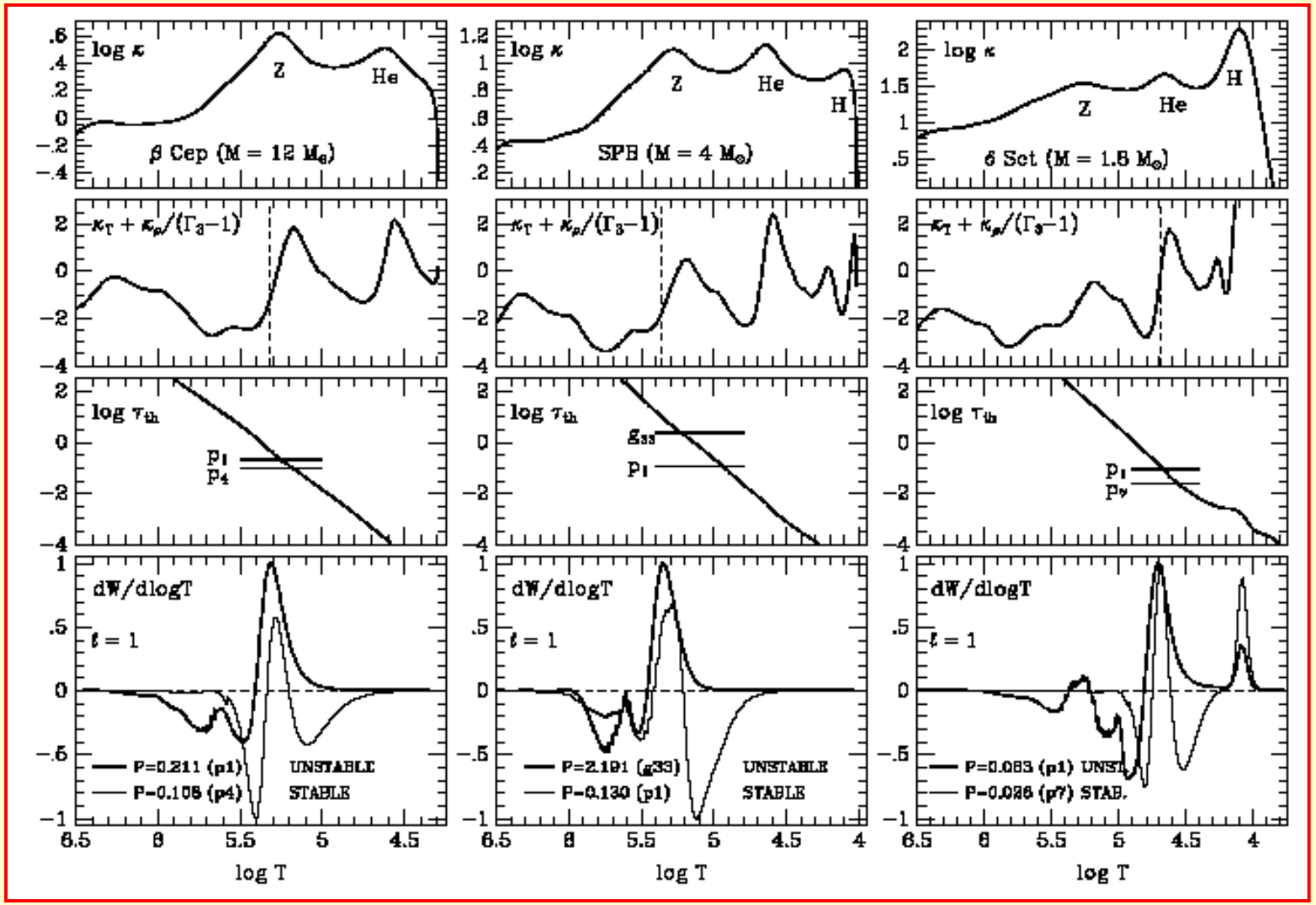

Pamyatnykh, 1999, Acta Astr., 49, 119

κ OPAL GN93 (Livermore, 1996):

Instability domains

in the Upper MS

X=0.70, Z=0.02

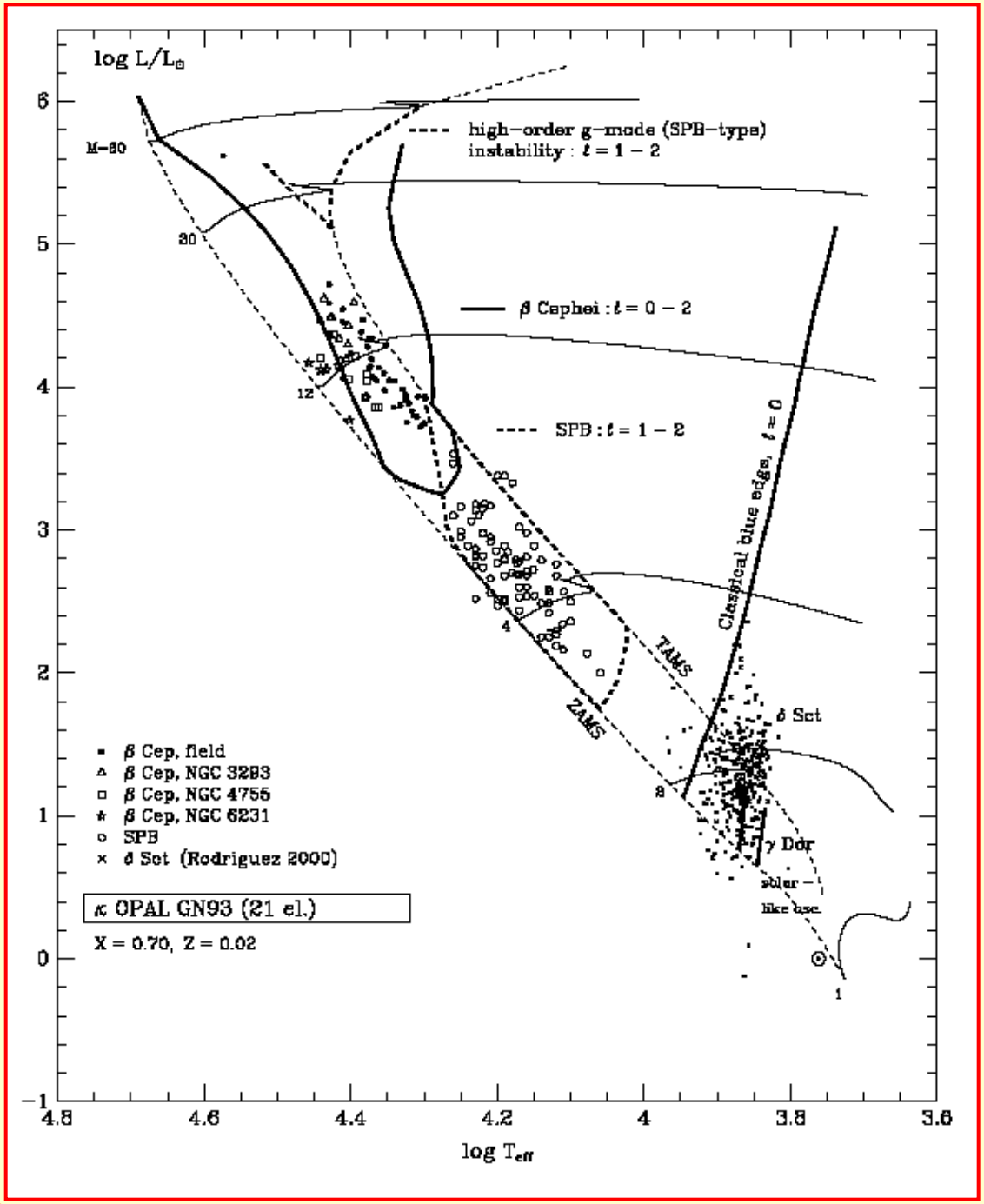

Pamyatnykh, 1999, Acta Astr., 49, 119

Effect of changes in the heavy element abundances on evolution and stability of the upper MS stars:

κ OPAL,
Z = 0.01, 0.015, 0.02

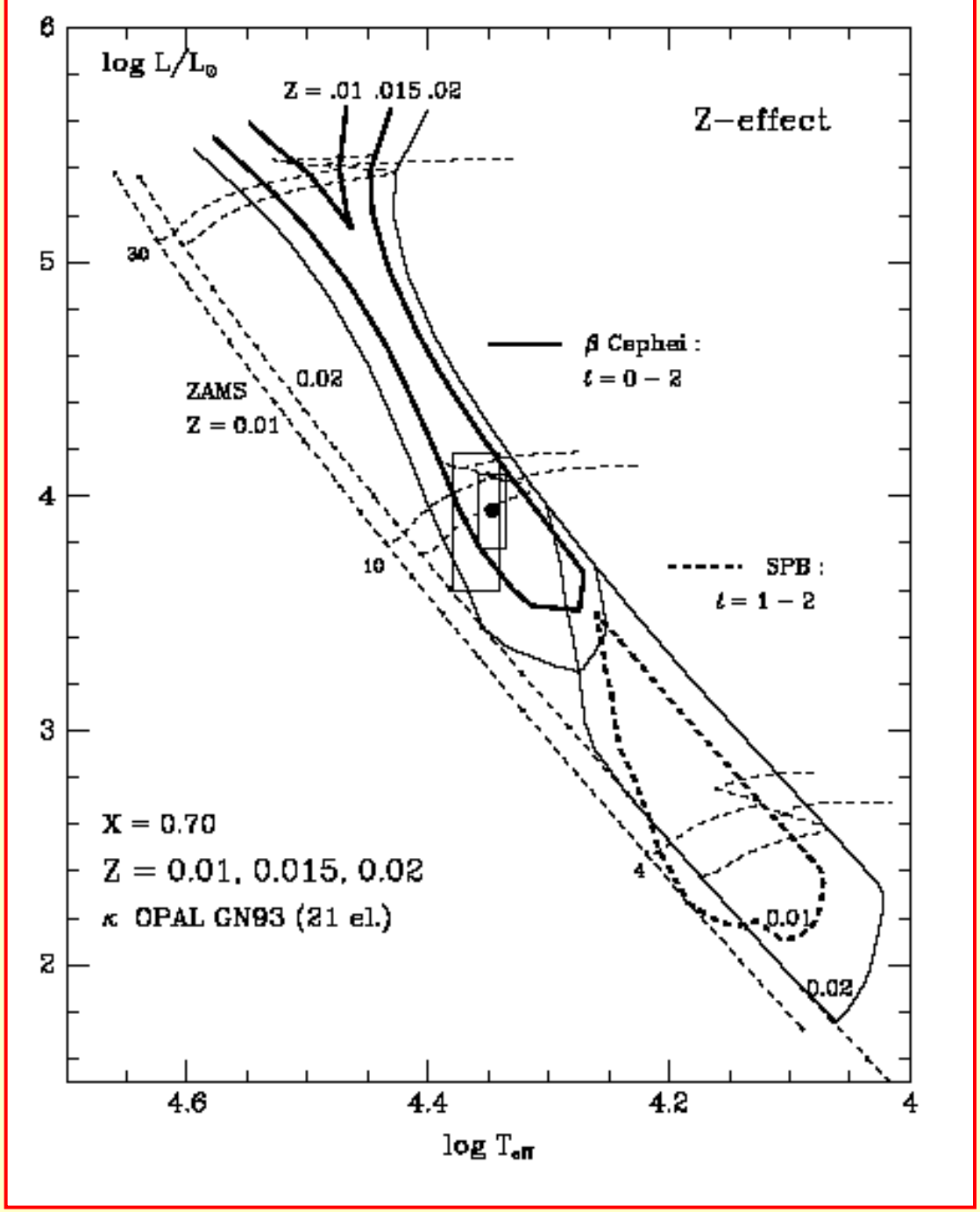

Pamyatnykh, 1999, Acta Astr., 49, 119

Opacity source	Z for β Cep instability
LAOL (< 1991)	no excitation
OPAL 1991	Z = 0.03-0.04
OPAL 1992	Z = 0.02-0.03
OPAL 1996	Z = 0.02-0.03
OP S92 >1993	Z = 0.02
OP A04 2005	Z = 0.01-0.02

With newest opacities and abundances it is possible to explain β Cep pulsations using models with significantly lower Z value than before.

INSTABILITY DOMAINS IN THE MAIN SEQUENCE

κ OPAL GN93 (Livermore, 1996)

X=0.70, Z=0.02

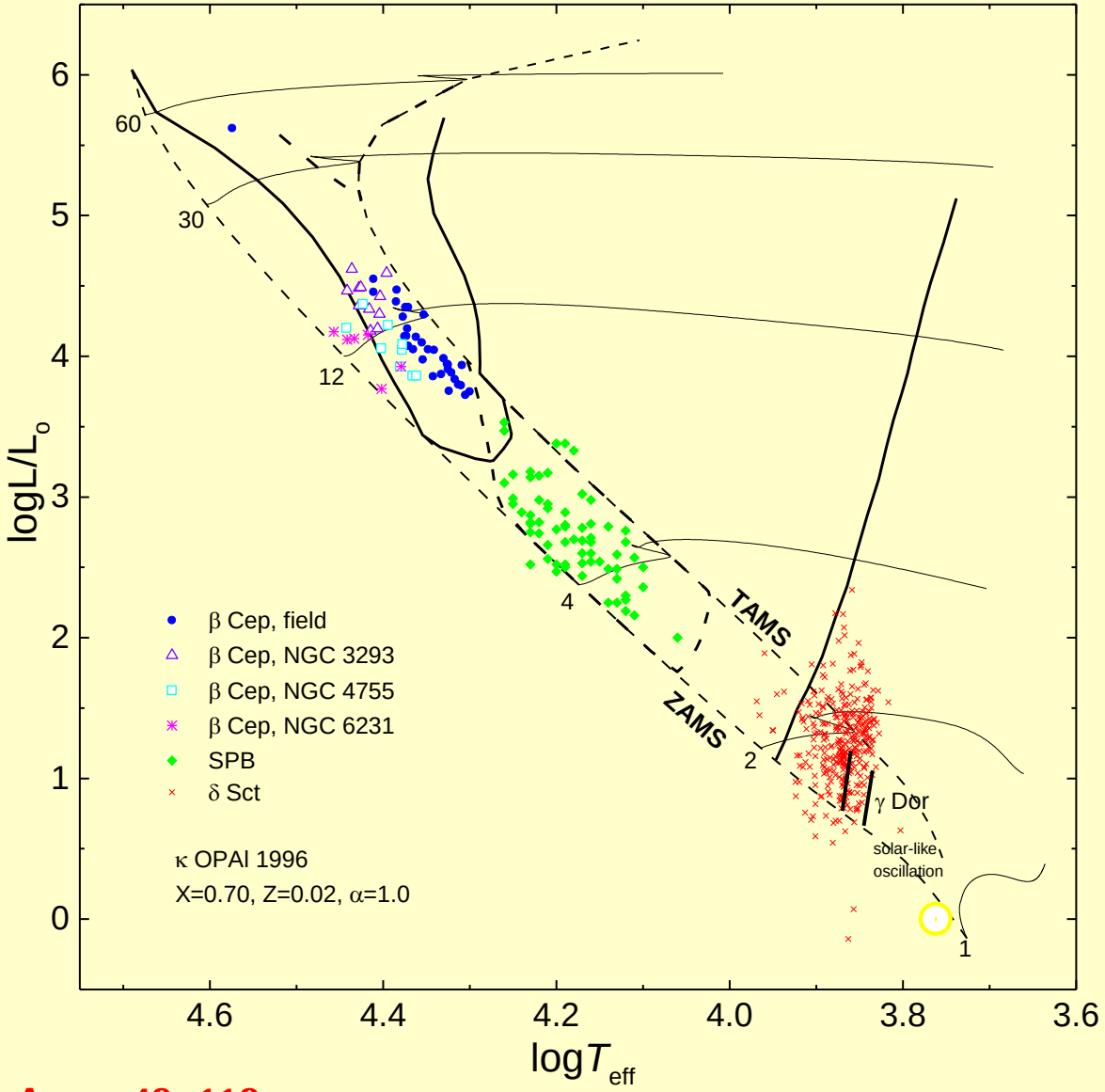

due to Pamyatnykh, 1999, Acta Astr., 49, 119

The END

Oscylacje nieradialne opisują za pośrednictwem harmonik sferycznych:

$$Y_l^m(\theta,\phi) = (-1)^m c_{lm}\ P_l^m\ (\cos\theta)\exp(i\,m\,\phi)$$

$$c_{lm}^2 = \frac{(2l+1)(l-m)!}{4\pi(l+m)!}$$

$$\lambda = \frac{2\pi}{k_{\rm h}} = \frac{2\pi R}{L}$$

$$k_{\rm h} = \frac{L}{R}$$

$$Y_l^m(\theta,\phi) = (-1)^m c_{lm}\ P_l^m\ (\cos\theta)\exp(i\,m\,\phi)$$

$$c_{lm}^2 = \frac{(2l+1)(l-m)!}{4\pi(l+m)!}$$

$$k_{\rm h} = \frac{L}{R}$$

$$\lambda = \frac{2\pi}{k_{\rm h}} = \frac{2\pi R}{L}$$

$$t_{\rm dyn} \simeq \left(\frac{R^3}{GM}\right)^{1/2} \simeq (G\bar{\rho})^{-1/2}$$

$$Q = \Pi \left(\frac{M}{M_\odot}\right)^{1/2} \left(\frac{R}{R_\odot}\right)^{-3/2}$$

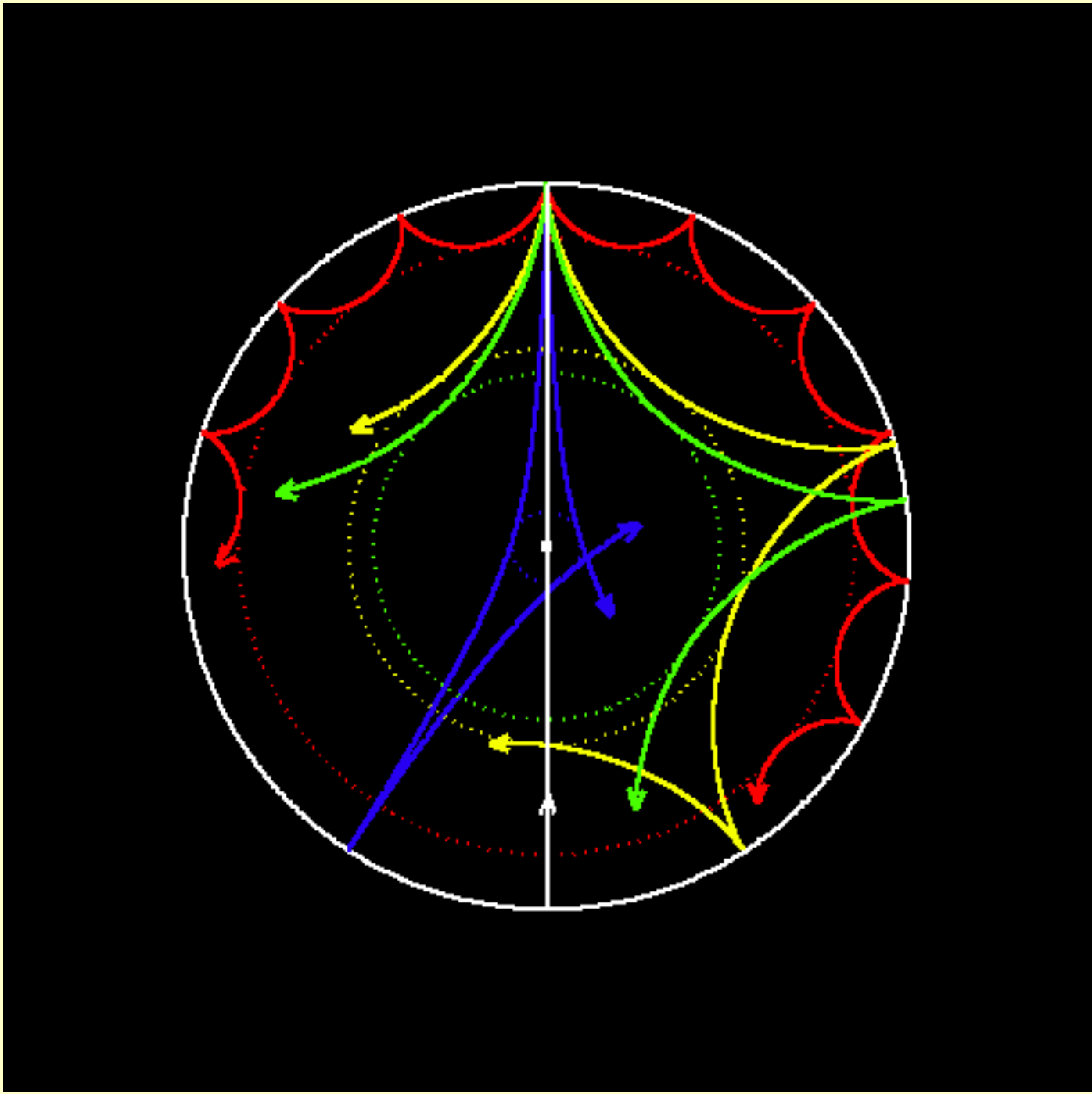

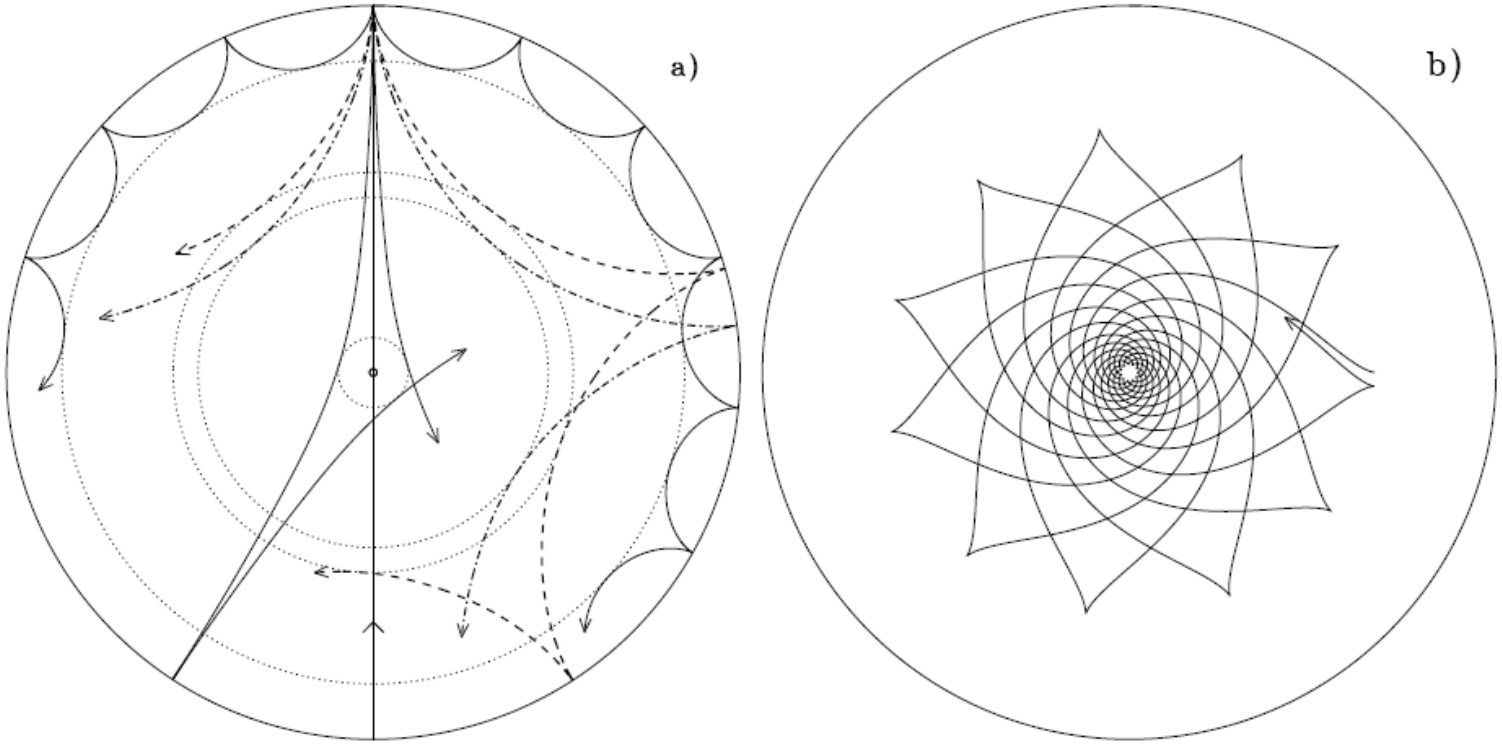

Fig. 5 Propagation of rays of sound or gravity waves in a cross-section of the solar interior. The acoustic ray paths (panel a) are bend by the increase in sound speed with depth until they reach *the inner turning point* (indicated by the dotted circles) where they undergo total internal refraction, at the distance r_t determined by Eq. (14). At the surface the acoustic waves are reflected by the rapid decrease in density. Rays are shown corresponding modes with frequency 3000 μHz and degrees (in order of increasing penetration depth) $l = 75$, 25, 20 and 2; the line passing through the centre schematically illustrates the behaviour of a radial mode. The gravity-mode ray path (panel b) corresponds to a mode of frequency 190 μHz and degree 5.

Cunha et al. 2007

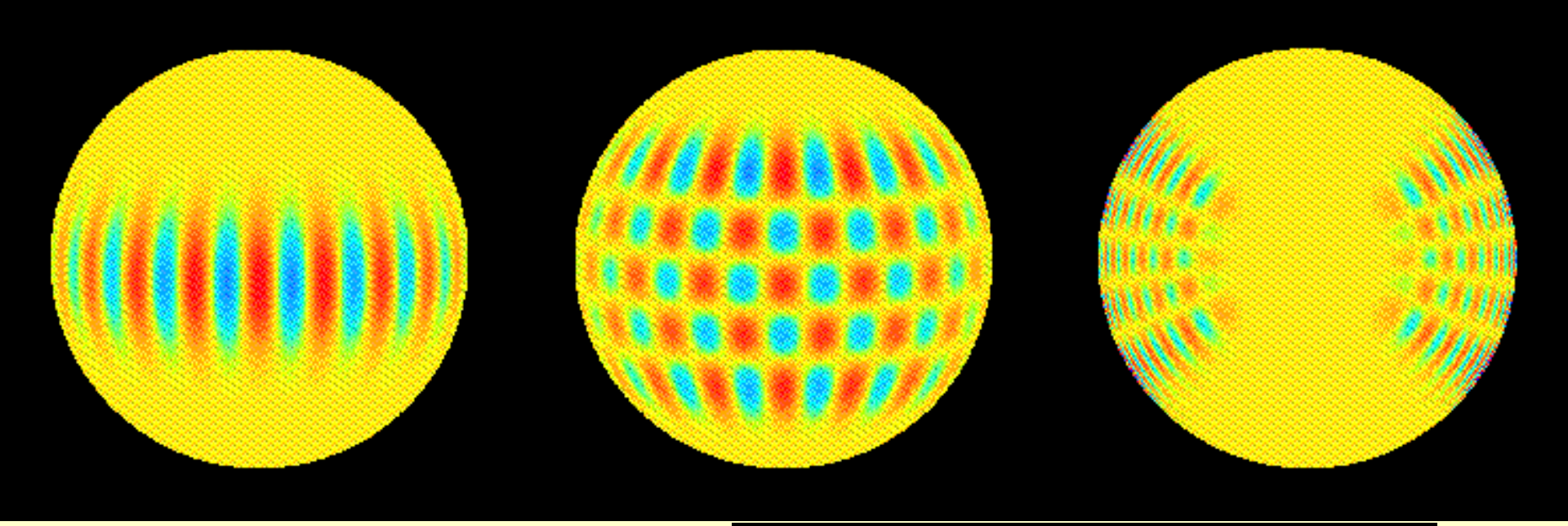

Akustyczne mody oscylacji Słońca

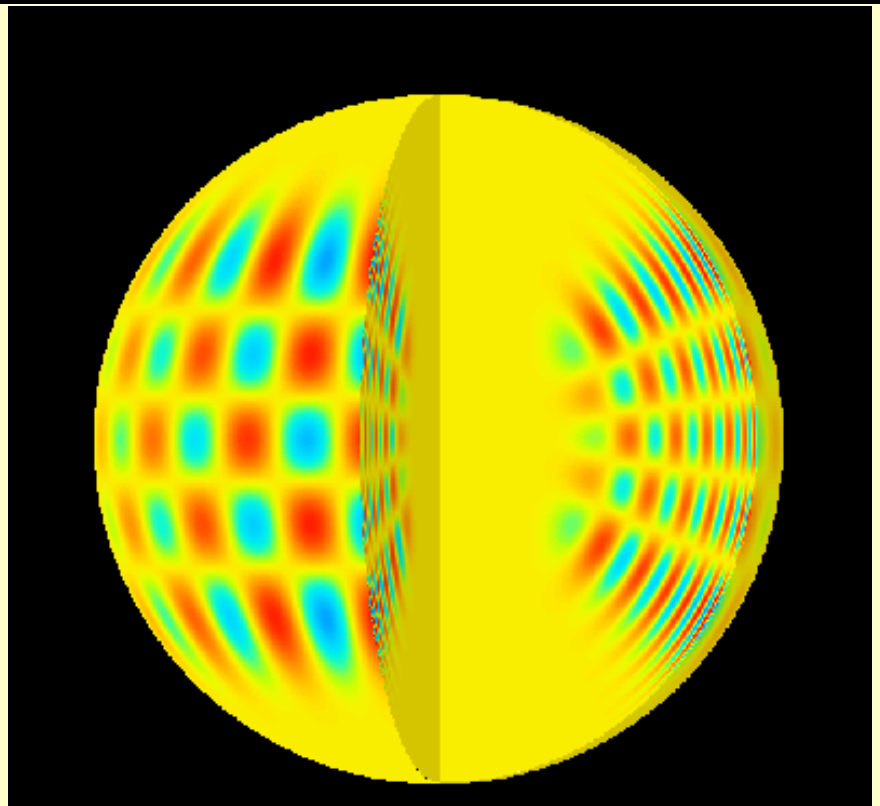

Współczynnik nieprzezroczystości κ jako funkcja temperatury i ciśnienia

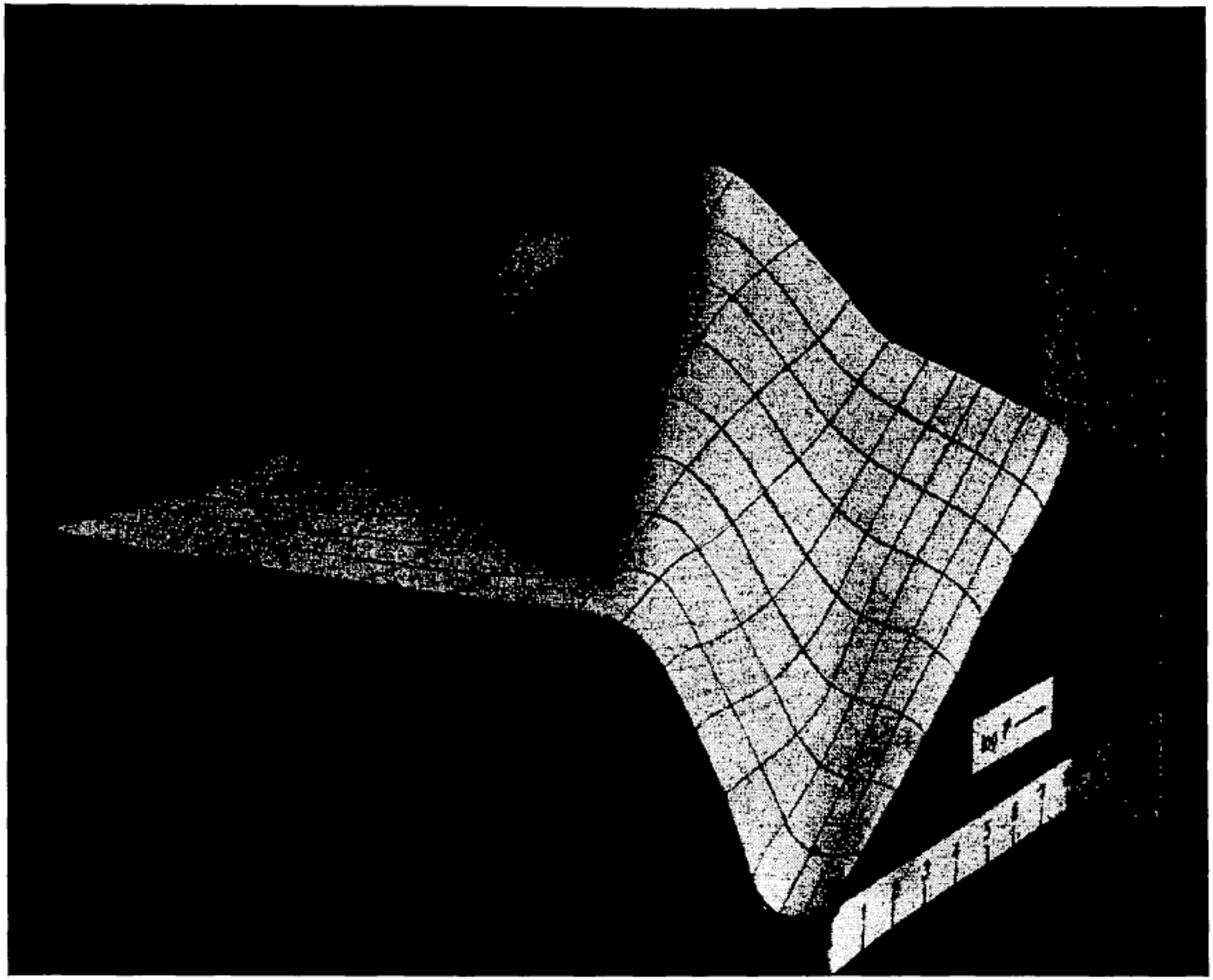

Fig. 1. A three dimensional model of the absorption coefficient $\varkappa$ as a function of $\log P$ and $\log T$ ($\varkappa$-surface). This model is based on the values of E. VITENSE (1951)

N. Baker, R. Kippenhahn, 1962, Z.f.Ap., 54, 114.

Stars whose luminosity varies periodically have been known for centuries. However, only within the last hundred years has it been definitely established that in many cases these variations are due to *intrinsic* pulsations of the stars themselves. For obvious reasons studies of pulsating stars initially concentrated on stars with large amplitudes, such as the Cepheids and the long period variables. The variations of these stars could be understood in terms of pulsations in the fundamental radial mode, where the star expands and contracts, while preserving spherical symmetry. It was realized very early (Shapley 1914) that the period of such motion is approximately given by the dynamical time scale of the star:

$$t_{\rm dyn} \simeq \left(\frac{R^3}{GM}\right)^{1/2} \simeq (G\bar{\rho})^{-1/2} \,, \tag{1.1}$$

where R is the radius of the star, M is its mass, $\bar{\rho}$ is its mean density, and G is the gravitational constant. Thus observation of the period immediately gives an estimate of one intrinsic property of the star, *viz.* its mean density.

It is a characteristic property of the Cepheids that they lie in a narrow, almost vertical strip in the HR diagram, the so-called *instability strip*. As a result, there is a direct relation between the luminosities of these stars and their radii; assuming also a mass-luminosity relation one obtains a relation between the luminosities and the periods, provided that the latter scale as $t_{\rm dyn}$. This argument motivates the existence of a *period-luminosity relation* for the Cepheids: thus the periods, which are easy to determine observationally, may be used to infer the intrinsic luminosities; since the apparent luminosities can be measured, one can determine the distance to the stars. This provides one of the most important distance indicators in astrophysics.

The main emphasis in the early studies was on understanding the causes of the pulsations, particularly the concentration of pulsating stars in the instability strip. As in many other branches of astrophysics major contributions to the understanding of stellar pulsation were made by Eddington (*e.g.* Eddington 1926). However, the identification of the actual cause of the pulsations, and of the reason for the instability strip, was first arrived at independently by Zhevakin (1953) and by Cox & Whitney (1958).

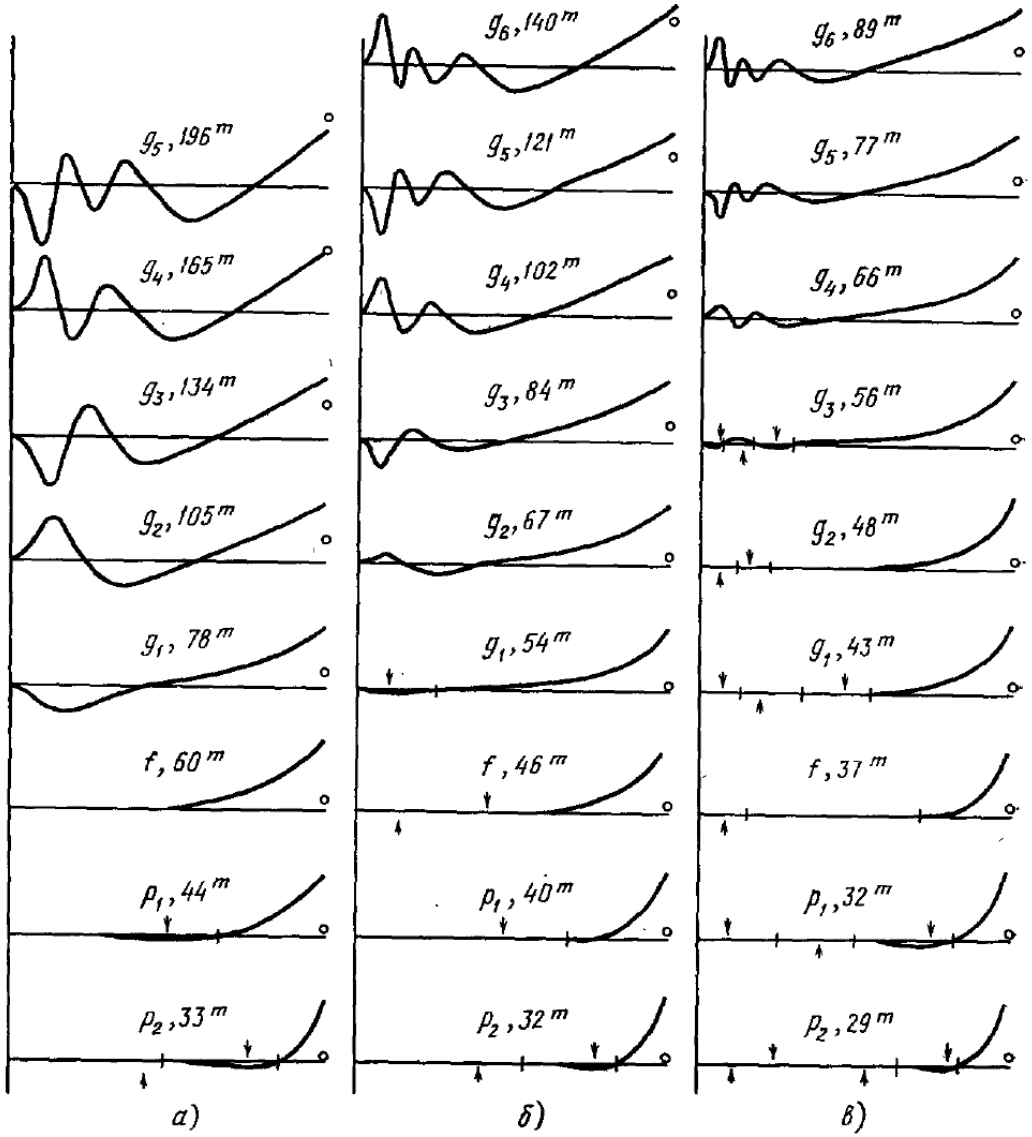

Рис. 3. Собственные функции квадрупольных колебаний политропных моделей Солнца [32].

По горизонтальным осям отложен безразмерный радиус $x = r/R_\odot$, слева — центр, справа — поверхность. По вертикали отложены нормированные амплитуды радиальных смещений $U(x)$. Где необходимо, положения узлов показаны штрихами и положения пучностей — стрелками. Относительные амплитуды тангенциальных смещений V на поверхности показаны точками. Для каждого колебания приведена его классификация по модам p, f, g и период в минутах. *а*) Политропа индекса 3; *б*) политропа индекса 3,4; *в*) политропа индекса 3,7.

Propagation diagram, ZAMS solar model

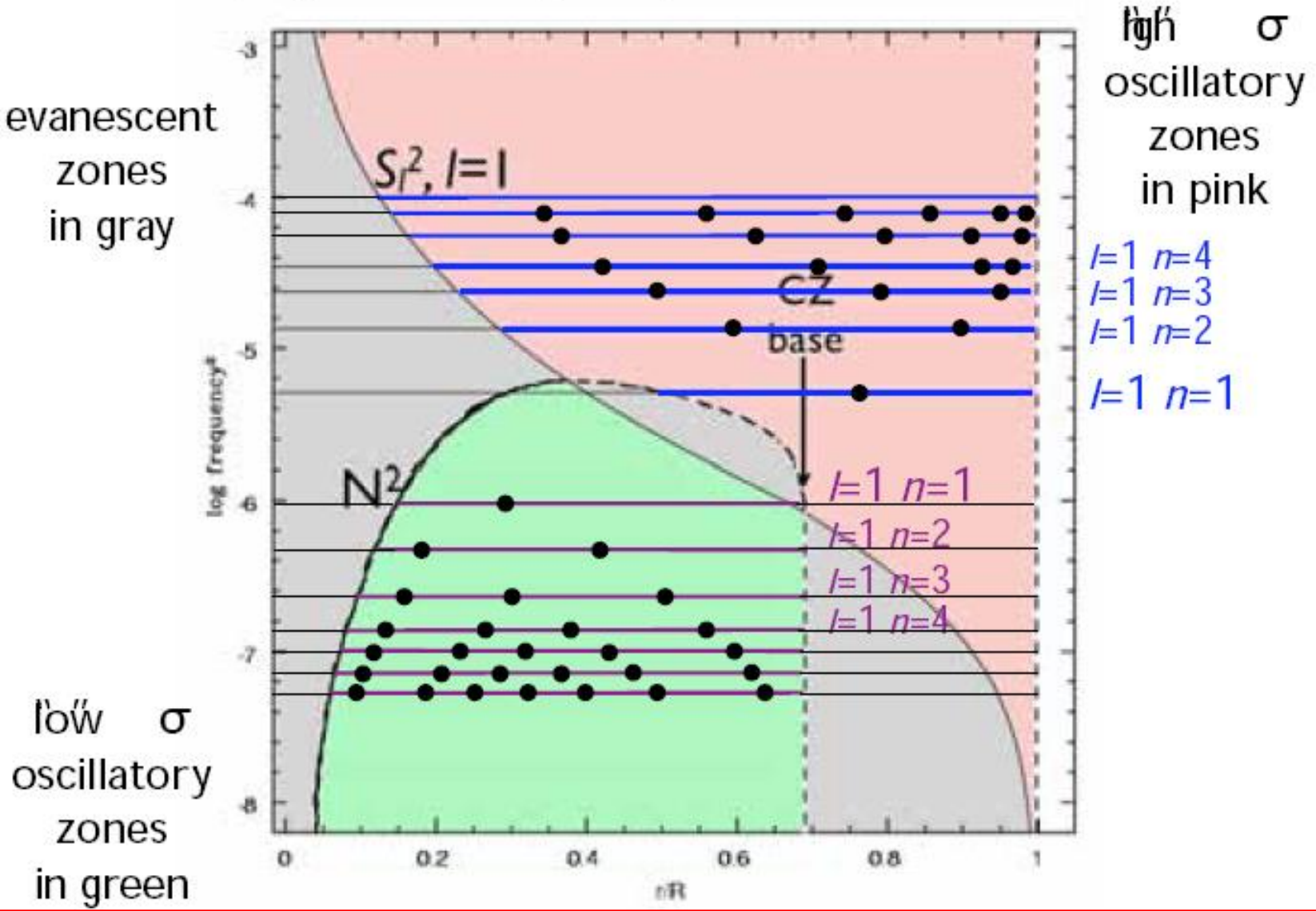

(Kawaler, Lecture 3)

$$W = -\int \mathrm{d}^3x\, \nabla_{\mathrm{ad}} \oint \mathrm{d}t\, \mathrm{Re}\left[\left(\frac{\delta P}{P}\right)^* \delta\, \mathrm{div}\, \mathbf{F}_{\mathrm{R}}\right]$$

$$\nabla_{\mathrm{ad}} = (\mathrm{d}\ln T/\mathrm{d}\ln P)_{\mathrm{ad}}$$

$$\delta\, \mathrm{div}\, \mathbf{F}_{\mathrm{R}} = \frac{1}{4\pi r^2}\frac{d\,\delta L_r}{dr}$$

$$\frac{\delta L_r}{L_r} = \frac{\mathrm{d}r}{\mathrm{d}\ln T}\frac{\mathrm{d}}{\mathrm{d}r}\left(\frac{\delta T}{T}\right) - \frac{\delta\kappa}{\kappa} + 4\left(\frac{\delta T}{T} + \frac{\delta r}{r}\right)$$

$$\tau_{\mathrm{th}}(r) = \int_r^R T c_P\, \mathrm{d}M/L$$

$$\kappa_T + \kappa_\rho/(\Gamma_3 - 1)$$

$$\Gamma_3 - 1 = (\mathrm{d}\ln T/\mathrm{d}\ln\rho)_{\mathrm{ad}}$$

$$\kappa_T = (\partial\ln\kappa/\partial\ln T)_\rho$$

$$\kappa_\rho = (\partial\ln\kappa/\partial\ln\rho)_T$$

$$\frac{1}{\kappa}\cdot\int\frac{dB_\nu}{dT}d\nu = \int\frac{1}{\kappa_\nu}\frac{dB_\nu}{dT}d\nu$$